Stony Brook University

Alterations in the Mineral and Collagen Matrix of Bisphosphonate-Treated Bone and Osteoblasts

A Dissertation Presented

by

Meghan Elizabeth Ruppel

To

The Graduate School

In Partial Fulfillment of the

Requirements

for the Degree of

Doctor of Philosophy

in

Biomedical Engineering

Stony Brook University

May 2009

Stony Brook University
The Graduate School

Meghan Elizabeth Ruppel

We, the dissertation committee for the above candidate for the

Doctor of Philosophy, hereby recommend

acceptance of this dissertation.

Lisa M. Miller, Ph.D- Dissertation Advisor
Adjunct Assistant Professor, Department of Biomedical Engineering

Stefan Judex, Ph.D- Chairperson of Defense
Associate Professor, Department of Biomedical Engineering

Yi-Xian Qin, Ph.D
Professor, Department of Biomedical Engineering

Roger Phipps, Ph.D
Bone Genomics and Cancer Research, The Main Institute for Human Genetics and Health

This dissertation is accepted by the Graduate School

Lawrence Martin
Dean of the Graduate School

Abstract of the Dissertation

Alterations in the Mineral and Collagen Matrix of Bisphosphonate-Treated Bone and Osteoblasts

By

Meghan Elizabeth Ruppel

Doctor of Philosophy

in

Biomedical Engineering

Stony Brook University

2009

Osteoporosis is a disease that affects nearly 75 million people worldwide. It occurs due to skewed activity of osteoblasts, which form new bone, and osteoclasts, which breakdown old bone. The disease is characterized by decreased bone mineral density (BMD), degradation of the trabecular architecture and increased fracture risk.

Prevention of bone loss by inhibition of osteoclast-mediated bone resorption appears to be the major mechanism for fracture risk reduction and increased BMD, seen with bisphosphonates (BPs) in osteoporosis. However, recent studies have shown that BPs may negatively affect bone quality. The goal of this dissertation was to determine the effect of bisphosphonate-treatment on the quality of existing and newly formed tissue. Understanding how bone quality might be altered will help to understand the long term affects of bisphosphonate-treatment.

Chemical composition of bone and mineralizing osteoblasts was determined using Fourier transform infrared imaging and matrix morphology was examined using nano-transmission x-ray tomography. We found that, while microdamage was not accumulated in areas of increased mineralization, formation of microcracks led to changes in the mineral stoichiometry and collagen cross-links. Microdamage accumulation and changes in bone composition due to microcrack formation may lead to changes in post-yield mechanical properties and increased fragility.

Further, we found that the rate of collagen deposition and mineralization were temporarily slowed by risedronate-treatment. The morphology of the mineral formed by the risedronate-treated cells was not altered. This paired lag in activity appears to be due to decreased function of osteoblasts cells, caused by BP-treatment.

While these results are difficult to directly extrapolate to the clinical setting, the concept that chemical composition and structure can be directly linked to mechanical properties of bone remains important. Therefore, further studies, specifically determining if BPs have long-term effects on osteoporotic patients needs to be undertaken.

Table of Contents

List of Abbreviations

ACP	Amorphous calcium phosphate
ALN	Alendronate
ALP	Alkaline phosphatase
ATP	Adenosine triphosphate
BMD	Bone mineral density
BMU	Basic multicellular units
BP	Bisphosphonate
BPs	Bisphosphonates
CCD	Charge-coupled device
FTIR	Fourier transform infrared spectroscopy
FTIRI	Fourier transform infrared imaging
HAP	Hydroxyapatite
IR	Infrared
Nano-TXM	Nano-transmission x-ray microscopy
OCN	Osteocalcin
RIS	Risedronate
SD	Standard deviation
SPS	Sulfonated polystyrene
SSRL	Stanford Linear Radiation Laboratory
TXM	Transmission x-ray microscopy

List of Equations

List of Figures

List of Tables

Acknowledgements

There are many people that I would like to thank, whom have supported me and my long educational journey. First I would like to thank Dr. Lisa Miller for her guidance and teaching in the area of synchrotron science and bone chemistry. She has been nothing but a true mentor from the day I started in her laboratory and I am extremely grateful for all of the time she has spent working with me as well as the continuous educational encouragement she has provided.

I would also like to thank my thesis committee members, Dr. Stefan Judex, Dr. Yi-Xian Qin and Dr. Roger Phipps. They have all been helpful throughout the dissertation process, providing insight and comments to my work.

My collaborators, Dr. Roger Phipps, Dr. Robyn Fuchs, Dr. Yizhi Meng, Dr. Cathy Carlson, and Dr. David Burr have all provided me with unlimited knowledge, support and assistance in the area of bone physiology and chemistry. They have all been an absolute pleasure to work with on this and other projects we have undertaken.

Over my 4 years within the Miller Research Group I have received much help from my fellow group members. I would like to thank them for their help in and around the lab, assistance during beamtime, support on this and other projects, and for their extensive knowledge in fields I would have otherwise known nothing about. You are all not only co-workers but true friends as well, thank you for all of your continued support. Good luck in your work and future endeavors.

I would like to thank my family and friends, especially my parents who have been nothing but supportive throughout my whole educational experience, even when they joked that I was going to be a career student.

Lastly, I would like to thank my fiancé Jeff. You have helped restore the happiness in my life and made me realize that I was more than capable of achieving this dream. I cannot wait to be your wife and start our future together.

Publications

1. M.E. Ruppel, R.J. Phipps, L.M. Miller (2009). Risedronate-treatment temporarily delays collagen deposition and matrix mineralization of MC3T3-E1 osteoblasts. *Bone*. Submitted

2. D.B. Burr, M. E. Ruppel, L.M. Miller (2009). Bone Fragility-Microscopic and Nanoscale Structure. *US Musculoskeletal Review.* Submitted.

3. M.E. Ruppel, L.M. Miller, D.B. Burr (2008). The effect of the microscopic and nanoscale structure on bone fragility. *Osteoporos. Int*. 19(9): 1251-65 [PMID: 18317862]

4. R.K. Fuchs, M.R. Allen, M.E. Ruppel, T. Diab, R.J. Phipps, L.M. Miller, D.B. Burr (2008). In situ examination of the time-course for secondary mineralization of Haversian bone using synchrotron-assisted Fourier transform infrared microspectroscopy. *Matrix Biol.*, 27(1): 34-41 [PMID: 17884405]

5. M.E. Ruppel, D.B. Burr, L.M. Miller (2006). Chemical Makeup of Microdamaged Bone Differs from Undamaged Bone. *Bone,* 39 (2): 318-24. [PMID: 16584933]

6. L.M. Miller, M.E. Ruppel, C. H. Ott, R.J. Smith, A. Lanzirotti (2005). Development and Applications of an Epifluorescence Module for Synchrotron X-ray Fluorescence Imaging. *Rev. Sci. Instr*., 76: 066107.

Chapter I: Introduction

I.I Bone Composition

Bone is an organ with a hierarchical structure (**Figure 1**) that is composed of organic and mineral components, mainly consisting of a matrix of cross-linked type I collagen mineralized with nanocrystalline, carbonated apatite [1-4]. Because bone is an anisotropic material, it is important to study its quality and structure on many levels, including the microscopic and nanoscale. Collagen fibers, which provide bone with its ductile properties, are approximately 1 μm in diameter [5-8], while mineral crystals, which give bone its rigidity, range from 5-60 nm in diameter [9-12]. While the collagen and mineral each contribute certain mechanical properties to the tissue, the interaction of the two phases of bone also add to its mechanical properties.

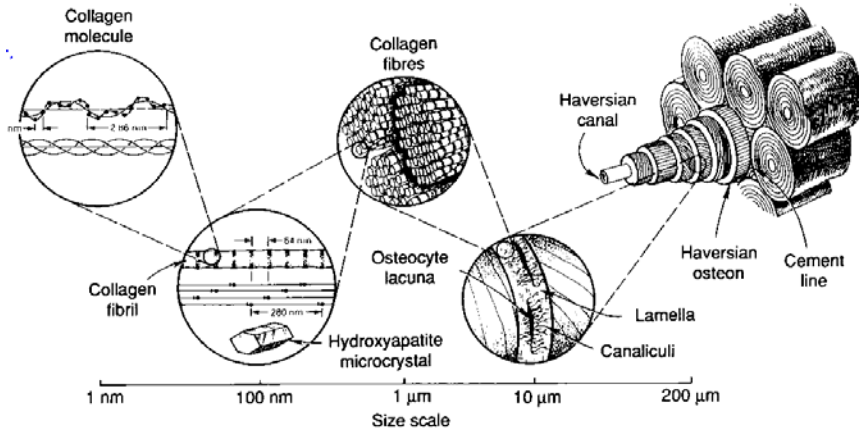

Figure 1: Schematic showing the hierarchal structure of bone and the size scale for each component of the tissue [1].

Type I collagen fibrils with diameters of ~100 nm are rectilinearly organized to form collagen fibers [13, 14]. Within bone, collagen fibrils are organized in parallel fibers to maximize strength and stiffness [14-18]. The mineral crystals in bone have a plate-like structure and are closely packed and parallel to one another [19-21].

Interaction of the mineral crystals and collagenous matrix contributes significant mechanical properties to bone. Mineral crystals occupy 35 nm hole

zones within the collagen matrix that are formed when the collagen fibrils come together [9, 22-25]. Within the mineralized matrix, it has been shown that collagen fibrils and mineral are oriented parallel to one another [9, 11, 12, 22, 24, 26] to optimize mechanical strength [27]. Additionally, it appears that collagen helps to distributed stresses across the whole mineralized matrix, protecting mineral crystals from large stresses they could not withstand on their own [28-30].

Stoichometrically, bone mineral is poorly crystalline hydroxyapatite ($Ca_{10}[PO_4]_6[OH]_2$). However, the exact structure of the mineral apatite in bone is hard to determine because the cationic calcium sites and the anionic phosphate sites can become highly substituted within the collagenous matrix. The two most abundant anionic substitutions are carbonate (CO_3^{2-}) and acid phosphate (HPO_4^{2-}) which primarily substitute into the PO_4^{3-} sites of the apatite lattice [31-34]. Carbonate substitutions can make the bone lattice less stable and can lead to a decrease in crystallinity and increased solubility [35-37]. Additionally it is known that higher acid phosphate content is associated with immature, young tissue [38-40].

Cationic substitutions can also alter the mechanical integrity of bone. For example, even though sodium fluoride treatment can increase bone mineral density and stimulate osteoblasts [41, 42], it can decrease elasticity and bone strength by altering crystal morphology [43-46]. Further, excessive lead in the body (from lead exposure) can be incorporated into the calcified matrix of bone, decreasing BMD [47-49].

I.II Bone Formation *in vitro* and *in vivo*

Bone forms in a similar way *in vivo* as it does *in vitro*. Ascorbic acid within the body helps stimulate osteoblasts to form a collagenous matrix within the extracellular space, called osteoid. A well developed matrix of collagen is essential for mineralization to begin [50-55]. Extracellular calcium and phosphate ions eventually form tiny apatite crystals within the osteoid. These initial crystals grow in size and act as nucleation sites for further mineralization [54, 56]. The osteoid typically begins to mineralize within 5-10 days [57] during primary

mineralization [58, 59]. The osteoid becomes 65-70% mineralized during primary mineralization [58, 60], and slowly increases to a physiological limit during secondary mineralization. Matrix proteins, like alkaline phosphatase (ALP) and osteocalcin (OCN) are also believed to play a role in matrix mineralization [56].

Within the skeleton bone remodeling is a continuous process, whereby osteoclasts breakdown old and damaged bone and osteoblasts form new tissue. During remodeling, bone that gets replaced (called secondary bone) gets replaced in the same way that primary bone gets formed, but secondary mineralization takes significantly longer during secondary bone formation [58, 61, 62].

Proliferation, differentiation and mineralization of MC3T3-E1 osteoblasts have been very well characterized [51, 53, 63]. The process by which these cells form a collagenous matrix and deposit mineral onto that matrix is similar to that which occurs in woven bone tissue. The cells undergo an initial period of proliferation where they replicate and divide. Addition of ascorbic acid acts to increase procollagen hydroxylation [64], which causes the formation of a triple-helix structure. Collagen fibrils are secreted by the cells and an insoluble, type I collagen matrix begins forming within 24 hours [53]. Collagen fibrils, which are made of several collagen molecules, overlap to form the matrix, which develops 60-70 nm axial periodicity, around 7 days [53].

After the synthesis of the collagen matrix has begun, the cells begin activation of osteoblast marker genes [65]. ALP, which helps process phosphate, is expressed starting around 2-3 days and OCN, which acts as a biomarker for bone formation, is expressed between days 4-6. The presence of a collagenous matrix, release of osteoblast marker genes, and the addition of phosphate help to initiate mineralization. The zones in between the collagen fibrils are filled with nodules of mineral apatite, specifically $Ca_{10}[PO_4]_6[OH]_2$ beginning at about 2 weeks. The formation of these mineral nodules within the extracellular matrix is initiated and assisted by matrix vesicles. Small vesicles, with diameters of 60-400 nm, that are filled with needle-like crystals of mineral, act as nucleation sites for

nodule formation [53, 66-68]. The matrix vesicles are secreted by the osteoblasts and interact with the collagen matrix [63].

The process by which collagen and mineral are formed and deposited in bone is important to maintain its mechanical properties and any alterations to the collagen or mineral can have adverse effects. MC3T3-E1 cultures that have been grown in the absence of ascorbic acid do not produce nearly as much collagen as those grown with ascorbic acid [51] and it has been shown that production of the collagenous matrix allows the cells to form multiple cell layers [53], which assists in mineralization. *In vivo* mutated or low quantities of type I collagen, which occurs with osteogenisis imperfecta, causes weaker and more brittle bones [69, 70]. Additionally, decreased collagen fibril diameter [13, 14] and alterations in mineral crystal size [71-73] have been demonstrated in osteoporotic tissue.

I.III Osteoporosis

Osteoporosis is a wide spread bone disease that affects approximately 75 million people in Japan, the USA, and Europe [74]. On a cellular level, osteoporosis is characterized by uneven metabolic activity of osteoblasts and osteoclasts, which results in a breakdown of bone microarchitecture as seen in **Figure 2** [75-80]. Osteoporotic patients also have increased fracture risk [81-85] and decreased BMD [86-88]. Evaluation for osteoporosis includes assessment of a patient's bone properties in terms of their fracture risk, via BMD measurements. However, osteoporosis quantifies more than just a patient's likelihood to experience a fracture; there are processes occurring within the bone tissue that compromise the overall strength of their skeleton.

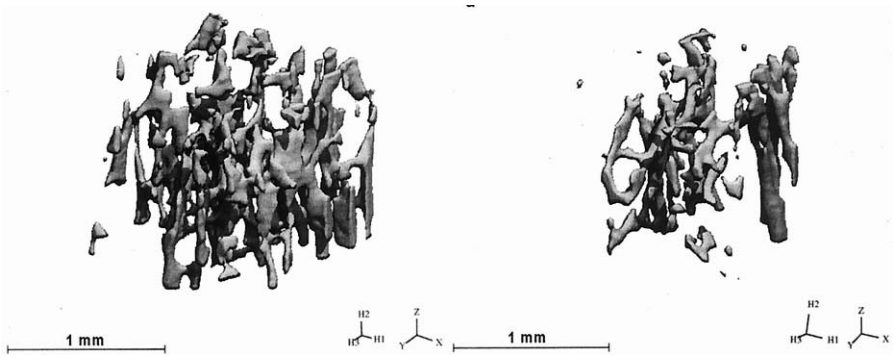

Figure 2: Three-dimensional μCT images of tibia secondary spongiosa in (A) an age-related control and (B) a 23 days-suspended rat [77].

To date, the most common clinical approach for diagnosing osteoporosis is by the measurement of BMD. Osteopenia is defined as a bone mineral density 1 to 2.5 standard deviations lower than normal peak BMD, while osteoporosis represents a BMD more than 2.5 standard deviations below normal levels [74]. Higher BMD is typically associated with lower fracture risk, however it has been shown that the small decreases in BMD that occur with age are a minimal contributor to the exponential increase in fracture risk after the age of 55 [89]. Additionally there is a large overlap in BMD values of osteoporotic patients and those that do not experience fractures [90], which demonstrates that BMD alone cannot predict bone fragility.

Although BMD can help determine a patient's fracture risk, bone fragility is a composite description of bone's mechanical properties, where fragility is directly related to bones susceptibility to fracture and it is inversely related to a bone's fracture resistance. Thus, mechanical properties such as the hardness and toughness of the tissue, and the load under which it will fracture, can provide direct quantitative measures of fragility. However, measurements such as these are often not feasible in a clinical setting, so the underlying contributors to fragility must be understood.

While bone quantity, as measured by BMD, is the best understood contributor to fragility in osteoporosis, other contributors to bone fragility include bone's architecture, geometry, and material properties [8, 91-95]. Taken together, these latter contributors have been defined as bone quality [96-98].

In order to obtain a precise measure of fragility, bone quality must be characterized for all levels of bone structure. In the clinic, measurements of whole bone properties are made. However, since bone is an anisotropic material, correlation with the macro-, micro- and nanoscopic levels is also extremely important. Like all composite materials, each constituent of bone has a different contribution to the overall quality of the tissue. Since bone fragility is defined as susceptibility to fracture, understanding how each element of bone tissue plays a role in its overall quality is an important step in defining bone fragility prior to osteoporotic fracture. Additionally, examining bone on the micro and nanoscopic levels may give more insight into why osteoporosis occurs.

I.IV Bisphosphonates

BPs (**Figure 3**) are a current class of treatments designed to help fight the damaging effects of osteoporosis. BPs are designed to decrease fracture risk. and it is believed they do this by preserving bone microarchitecture [99]. They have also been shown to increase BMD by extending the mineralization times for the basic multicellular units (BMU) by inhibiting osteoclasts [100, 101]. BPs have been shown to induced osteoclast apoptosis as well as suppress their proliferation and activity [102-106].

There are two types of BPs; nitrogen and non-nitrogen containing. Non-nitrogen containing BPs, like etidronate and clodronate, are metabolized by the cell and get incorporated into adenosine triphosphate (ATP). These new forms of ATP are toxic because the enzyme that normally cleves the oxygen-phosphate bond in normal ATP cannot cleave the carbon-phosphate bond in the ATP analog. These analogs then build up within the cell because they cannot be used for energy, leading to apoptosis and necrosis of the osteoclast [107]. Nitrogen containing BPs, like risedronate (RIS), alendronate (ALN), and ibandronate, inhibit enzymes in the mevalonate pathway [105, 106, 108]. G proteins, like Rho, Rac, Rab and Ras perform important functions within osteoclasts, and if these proteins do not function correctly the cells will die [109]. In order for these proteins to function correctly they need either a 20 or 15-carbon side chain.

Nitrogen-containing BPs inhibit production of these side chains, leading to osteoclast apoptosis and necrosis.

BPs have been shown to have high binding affinity for bone mineral due to the presence of their two phosphate groups [110-113]. Once administered *in vivo*, BPs bind to bone. While only small amounts are naturally desorbed from the bone surface over time [113], large amounts are released from the surface by osteoclasts during bone resorption [105, 106]. Studies of animals treated with BPs have demonstrated that they target and bind to hydroxyapatite and can inhibit crystal formation and dissolution [114-117].

Through interaction with osteoclasts BPs decrease the number of remodeling sites in bone [118], which leads to a decrease in bone formation [119, 120]. Because of slowed remodeling overall tissue mineralization increases. Increased amounts of fully mineralized bone have been shown to increase the brittle properties of the tissue [121-123].

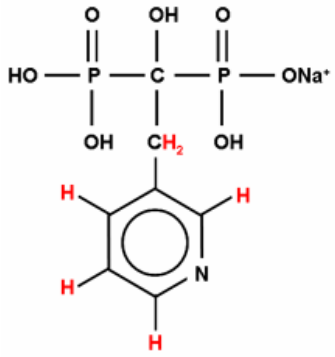

Figure 3: Chemical structure of the bisphosphonate, risedronate, illustrating the non-labile hydrogen's that will be deuterated for the proposed experiments.

The inhibitory role of BPs on osteoclasts has been extensively studied in culture [104, 124-126] and *in vivo* [104, 127]. However, the role of BPs on osteoblasts is only beginning to be investigated, but some studies have shown that they inhibit the formation and dissolution of mineral crystals in culture [116, 128-132]. Others have shown that BPs increase the differentiation of osteoblasts [133-135]. Additionally others have shown that BPs also affect osteoblasts *in vivo* leading to decreased bone formation [136-139] Therefore, investigation into how BPs affect the chemical composition, morphology, and overall quality of existing

and newly formed bone is important to understanding the quality of the tissue and the long term affects of drug treatment.

I.V Microdamage

Microdamage (**Figure 4**) forms in response to applied loads placed on the body during normal activities [140-143]. When bones are loaded, small cracks form as a result of energy absorption and dissipation. Microcracks are typically 100-300 μm in length [144], oriented parallel to the longitudinal axis of bone [145], form at cement lines and interlamellar boundaries [146] and are isolated to interstitial bone [144, 147].

It is proposed that in healthy individuals areas of bone containing microdamage are targeted during the remodeling and repair of the tissue [148-150]. However, based on more recent studies, it appears that microdamage can occur due to various physiological triggers. For example, targeted remodeling is believed to occur in overuse fractures in dogs [140, 142], and in areas of cyclic-loading induced microdamaged in rats [151]. However, microdamage can also be associated with the process of bone remodeling [140, 152, 153]. It is believed that at the beginning of remodeling, when bone is being resorbed, there is less bone to help sustain loading. The remaining bone is then subjected to higher strains which could lead to microdamage formation.

Microcracks can be detected by bulk staining with fuchsin [148, 154]. There are two types of microdamage; microcracks and diffuse microdamage. In this work we focused on microcracks that appear as clear, distinguishable, and linear cracks. Diffuse damage tends to appear as a cloud of fuchsin stain.

Fatigue loading, to physiologically relevant strain levels, is believed to be the leading cause of microdamage [140, 142, 155]. Linear microcracks tend to form under compressive loads [156, 157], while diffuse damage results from tensile loading [156]. In humans microdamage accumulation has been shown to increase with age which could play a role in increased fractures and fragility in the elderly [144, 158-160]. This increase is linked to slowed remodeling that occurs with age [161].

It has been suggested that microcracks are an indication of impending failure [162] and that stress fractures are inevitable if microcracks go unrepaired [163, 164]. Microdamage accumulation has been linked to mechanical instability; such as a decrease in elastic modulus. Stiffness, ultimate strength, and energy to failure are also compromised with microdamage accumulation, leading to decreased fracture resistance [165, 166]. Reduced tensile strength [165] and fracture toughness [167] have also been attributed to microdamage accumulation.

Further, microdamage has been associated with increased blood flow [168], decreased interstitial fluid flow [168], and plays a role in calcium homeostasis [169].

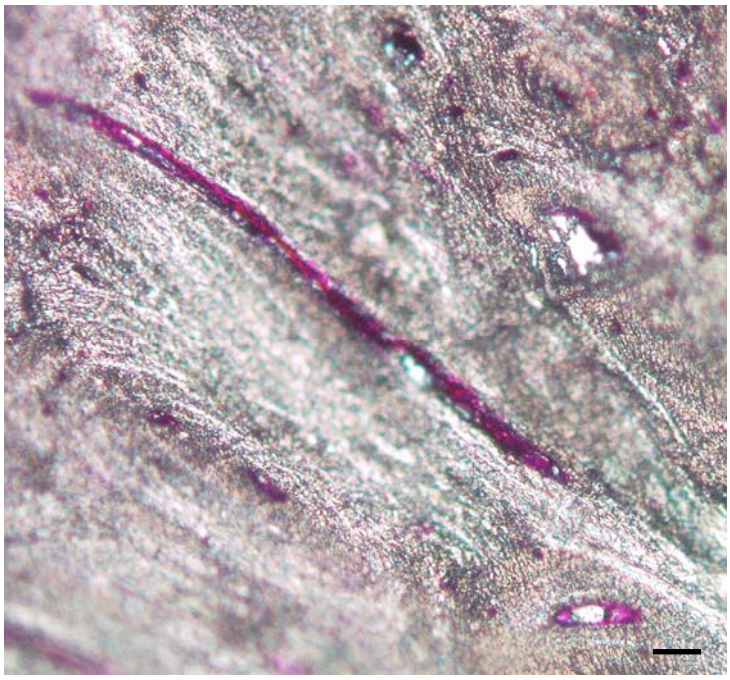

Figure 4: 100X image of a section from the L3 vertebra of a beagle. Bone was stained with fuchsin (purple) to demonstrate areas of microdamage. Scale bar is 5 μm.

During high-dose BP treatment, the microdamage burden in dogs has been shown to increase up to 322% and the toughness of bone has decreased [122]. It is thought that because osteoclast activity is slowed by BPs, areas containing damage are not targeted for remodeling. However, microdamage could result from increased mineralization, also seen with BP treatment [100,

121]. In dogs administered BP doses comparable to that received by postmenopausal women, microcrack frequency also increased, but was not paired with decreased mechanical stability [170]. However, examination of tissue from humans on long term BP-treatment revealed no increase in microdamage when bone remodeling was significantly suppressed [171, 172]. Regardless of the cause, increased accumulation of microdamage over the course of BP treatment, paired with altered bone chemistry, could ultimately lead to increased fragility of already susceptible tissues.

I.VI FTIRI and Nano-TXM

Two techniques that can be used to study the quality of bone and mineralizing tissue on the micro- and nanoscale, are Fourier Transform infrared imaging (FTIRI) and nano-transmission x-ray microscopy (nano-TXM), respectively.

FTIRI

Infrared (IR) light is located in the middle of the electromagnetic spetrum, between visible light and microwaves. FTIRI combines light microscopy and IR spectroscopy and takes advantage of the fact that bonds between organic compounds absorb light within the infrared region of the electromagnetic spectrum [173]. Molecular bonds naturally vibrate at a specific frequency, based on the atoms within the molecule. The energy absorbed using FTIRI relates to the frequency at which specific molecular bonds vibrate, and only precise frequencies of IR radiation that match the natural vibrations of the probed molecules will be absorbed. The absorbed IR radiation will amplify the natural vibrations of the molecule by stretching, bending, wagging, and/or deforming the bonds. FTIRI allows correlation of the microstructural features of a sample, to be correlated with chemical composition.

The natural frequency at which at bond will vibrate can be determined by using Hooke's law [173]:

Equation 1 $$\nu = 1/(2\pi c)\sqrt{K/\mu}$$

K is the force constant and varies from one bond to another, c is the velocity of light (3 x 10^{10} cm/sec). The reduced mass, μ, can be determined from the atomic weights of the two atoms within the bond.

Equation 2 $\mu=(m_1m_2)/(m_1+m_2)$

IR imaging systems couple a spectrometer that generates the IR light, to a microscope so that point and area imaging of a sample can be performed. Broadband IR light is either transmitted or reflected through a sample and collected. Changes in the intensity of the absorbed light can be plotted versus frequency to generate an infrared spectrum. The infrared spectrum reveals the wavelength at which and the amount of energy a sample absorbed light. This can be further used to determine the chemical components within the sample.

Biological samples can be probed using FTIRI to determine what molecules they are composed of. According to the Lambert-Beer law, the intensity of a peak in the absorbance spectrum is directly proportional to the concentration of molecular bond within the sample.

Equation 3 $A=\varepsilon bc$

A is the absorption intensity of the peak, ε is the molar absorption coefficient, b is the sample thickness, and c is the concentration. Using FTIR and FTIRI, the biochemistry of biological, geological, environmental, and material samples can be probed [174]. Typically, biological samples are composed of lipids, proteins, nucleic acids and carbohydrates.

More specifically, FTIRI is a valuable technique for examining the mineral and protein content of bone and mineralized tissue [175, 176]. Further, it can be used to study the compositional changes caused by bone disease [71, 177-181]. Utilizing a globar source, bone can be studied with a spatial resolution of 30-50 μm [182-184], which can be further increased to the diffraction limit of 3-15 μm with the use of a synchrotron [39, 179, 185-187]. Utilizing this technique, the mineralization, carbonate accumulation, crystallinity, collagen cross-linking, and collagen content of bone and mineralizing osteoblasts can be studied. Further, changes in chemical composition of bone can be linked to the mechanical properties of the tissue [188].

Nano-TXM

Xradia™ has recently developed the nanoXCT™; a nano-TXM capable of performing x-ray absorbance and phase contrast 2-D imaging as well as 3-D computed tomography. This instrument has recently been installed at beamline BL6-2 at the Stanford Synchrotron Radiation Laboratory (SSRL) and is capable of imaging biological tissue with a spatial resolution less than 40 nm in 3-D tomographic mode and 2-D phase contrast and absorption modes. The nano-TXM at SSRL is based on zone plate optics, which function in absorption mode from 5-14 keV and Zernike phase contrast at 8keV [189, 190].

The instrument at SSRL operates similar to an optical microscope. The synchrotron light is provided through a 54-pole wiggler, and vertically collimated by a platinum-coated bent-flat mirror. The x-rays then pass through a liquid-nitrogen cooled double silicon crystal (111) monochromator. The beam is focused onto a toroidal mirror, which focuses it through a slit that reduces the beams vertical translation. The nano-TXM focuses the x-ray beam through its condenser lens onto the sample. The resulting x-rays are magnified by the micro zone plate, onto a liquid nitrogen cooled charge-coupled device (CCD).

Phase contrast mode was utilized in this work. The phase and amplitude of light can be changed when it is passed through a sample because different structures within the sample have different indexes of refraction. Highly refractive structures bend light to a much greater extent than those with lower refractive indexes, which gives rise to changes in the phase of light passing through them. Specifically in biological samples, phase contrast can illuminate small features, such as micron and nanometer structure within a cell. Phase contrast images are generated from the nano-TXM, by converting the differences in phase and amplitude of the x-rays into a grey-scale image.

This instrument provides information about biological samples that can be used in conjunction with other imaging techniques. Cells and bacteria are typically studied using visible light and electron microscopy. Nano-TXM combats the resolution inadequacies of visible microscopy and does not require sample sectioning like electron microscopy, as the x-rays can penetrate 1-20 μm.

Samples can be “virtually sectioned” and imaged with 40 nm resolution, without disturbing critical spatial information of the sample.

While this technique is fairly new, its usefulness in imaging of several biological tissues has previously been demonstrated [189]. Specifically, it enables the imaging of the nanoscale structure of mineralized bone tissue, such as how the individual collagen fibrils are oriented and the structure of the mineral within the collagen matrix. Results can be correlated with mechanical information from nanoindentation [191, 192] to provide an understanding of bone fragility at the nanoscale.

I.VII Hypotheses and Specific Aims

While it has been shown that BP-treatment increases BMD and reduces fracture risk through regulation of osteoclast function, it has also been shown that BPs cause increased tissue mineralization and can act on osteoblasts. If osteoclast and osteoblast function are being altered by BP-treatment, we hypothesize that the chemical composition and morphology of existing and newly formed bone might also be affected. Therefore, the goal of the current study is to determine if the chemical composition and structure of existing and newly formed bone are affected by BP-treatment both in bone tissue and mineralizing osteoblast cultures. This goal will be investigated by studying existing bone from animals that have been treated with the nitrogen-containing BPs, ALN and RIS, and by examining the chemical composition and morphology of mineral formed by MC3T3-E1 mouse osteoblasts treated with RIS.

Chapter II will address **specific aim 1**, which is to compare the chemical composition of BP-treated and untreated bone in areas of microdamage and undamaged tissue, to determine the long term effects of BP treatment on bone composition. Because BPs slow down the turnover process, we hypothesize that BP-treated bone will be older resulting in higher levels of mineralization and carbonate accumulation and lower acid phosphate content than untreated bone. Additionally, since highly mineralized bone can be correlated with brittleness, we

hypothesize that microdamage will be concentrated in areas of the tissue that have become overmineralized.

Chapter III and IV will address **specific aim 2**, which is to examine the degree of mineralization, collagen content, collagen fibril orientation and morphology of the mineralized matrix formed by MC3T3-E1 osteoblasts, as a function of time and RIS-treatment. *In vivo* [131, 136, 137, 139, 193-200] and *in vitro* [134, 201-203] studies have both shown decreased mineralization with BP treatment. Additionally groups have demonstrated decreased collagen production and deposition with BP-treatment [135, 203, 204]. Therefore we hypothesize that supplementation of media with risedronate will cause a decrease in the mineralization and collagen deposition of osteoblast cells in culture. Additionally, as BPs have been shown to bind to mineral we hypothesize that mineral structure could be altered in the RIS-treated cells. Further we believed that the collagen fibril orientation of the matrix formed by MC3T3-E1 osteoblasts will not be altered by RIS-treatment.

Chapter II: Chemical makeup of microdamaged bone differs from undamaged bone [205]

II.I Abstract

Microdamage naturally occurs in bone tissue as a result of cyclic loading placed on the body from normal daily activities. While it is usually repaired through the bone turnover process, accumulation of microdamage may result in reduced bone quality and increased fracture risk. It is unclear whether certain areas of bone are more susceptible to microdamage than others due to compositional differences. This study examines whether areas of microdamaged bone are chemically different than undamaged areas of bone. Bone samples (L3 vertebrae) were harvested from 15 dogs. Samples were stained with basic fuchsin, embedded in poly-methylmethacrylate, and cut into 5 micron-thick sections. Fuchsin-staining was used to identify regions of microdamage, and synchrotron infrared microspectroscopic imaging was used to determine the local bone composition. Results showed that microdamaged areas of bone were chemically different than the surrounding undamaged areas. Specifically, the mineral stoichiometry was altered in microdamaged bone, where the carbonate/protein ratio and carbonate/phosphate ratio were significantly lower in areas of microdamage, and the acid phosphate content was higher. No differences were observed in tissue mineralization (phosphate/protein ratio) or crystallinity between the microdamaged and undamaged bone, indicating that the microdamaged regions of bone were not over-mineralized. The collagen cross-linking structure was also significantly different in microdamaged areas of bone, consistent with ruptured cross-links and reduced fracture resistance. All differences in composition had well-defined boundaries in the microcrack region, strongly suggesting that they occurred after microcrack formation. Even so, because microdamage results in an altered bone composition, an accumulation of microdamage might result in a long term reduction in bone quality.

II.II Introduction

Microdamage occurs in bone tissue as a result of cyclic loading placed on the body during daily activities [140-143]. Normally, the bone remodeling process specifically targets these microcracks for repair [142, 151, 152]. Current anti-resorptive bisphosphonate treatments for osteoporosis allow the microdamage burden to increase [122] because these drugs reduce targeted bone remodeling that would normally repair the damage [141]. The increased accumulation of microdamage may also be the result of increased tissue mineralization [100, 121] that occurs secondary to remodeling suppression and that may make the bone more brittle. However to date, little is known about the microscopic tissue composition where microdamage occurs and whether certain areas of bone are more susceptible to microdamage than others due to compositional differences.

Bone is made up of organic and mineral components, mainly type I collagen and nanocrystalline biological apatite [4]. The exact structure of the apatite mineral is not well-defined because substitutions into the mineral apatite lattice can occur in the cationic calcium sites (e.g. Na^{+}, K^{+}, Fe^{2+}, Zn^{2+}, Sr^{2+}, Mg^{2+}, Pb^{2+}) and anionic phosphate sites (e.g. F^{-}, Cl^{-}, HPO_4^{2-}, CO_3^{2-}). These substitutions can affect bone's chemical and physical properties such as solubility, density, hardness, and growth morphology [4, 206]. Bone composition has been shown to change with age [183, 207] and is also affected by disease [62, 181, 187, 208-212] and treatment for disease [39, 100, 121, 208].

Infrared (IR) spectroscopy is a valuable technique for examining bone composition because it is sensitive to both the protein and mineral component of bone [175, 213]. By putting infrared light through a microscope, bone composition can be studied with a spatial resolution of 30-50 μm [182-184]. Spatial resolution can be improved to the diffraction limit (3-15 μm) using a synchrotron infrared source [39, 179, 185-187].

The goal of this study was to examine whether areas of microdamaged bone are chemically different than undamaged areas, and could therefore be predisposed to sustaining damage. It has been demonstrated that BPs slow

down the turnover process, and so we hypothesized that BP-treated bone would be older resulting in higher levels of mineralization and carbonate accumulation and lower acid phosphate content than untreated bone. By using infrared microspectroscopy, the mineral and protein content and stoichiometry were examined in regions of microdamage and the surrounding undamaged areas. Because the microcracks were less than 10 μm wide, a synchrotron infrared source was necessary to improve the spatial resolution of the technique.

II.III Materials and Methods

Experimental Design

A detailed description of the experimental design has been previously presented [122]. For this study, a subset of fifteen beagle dogs ranging in age from 1-2 years old was examined. The dogs were equally divided among those that received a daily saline injection, 0.5 mg/kg/day of oral risedronate, or 1.0 mg/kg/day of oral alendronate for 12 months. These doses were 5-6 times higher than those administered to osteoporosis patients. The dogs were fed normal dog chow and provided water ad libitum. They were kept separate in environmentally controlled rooms for the length of the study as well as one month prior to the start of the study. After 12 months of treatment, the dogs were sacrificed using a high dose of sodium pentobarbital (0.22 mL/kg i.v.), and the L3 vertebra were removed.

Tissue Preparation

The L3 vertebrae were bulk stained with basic fuchsin, embedded in poly-methyl methacrylate, and then cut into 5 μm sections with a sledge microtome fitted with a tungsten carbide knife. Bulk staining with basic fuchsin prior to embedding and histological sectioning enables visualization of microdamage and differentiation between microdamage and artifactual cracks induced during histological preparation [154, 214, 215].

Infrared Microspectroscopy

The process of IR microspectroscopy performed on bone has been previously described [39, 186, 187, 210]. In short, the bone sections were

supported between two aluminum disks (13 mm diameter) that each contained a narrow slit (9 mm x 3 mm). The microdamaged area of bone and the surrounding undamaged area were visible through the center of the slit. Microdamaged areas were defined as those that stained positive (i.e. purple) with basic fuchsin. Undamaged areas were defined as the surrounding unstained areas. Microcracks were approximately 3-10 μm in width and 20-100 μm in length. Regions for IR imaging were defined as a rectangular area to include the microcrack and the surrounding undamaged tissue within a radius of approximately 200 μm from the microcrack. This area of analysis is larger than the area analyzed by Verborgt et al., [216] and reflects the finding that microcracks alter fluid flow velocity around the crack for a distance of up to 180 μm [217].

IR microspectroscopy was performed using a Thermo Nicolet Continuμm infrared microscope coupled to a Nicolet Magna 860 FTIR (Thermo Nicolet Instruments, Madison, WI, USA). Infrared light from the National Synchrotron Light Source Beamline U10B, Brookhaven National Laboratory (Upton, NY) was used. An MCT-B detector, cooled to 77 K, was used for its extended infrared sensitivity from 4000 and 500 cm^{-1}, which was necessary for imaging the v_4 phosphate band from 500 – 650 cm^{-1}.

The sample was mounted on a motorized microscope stage and raster-scanned through the synchrotron IR beam (15 μm diameter), collecting a grid-like pattern of IR spectra spaced in 10 μm increments. Spectra of the bone were collected in transmission mode using confocal 32X Schwarzschild objectives. The spectral resolution was 4 cm^{-1} and 256 scans were accumulated per point using Atlμs software (Thermo Nicolet Instruments). For each IR image, 200 – 1000 spectra were collected in absorbance mode, where the background spectrum was collected from an empty sample holder. The resulting IR map included spectra from both the undamaged and microdamaged areas, which were separated after data collection based on fuchsin staining.

For each animal, IR microspectroscopic images were collected from 2-3 areas of microdamage in the L3 vertebrae, including the surrounding undamaged area.

Infrared Data Analysis

For each spectrum, a linear baseline correction was first performed to account for changes in synchrotron beam current. Protein and mineral contents were analyzed using the area under the amide II protein band (1595-1510 cm^{-1}), the v4 phosphate band (500-650 cm^{-1}), and the v_2 carbonate band (905-825 cm^{-1}). The integration results were expressed as ratios (phosphate/protein, carbonate/protein, and carbonate/phosphate) to account for any variations in sample thickness. Crystallinity was determined as a peak height ratio of 603/563 cm^{-1} [187]. Acid phosphate content was calculated as a ratio of acidic phosphate (538 cm^{-1}) over the peak area of the v_4 phosphate band [187]. Collagen cross-link structure was analyzed as a peak height ratio of 1660/1690 cm^{-1} [218].

In a small number of instances (<10%), microcrack spectra contained embedding medium, indicating a space in the tissue where the microcrack formed. These spectra were removed from the data analysis. Animals from all treatment groups were pooled for comparison of microdamaged vs. undamaged areas because previous studies showed that treatment with these agents and doses did not affect tissue composition significantly [121]. A mean ± standard deviation (SD) was determined for each bone composition parameter. Independent t-tests were performed between the microdamaged and undamaged areas for each bone parameter using Prism 3 (GraphPad). Statistical differences were considered significant for $p<0.05$.

II.IV Results

Fuchsin-stained microcracks could be easily identified from optical images (**Figure 5A**). In the IR data, the absorption intensities of both the protein and mineral peaks in the microdamaged areas were slightly decreased compared to surrounding undamaged areas. This was observed because the formation of a microcrack causes the collagenous matrix to be stretched and sometimes

broken, and mineral crystallites to be lost in the immediate area of the crack [219]. In fact, the exposed collagen fibers and charged mineral ions at the surface of the microcrack are the mechanism behind the binding of basic fuchsin [154, 215].

All data were plotted as ratios to account for loss of material in the microdamaged regions and any other thickness variations in the sample. IR imaging easily discriminated the carbonate/phosphate (**Figure 5A**), carbonate/protein (**Figure 5B**), acid phosphate content (**Figure 5C**), and collagen cross-linking (**Figure 5F**) in the area of the microcrack from regions of bone surrounding the crack. Statistical analysis of these parameters for all samples was consistent with the IR images.

The amount of carbonate in the microdamaged areas, normalized to protein or phosphate content, was consistently lower than in the undamaged areas (**Table 1; Figures 6A, 6B**). However since the data are plotted as a ratio to account for sample thickness variations, it is not certain whether the decreased ratio in the microcracks is due to higher carbonate or lower protein and/or phosphate. Conversely, the fraction of acid phosphate in the total phosphate content is increased significantly ($p < 0.03$) in the microdamaged areas of bone (**Table 1; Figure 6C**).

The level of mineralization in bone is represented by the phosphate/protein ratio. No differences were observed in the mineralization when comparing microdamaged areas to undamaged bone (**Figure 6D**). The mineral crystallinity also remained unchanged between damaged and undamaged regions of bone (**Figure 6E**).

Differences in the cross-linking of collagen can be seen from the amide I protein band. Specifically, the peak height ratio of 1660/1690 cm^{-1} represents a measure of the nonreducible/reducible collagen cross-links in bone [218, 220]. There was a significant decrease ($p < 0.02$) in the cross-linking ratio in microdamaged regions of bone (**Figure 6F**).

II.V Discussion

It has been suggested that the accumulation of microdamage in bone may be the result of increased average tissue mineralization that makes bone more brittle [100, 121]. However, less is known about the microscopic composition of bone tissue, and whether compositional differences make certain areas of bone more susceptible to microdamage than others.

Bone is composed of a cross-linked collagenous protein matrix mineralized by poorly crystalline apatite. The exact structure of bone apatite is not well-defined because both the cationic calcium sites and the anionic phosphate sites can become highly substituted. These substitutions can affect bone's chemical and physical properties such as solubility, density, hardness, and growth morphology [4, 206].

Two of the most abundant anionic substitutions in bone mineral are carbonate (CO_3^{2-}) and acid phosphate (HPO_4^{2-}) which primarily substitute into the PO_4^{3-} sites of the apatite lattice [31-34]. Carbonate incorporation has been reported to increase [34, 221], decrease [183, 222], and remain constant [61] during aging. Its content is also altered in disease states such as osteoporosis [62, 71], osteogenesis imperfecta [211], and osteoarthritis [210].

While many changes in bone's carbonate content have been observed, the role of carbonate substitution on the physiological or mechanical properties of bone is still poorly understood. It has been shown that carbonate substitution tends to reduce the stability of the hydroxyapatite lattice, rendering the bone mineral more soluble [35, 36]. The replacement of PO_4^{3-} by CO_3^{2-} also causes a charge imbalance, which can be compensated by a loss of Ca^{2+} ions from the crystal lattice. These defects created in the crystal lattice lead to crystallographic microstrain and altered crystal morphology [35, 223]. These factors could strongly influence how microcracks are initiated or grow in bone.

In this work, we find that the carbonate content is significantly decreased in microdamaged regions of bone (**Figures 6A and 6B**). These results are consistent with Raman microscopy studies of mature bovine bone by Morris and coworkers, in which a different spectral component in the v_1 phosphate band was

observed in areas of microdamage [224, 225]. In the Raman work, this new phosphate band was attributed to a more stoichiometric and less carbonated apatite species.

Whereas we attributed the loss of carbonate to the deposition of more stoichiometric mineral crystallites, the loss of carbonate in the damaged regions could possibly mean that recently deposited mineral crystallites are preferentially lost. During the process of microcrack formation, mineral crystallites are displaced from the collagen fibrils. In this environment, the free mineral crystals likely dissolve and reform. Since carbonated apatite is more soluble than non-carbonated (stoichiometric) apatite, highly carbonated crystallites would preferentially dissolve and the carbonate content in the mineral would decrease.

Acid phosphate (HPO_4^{2-}) is another ion that substitutes into the apatite mineral lattice of bone. It is usually present at high concentrations in young, immature bone, and decreases with bone age [38-40]. **Figure 6C** shows that microdamaged bone has a higher acid phosphate content than undamaged bone. Again, these results are consistent with the Raman work by Timlin et al. [224]. Although the Raman study did not describe the nature of the stoichiometric apatite phase, the spectrum of the microdamaged area also contained a feature around 1003 cm^{-1}, attributed to acid phosphate. Thus, the mineral in the microdamaged areas of bone can be described as an immature, acid phosphate-containing, more stoichiometric, and less carbonated apatite.

Tissue mineralization may make bone more brittle [61] and increase the occurrence of microcracks [121]. Although the stoichiometry of the mineral in the microdamaged areas differed from undamaged bone, as evidenced by the altered carbonate and acid phosphate content, no differences were observed in the level of mineralization, i.e. the phosphate/protein ratio (**Figure 6D**). However, the FTIR absorption intensities of both the protein and mineral peaks in the microdamaged areas were slightly decreased compared to surrounding undamaged areas. We attribute these decreases to (1) stretching and some breakage of the collagen matrix, and (2) displacement and dissolution of bone mineral in the area of the crack. Thus, the quantities of bone protein and mineral

in the microdamaged areas decreased, but the ratio of phosphate mineral to protein was not affected.

We also did not observe any changes in mineral crystallinity (**Figure 6E**), which can affect the bone's mechanical properties [226]. These findings indicate that the microdamaged areas of bone were not over-mineralized, suggesting that these local regions of tissue were not more brittle.

The collagen matrix provides the nucleation site for the deposition of mineral [21]. Collagen quality and cross-link maturity play a role in the biomechanics of bone, specifically contributing to its plastic, ductile properties [5, 6]. Increased non-enzymatic cross-linking of collagen makes the bone tissue more brittle and reduces the resistance of the bone tissue to crack growth [227]. This may be one reason for the observation that the energy required both to initiate and to propagate cracks in bone is significantly reduced as one ages [228].

Here, we examined the 1660/1690 cm^{-1} ratio of the amide I band, which can be related to the amount of nonreducible/reducible collagen cross-links in bone tissue [218]. This ratio has been shown to increase with collagen maturity [218], with fracture healing [222], and in osteoporosis [220], but remains unchanged in osteomalacia [229]. In microdamaged bone, we find that the collagen cross-linking ratio was lower than undamaged bone (**Figure 6F**), indicating an altered collagen cross-linking chemistry in the microdamaged areas. A lower ratio is consistent with studies on collagen where cross-links have been reduced or broken [218], or when collagen has been denatured [230]. It has also been suggested that the rupture of collagen cross-links is the last step prior to fracture formation [231]. Thus, our results suggest that cross-links have been ruptured in the microdamaged regions of bone, which can compromise its mechanical properties such as decreasing fracture resistance.

It should be noted that the collagen cross-link ratio is not a direct measure of the cross-link content in bone, but rather a measure of the effect that cross-links have on collagen's structure. Specifically, the amide I band (1600 – 1700 cm^{-1}) represents the total amount of protein in the bone. The intensity of this

peak (as represented by the integrated area) is directly proportional to the concentration of protein in the sample. The shape of this peak is determined by the structure of collagen in the sample. Thus, changes in this ratio reflect how collagen's structure is changed by cross-link differences. Thus, it is possible that changes in this ratio arise from other factors that affect collagen's structure, unrelated to collagen cross-linking.

One limitation of this study is that it cannot assess whether altered bone composition caused the microdamage to occur, or whether it was an effect of the fracture formation. However in the former case, we would expect a spatially heterogeneous composition in the undamaged bone, where certain regions had chemical and mechanical properties that were more susceptible to microdamage. Instead, we found the undamaged bone composition to be quite homogeneous, as evidenced by small standard deviations for all chemical composition parameters (**Table 1**), and consistent with our earlier findings [121]. In addition, the IR images showed discrete, but significant chemical differences between the undamaged and microdamaged bone. Thus, the uniformity of the undamaged bone and the discrete differences between microdamaged and undamaged regions strongly suggests that the compositional differences we observed are an effect of the microdamage and not a cause of it.

Another limitation is the possibility that the bisphosphonates altered the physical properties of the bone matrix. Our earlier work demonstrated no compositional differences at the microscopic level between drug-treated and control groups, except for an increase in the mineral content itself [121]. None of our previous work has shown differences between alendronate and risedronate either [122, 123]. Moreover, in the current work, we compared damaged and non-damaged regions of bone within each individual sample – a paired design – so the effect of the damage itself can still be evaluated and compared to the non-damaged state. This is relevant from a clinical standpoint, given that people being treated with bisphosphonates also accumulate microdamage [232].

Changes in mineral composition under pressure or stress are commonly seen in geological minerals and synthetic apatites [224, 233] and have also been

observed in bone with mechanical loading/deformation [225]. During the process of microcrack formation, collagen cross-links are broken and mineral crystallites are displaced from the collagen fibrils. In this environment, the free mineral crystals likely dissolve and reform [206]. Since carbonated apatite is more soluble than non-carbonated (stoichiometric) apatite [35, 36], highly carbonated crystallites would preferentially dissolve and the carbonate content in the mineral would decrease. Thus, the resulting chemical environment in the microdamaged region would consist of ruptured collagen cross-links (decreased cross-link ratio), decreased carbonate content (carbonate/phosphate), and an unchanged overall mineral content (phosphate/protein), which is consistent with the results presented here.

Even though the observed chemical changes likely occur as a result of microcrack formation, and may not be a causative factor in the process, the accumulation of microdamage leads to altered bone composition nonetheless. We previously demonstrated that microdamage accumulation in both cortical and cancellous bone following one year treatment with alendronate or risedronate in intact dogs is associated with compromised material properties [122, 123]. We have more recently demonstrated that this occurs even at clinical treatment doses of these bisphosphonates [136]. However, our most recent data suggest that the accumulation of microdamage by itself does not explain the reduced toughness of bone [136]. Changes in the composition of the bone matrix as an effect of microcracking, however, could be related to the reduced material properties. The observations described in the current paper provide the mechanistic explanation for the compromised material properties, i.e. reduced toughness does not occur as a direct result of the damage itself, but as an indirect result of physical changes in the matrix caused by the microcrack. The changes in material properties that we have observed in our previous work are largely the result of reduced post-yield properties of bone. Post-yield properties are influenced primarily by the collagen moiety in bone and by cross-linking of collagen [234, 235]. By showing disruption of collagen cross-linking as an effect of microcracking, the current work provides an explanation for the previous

observation that post-yield properties are compromised. This is relevant from a clinical standpoint, given that people being treated with bisphosphonates also accumulate microdamage [232]. With long term treatment the accumulation of microdamage and the accompanying changes in bone composition could eventually increase bone fragility that occurs in postmenopausal women.

II.VI Acknowledgements

We would like to thank Randy Smith of the NSLS for assistance at NSLS Beamline U10B. M.R. was supported by the U.S. Department of Energy's Student Undergraduate Laboratory Internship (SULI) Program. The NSLS is supported by the United States Department of Energy under contract DE-AC02-98CH10886. Parts of this study were supported by NIH grants P01 AG05793 and R01 AR047838. Merck and Co., Inc. and Procter and Gamble Pharmaceuticals, Inc. kindly provided the bisphosphonates.

II.VII Tables

Table 1. Bone composition for undamaged versus microdamaged bone

Parameter	Undamaged	Microdamaged	p-value
Carbonate/Phosphate	0.0681 ± 0.0016	0.0570 ± 0.0020	0.0002
Carbonate/Protein	0.0489 ± 0.0017	0.0413 ± 0.0016	0.003
Acid Phosphate	0.0039 ± 0.0001	0.0043 ± 0.0001	0.027
Phosphate/Protein	0.735 ± 0.026	0.727 ± 0.022	0.815
Crystallinity	1.00 ± 0.012	0.974 ± 0.0222	0.395
Collagen Structure	2.59 ± 0.057	2.38 ± 0.054	0.0145

II.VIII Figures

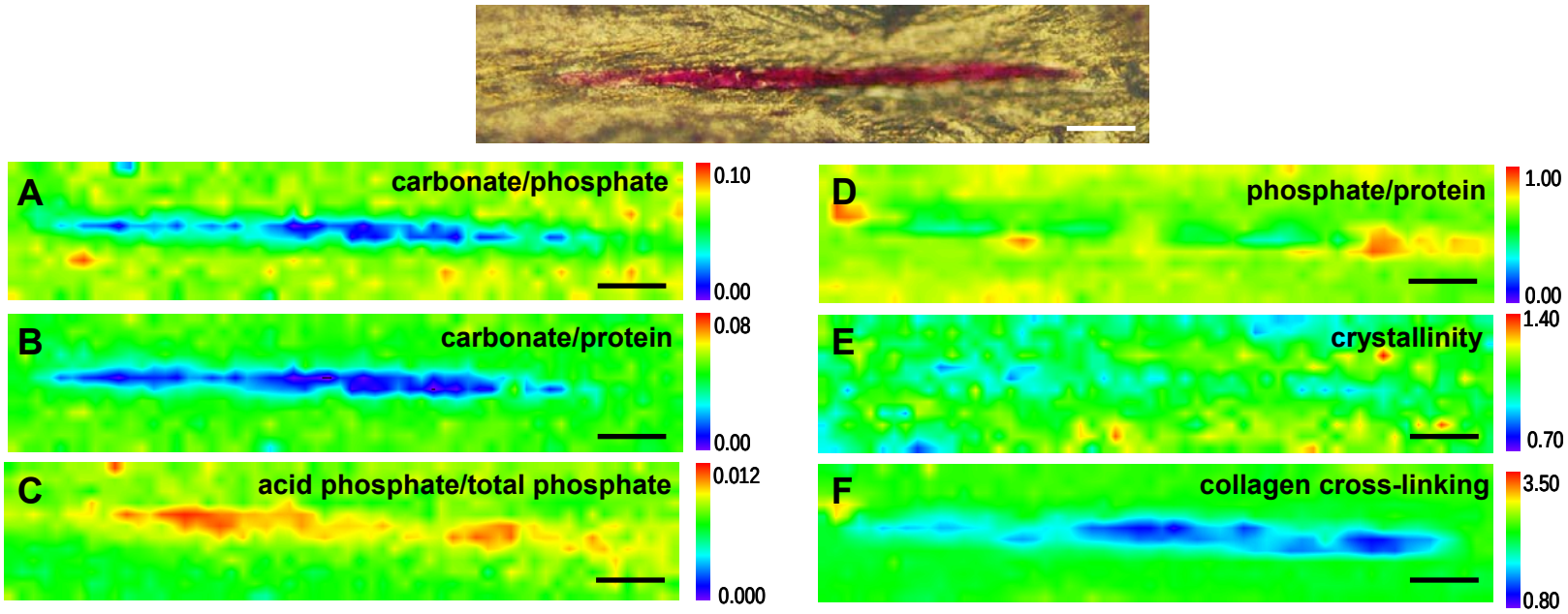

Figure 5: (Top) Visible image of a microcrack indicating the area imaged with the IR microscope. The fuchsin stain (magenta) highlights the microcrack. Data were collected within the crack and from the surrounding area. (A) – (F) represent the corresponding IR images of the same area. The individual images illustrate the (A) carbonate/phosphate ratio, (B) carbonate/protein ratio, (C) acid phosphate/total phosphate ratio, (D) phosphate/protein ratio, (E) crystallinity, and (F) collagen cross-linking. Scale bar is 25 microns.

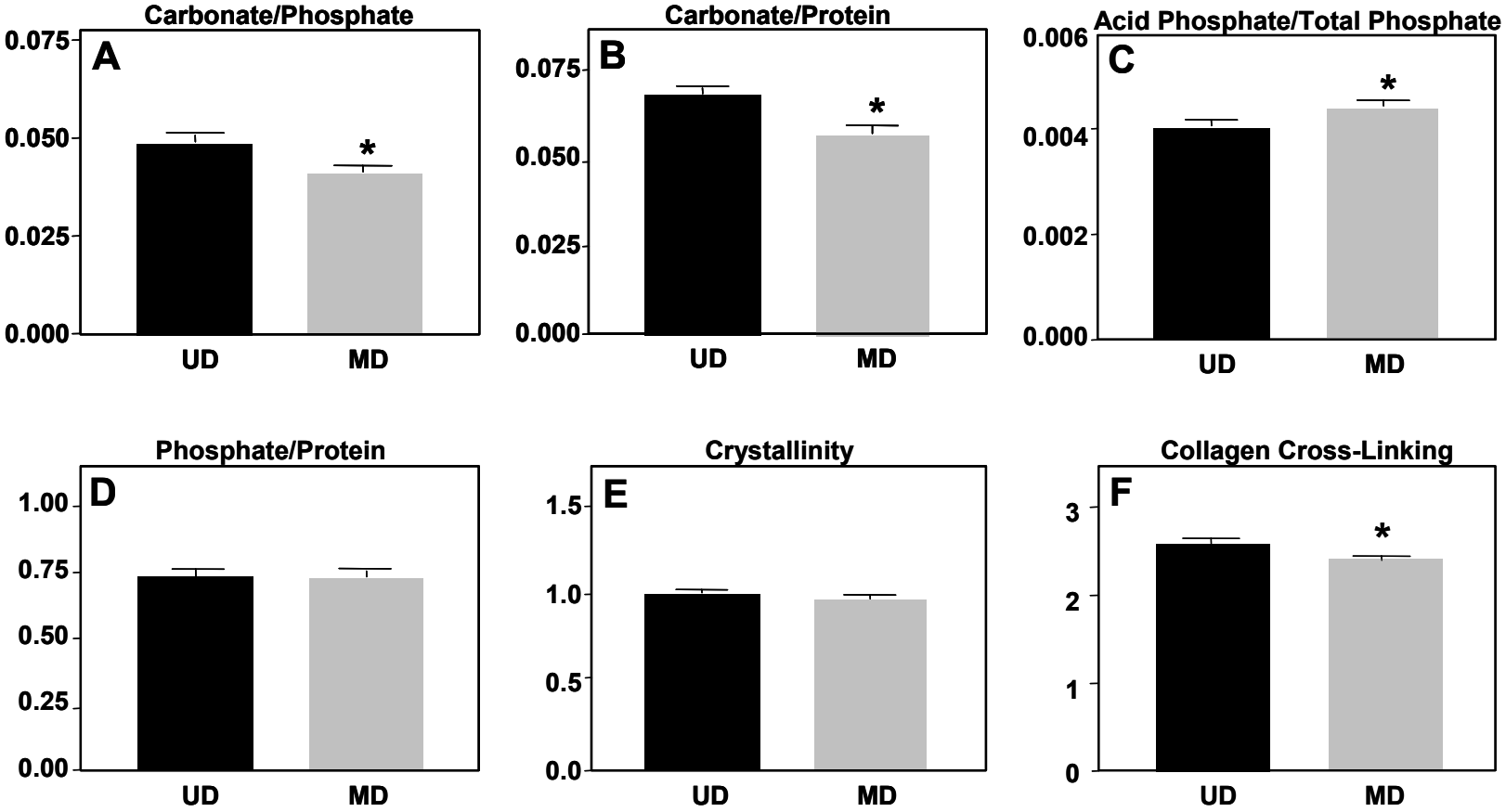

Figure 6: Comparison of bone composition in microdamage (MD) versus undamaged (UD) bone for (A) carbonate/phosphate, (B) carbonate/protein, (C) acid phosphate/total phosphate, (D) phosphate/protein, (E) crystallinity, and (F) collagen cross-linking. Error bars represent the standard deviation from the mean. (*) indicates a significant difference ($p<0.05$) between undamaged and microdamaged bone.

Chapter III: Risedronate-treatment temporarily delays collagen deposition and matrix mineralization of MC3T3-E1 osteoblasts [236]

III.I Abstract

Prevention of bone loss by inhibition of osteoclast-mediated bone resorption is the major mechanism for fracture risk reduction seen with BPs in osteoporosis. Some recent studies have shown that under certain conditions BPs may stimulate osteoblast formation or prevent osteoblast and osteocyte apoptosis, but whether they have direct effects on the quality of newly forming bone matrix is unknown. The goal of the present study was to determine if risedronate (RIS) treatment alters the quality of newly formed tissue. RIS-treated and untreated MC3T3-E1 mouse osteoblasts were mineralized in culture for 0, 4, 11, 14, 21, and 28 days. Fourier transform infrared imaging (FTIRI) was used to study the chemical composition of the matrix produced, including level of mineralization and collagen content as a function of time and drug treatment. Mineral formation was quantified via osteocalcin (OCN) production. Our results showed that mineralization and collagen content increased over time in control and RIS-treated cells; however both were significantly lower at day 14 and day 21 in RIS-treated cultures. OCN increased significantly between day 4 and 28 for control and RIS-treated cells, and there was no significant difference between the two groups at any time point. Thus, these studies showed that matrix synthesis and mineral deposition are temporarily slowed by RIS-treatment. We hypothesize that this delay resulted from RIS inhibition of protein prenylation within the osteoblasts. This could have caused disrupted collagen production and cross-linking, leading to decreased mineralization. Understanding how RIS directly affects the mineralization and matrix production of osteoblasts is important to determine long term effects of the drug.

III.II Introduction

Osteoporosis is a wide spread disease that affects nearly 75 million people in the USA, Japan, and Europe combined [74]. Osteoporosis is characterized by loss of bone mass and microarchitecture, resulting from an imbalance of osteoclast-mediated bone resorption and osteoblast-mediated bone formation.

BPs are a current class of drugs that are used to treat osteoporosis. BPs inhibit osteoclasts, thereby slowing bone remodeling and reducing osteoclast-mediated bone loss. Since BPs reduce remodeling they increase bone mineral density by extending the mineralization times for the BMU. BPs act on osteoclasts in one of two ways; non-nitrogen containing BPs are metabolized by the cell and form toxic analogs of ATP, while nitrogen containing BPs, like RIS, inhibit enzymes in the mevalonate pathway [105, 106, 108] leading to decreased osteoclastogenesis [124], decreased cell function, and increased apoptosis. Reduced osteoclast activity leads to decreased bone resorption and bone loss [124, 125, 197].

In normal bone remodeling, the actions of osteoclasts and osteoblasts are linked. BPs therefore reduce bone formation indirectly through their inhibition of bone resorption. It has recently been suggested that BPs may also have a direct affect on osteoblasts, but results have been conflicting. In some studies BPs inhibited the formation and dissolution of mineral formed by osteoblasts [116, 128-132, 202]. In other studies BPs have increased osteoblast differentiation and mineralization [133-135, 229, 237]. Differences in the affect of BPs on mineralization could be due to differences in their antiresorptive potency and their binding affinity for hydroxyapatite (HAP) [113]. In light of previous research, it is important to understand what role BPs might play in altering osteoblast function during treatment. Furthermore, understanding the affects specific BPs have on new bone formation is necessary to determine long term consequences they could have on bone chemistry, quality and strength.

The differentiation, proliferation, collagen deposition, and mineralization of MC3T3-E1 osteoblasts has been very well classified [51, 53, 63], and they have

been shown to be a suitable model of bone mineralization and collagenous matrix formation. After the synthesis of the collagen matrix has begun, the cells initiate activation of osteoblast marker genes [65] including alkaline phosphatase (ALP), which helps process phosphate, that is expressed starting around 2-3 days [51] and osteocalcin (OCN), which is expressed between days 4-6 [51, 238, 239] and peaks at day 14 [240]. Deposition of HAP within the extracellular matrix and the formation of nodules is initiated by matrix vesicles. These vesicles, with diameters of 60-400 nm, are filled with needle-like crystals of mineral, and act as nucleation sites for nodule formation [53, 66-68]. Matrix vesicles and mineral nodules are typically associated with the fibrous network of collagen however they can also be ectopic and not associated with the collagen network [63].

FTIRI is an important technique that has been extensively used to study the chemical composition of bone tissue in osteoporosis [71, 178, 181, 186, 209], osteoarthritis [210, 241] and osteomalacia [229]. Additionally, FTIR has been used to study the mineral and collagen content of the mineralized matrix formed by osteoblasts in culture [242-246] and has been shown to be more sensitive than von Kossa staining alone [247]. To date, most studies using FTIR have examined the cells and matrix in bulk, after it has been processed into a KBr pellet. While the information from these studies is useful, all spatial information is lost. In this study we have grown the MC3T3-E1 cells directly on an infrared reflective slide in order to study and spatially correlate mineralization and collagen deposition over time.

The goal of this study was to understand the effects of RIS on mineralizing osteoblasts, specifically the mineral and collagen production, distribution and interaction. Previous studies have shown that collagen deposition [135, 203, 204] and mineralization [134, 201-203] can be delayed due to BP-treatment, we hypothesize that a similar affect will be observed here. Understanding this relationship is important for identifying the affects long term osteoporosis treatment might have on bone quality.

III.III Materials and Methods

Cell Culture

A mineralizing sub-clone (sub-clone 4) of MC3T3-E1 mouse osteoblasts (ATCC, Manassas, VA) was grown in α-MEM with 10% fetal bovine serum (Sigma-Aldrich, Missouri), 1% sodium pyruvate (Sigma-Aldrich, Missouri), 1% Penicillin-streptomycin (Sigma-Aldrich, Missouri) and 1% Amphotericin β (Sigma-Aldrich, Missouri) at 37^{o}C in a fully humidified atmosphere of 5% CO_2 in 35 mm diameter (9.5 cm^2 growth area) 6-well plates (Corning Inc., New York) Approximately 1 week after plating the cells were confluent (day 0) and the medium was supplemented with 5 μg/mL ascorbic acid (Sigma-Aldrich, Missouri) and 4 mM sodium phosphate monobasic (Sigma-Aldrich, Missouri) to initiate mineralization. RIS-treated cells were also supplemented with 10 μM RIS. Medium, supplements and RIS were changed every 2-3 days and samples were removed after 0, 4, 11, 14, 21, and 28 days in mineralizing media.

The sub-clone of MC3T3-E1 cells used in this study (sub-clone 4) has been shown to form a mineralized matrix that stains positive with von Kossa staining [63]. This sub-clone also expresses high levels of mRNA's for OCN, parathyroid hormone/parathyroid hormone-related protein and bone sialoprotein. However, it does not produce significant amounts of ALP and so it cannot hydrolyze β-glycerol phosphate for use during mineralization. Therefore sodium phosphate was used.

For infrared data collection the cells were grown on a 1.0 x 0.5 inch piece of infrared reflective slide (Kevley Technologies, Ohio). The slides were sterilized in 95% ethyl alcohol for 24 hours, dried, and spin-coated with 8 mg/ml sulfonated polystyrene (SPS) (Polymer Source, Inc., Montreal Canada) dissolved in dimethylformamide for 30 seconds at 2500 rpm [248]. After SPS deposition, the slides were placed in a vacuum oven at 150^{o}C for 24 hours to remove the solvent and attach the polymer to the slide. The resulting SPS coating was ~20 nm. SPS has been shown to provide a suitable substrate for osteoblast mineralization to occur because the charged surface of the SPS causes proteins to self assemble into fibrillar networks [55, 248, 249].

The coated slides were used within 24 hours of SPS deposition and were added to the culture dishes when the cells were first plated. At the end of each time point, the slides were removed from the medium and washed twice in distilled water, once in 75% ethyl alcohol, and dried. A total of 44 samples (control: day 0, 4, 11, 14, 21, 28; RIS: day 4, 11, 14, 21, 28, n=4 for each time point) were grown.

Risedronate

RIS monosodium hemipentahydrate powder was obtained from Procter & Gamble Pharmaceuticals (Cincinnati, OH). The drug was dissolved in sterile water, the pH adjusted to 7.4 with 1 M NaOH, then filter-sterilized through a 0.22 μm filter before use.

FTIRI

Infrared data were collected using a Spectrum Spotlight 300 FT-IR imaging system (PerkinElmer, Waltham, Massachusetts). Low resolution IR images were collected on a ~50 mm^2 area in reflection mode on each sample, in imaging mode using a 25 μm pixel size, 2 scans per point at 8 cm^{-1} resolution where the background was an empty IR reflective slide. Based on the results of the low resolution images, one high resolution map per sample was then collected on a ~7 mm^2 area in image mode, using a 6.25 μm pixel size, 4 scans per point, at 8 cm^{-1} resolution. The high resolution maps at later time points were collected in an area that contained both mineralized and non-mineralized regions. Areas where more than 5% of the pixels had an amide II absorbance greater than 1.0 were also avoided.

To ensure that the choice of high resolution maps was not biased to areas of high mineralization in later timepoints, intra-sample variance and inter-sample variance were determined. Three high resolution maps were collected within day 11 and day 28 control and RIS-treated cells. The intra-sample median variance was ~10^{-5} for each sample. The inter-sample median variance between control and RIS-treated samples was ~10^{-3} for samples that had significance differences. Therefore, because the intra-sample variance was 2 orders of magnitude smaller

than the inter-sample variance, the differences we saw across time points were in fact significant.

FTIRI Data Analysis

Protein was analyzed using the area under the amide II protein band (1595-1510 cm^{-1}; baseline 1800 cm^{-1}). Mineral phosphate was analyzed using a region of the v_1, v_3 phosphate peak (1060-990 cm^{-1}; baseline 1180-980 cm^{-1}). The phosphate peak contains contributions from both cellular and mineral phosphate. If just a cell layer was present, the cellular phosphate peak (1250-1220 cm^{-1}) and the total phosphate peak (1150-990 cm^{-1}) would be approximately the same size. However, when mineralization occurs the region of the between 1060-980 cm^{-1} gets larger as seen in the spectrum of bone (**Figure 7A**) and mineralizing osteoblasts (**Figure 7B**), and the total phosphate peak gets larger than the cellular phosphate peak. The C-H wagging/deformation peak (1350-1325 cm^{-1}; baseline 1360-1325 cm^{-1}) was also analyzed to determine the collagen content [250-253]. This region was chosen based on the IR spectrum of rat tail collagen (**Figure 7A**), which is known to contain only type I collagen. Also, this region was chosen, because this area of the IR spectrum of mineralizing osteoblasts does not contain any absorption bands attributed to other constituents.

The integration results were expressed as ratios (mineralization: mineral phosphate/protein and collagen content:collagen/protein) to account for any variations in sample thickness. At the later time points (day 21 and 28), the absorbance of the amide II peak was greater than 1.0 due to the increasing thickness of the cell layer over time. Spectra whose amide II absorbance was greater than 1.2 were removed from the analysis (~3% of the total spectra).

Measurement of Osteocalcin

OCN has been shown to be a biomarker for bone formation. At each time point medium from the cells was removed when the IR substrates were harvested. OCN content within the medium was measured for each sample using the colorimetric mouse osteocalcin EIA kit (Biomedical Technologies Inc.,

Massachusetts). The absorbance of the samples was measured at 450 nm using a SpectraMax Plus (Molecular Devices, Sunnyvale, California).

Statistical Analysis

For FTIR spectra, the median, 25th, and 75th percentile, values for each map were determined using SPSS version 14.0 statistical software (SPSS, Inc., Chicago, Illinois). A Kruskal-Wallis test was performed to test for differences in the mineralization, collagen content and OCN between all of the time points. A Mann-Whitney U-test was performed to determine statistically significant differences between control and RIS-treated cells at each time point and to further determine where differences across time points occurred. Differences were considered significant if $p<0.05$ on a two-tailed test.

III.IV Results

FTIRI

The IR spectra of fully mineralized bone and rat tail collagen (**Figure 7A**) were used to determine regions used for the IR analysis and for comparison to the mineralizing osteoblasts. The IR spectra of the mineralizing osteoblasts changed over time from day 0 to day 11, and day 0 and day 28 in control and RIS-treated osteoblasts (**Figure 7B**). The absorption intensities and area under the phosphate region (1060-990 cm^{-1}) of the infrared spectra grew from day 0 to day 11 where mineralization began, and increased in intensity and area again from day 11 to day 28 (**Figure 7**).

IR images of mineralization at each time point for control and RIS-treated cells are shown in **Figure 8**. Day 0 and day 4 images show “background phosphate” due to the contribution of the cellular phosphate of the MC3T3-E1 cells, as mineralization did not start until ~day 11. Mineralization of the MC3T3-E1 cells was first seen at day 11, with more mineralized area in the control cells. The amount of mineralization increased through day 28, however at day 14 and 21 the control samples appeared to be more mineralized than the RIS-treated samples. By day 28 the mineralization of the control and RIS-treated cells was similar.

IR images of collagen content at each time point for control and RIS-treated samples are shown in **Figure 9**. Little or no collagen matrix deposition can be seen before day 11; the collagen content increased significantly between day 11 and 28 in control and RIS-treated cells (CNTL p=0.014; RIS p=0.014). At days 14 and 21 however there appeared to be more collagen matrix in the control cells compared to the RIS-treated cells. By day 28 the control and RIS-treated cells showed similar amounts of collagen.

Composite red-green images of the collagen and mineral at day 11 and day 21 for control and RIS-treated cells are presented in **Figure 10**. The green channel represents the mineralization and the red channel represents the collagen content. When the images are overlaid correlation between the collagen matrix and mineral can be seen as yellow, starting around day 11 and progressing through day 21. At both time points the mineral was correlated with the collagen matrix for both control and RIS-treated cells.

The distribution of the level of mineralization changed over time (**Figure 11**, n=4, bin size of 0.0005). Starting at day 0, there was a single peak in the mineralization distribution. This peak can be attributed to the contribution of the cellular phosphate within the phosphate peak. For day 11 control cells, the distribution began to develop a second maximum, indicating that mineralization had started. This maximum increased in frequency and value for control cells at day 14, 21, and day 28. The second maximum did not appear until day 14 for the RIS-treated cells, and did not occur as frequently in the day 21 treated cells as in the control cells. The level of mineralization between control and RIS-treated cells was significantly different at day 14 (p=0.021) and day 21 (p=0.021) (**Table 2**). However, by day 28, the level of mineralization of the RIS-treated cells was indistinguishable from the control cells.

The distribution of the collagen content also changed over time (**Figure 12**, n=4, bin size of 0.0002). Very little collagen was present at early time points. In control cells, the deposition of a collagen matrix was seen by day 11 and collagen content increased from day 11 through day 28. The distribution for RIS-treated cells lagged and was significantly different from the collagen content of

control cells at day 14 (p=0.010) and 21 (p=0.021) (**Table 3**). However, by day 28 the collagen content of the control and RIS-treated cells was not different.

The median of the mineralization distribution over time for control and RIS-treated cells are shown in **Figure 13A**. For the control cells, there was a significant increase in mineralization between day 0 and day 11 (p=0.021) and day 0 and day 14 (p=0.021), showing the start of mineralization. This significant difference carried through day 21 (p=0.021) and 28 (p=0.021). Additionally, significant increase in the amount of mineral in the control cells occurred between day 11 and 21 (p=0.021), and day 11 and day 28 (p=0.021).

Further examination of the differences showed that there was a significant increase in mineralization of the RIS-treated cells between day 14 and 21 (p=0.021) and day 14 and 28 (p=0.021) that was not present in the control cells.

Medians of the collagen content distributions over time for both control and RIS-treated cells are shown in **Figure 13B**. In control cells there was a significant increase in collagen deposition between day 0 and 14 (p=0.014), day 0 and 21 (p=0.014), and day 0 and day 28 (p=0.014).

For the RIS-treated cells there were significant differences in collagen content between day 4 (p=0.014), 11 (p=0.014), 14 (p=0.018), 21 (p=0.0291) and day 28.

Osteocalcin

There were no significant differences in the amount of OCN produced by the control versus the RIS-treated cells at any time point (**Figure 14**; n=6). There was a significant difference in OCN between day 4 and day 11 for both control (p=0.037) and RIS-treated (p=0.037) cells. There was also a significant increase in OCN over the period from day 4 to day 28 for control (p=0.004) and RIS-treated (p=0.004) cells.

III.V Discussion

While the effects of BPs on osteoclasts have been well characterized, reports on direct effects on osteoblasts and bone formation are conflicting. Specifically, it is not known how BPs affect the timing of osteoblast-induced

collagen deposition and mineralization. In this study, we have used MC3T3-E1 osteoblast cells, which mineralize in culture and so provide an appropriate model of bone matrix production, to study the effects of RIS on newly formed bone tissue.

We found that at the onset of mineralization and collagen production (~day 14), treatment of osteoblasts with RIS caused a significant lag in mineral deposition and collagen production. This lag in mineralization was also present at day 21, but was recovered by day 28.

Many studies have shown that various BPs decrease mineralization of osteoblasts *in vitro* [134, 201-203] and *in vivo* [131, 136, 137, 139, 193-200].

Several mechanisms by which BPs decrease osteoblast mineralization *in vitro* have been proposed. Some attribute the decreased mineralization to altered osteoblast activity and function [204, 237, 254]. It has been shown that osteoblasts can internalize small amounts of RIS [126, 255], but they cannot metabolize it. Excess levels of internalized BPs leads to inhibition of protein prenylation [136, 256] that compromises the function of the osteoblasts and could cause a decrease in osteoblast mineralization activity. On the other hand, decreased mineralization has also been attributed to a decrease in the number of viable osteoblasts [201]. If there were fewer cells producing mineral, total mineralization would go down. However some studies show that decreases in mineralization are not due to cytotoxicity, but rather to a combination of inhibition of crystal growth and osteoblast function [203]. Lastly it has been proposed that inhibition of mineralization might be caused by the BPs interacting directly with the HA crystals [113, 202]. Idris and co-workers proposed that the mineralization effects were unrelated to cell growth, ALP activity, or inhibition of protein prenylation, because addition of farnesyltransferase inhibitor did not counteract the inhibitory affects of the BPs.

Three mechanisms for decreased mineralization that have been proposed to explain *in vivo* observations: 1) A direct effect on osteoblasts inhibits their ability to form mineral [131, 136, 139, 193, 203]; 2) inhibition of the remodeling process, where by bone formation is slowed because bone resorption has been

disrupted [119, 136, 195, 203]; 3) physiochemical interactions of the BPs which inhibits crystal growth [113, 203]. The second mechanism does not occur in most *in vitro* models because the cells studied are limited to osteoblasts only and there are no remodeling surfaces present, although it has been suggested that it is only osteoblast activity that is affected in areas of bone where only formation is occurring [131].

Consistent with our findings, other groups have seen temporary decreases in collagen production when osteoblasts were treated with various BPs. [135, 203, 204]. Garcia-Moreno and co-workers attributed the decrease in collagen production to a decrease in cell viability.

While collagen deposition is not altered when the collagen molecules are disrupted [257], mutated collagen fibrils and damaged collagen cross-links have been shown to cause alterations to the osteoblastic genes necessary for mineralization [243]. It has been suggested that the deposition of a normal collagen matrix is needed for OCN production [258] and mineralization to begin [259-263]. OCN levels in this study were not significantly different between control and RIS-treated cells, suggesting that the collagen matrix was normal; it was just being laid down at a slower rate in the RIS-treated cells.

Additionally, it has been shown that type I collagen promotes proliferation of mineral from matrix vesicles and that collagen fibrils work together with matrix vesicles to achieve mineralization [264-267]. So a lag in collagen deposition, as seen in the RIS-treated cells at day 14 and 21, could directly cause a delay in the mineralization of the matrix, which was also observed.

Collagen deposition has been shown to be necessary and directly related to the production of osteoblasts marker genes and mineral [50-55, 243]. Collagen and mineral are also known to be associated in bone, whereby mineral is deposited within hole-zones in the collagen matrix [19-21, 268]. As tissue ages the mineral crystals grow and begin to overlap with the collagen fibers within the matrix [9].

In this study we saw that as early as day 11 (**Figure 4**), when mineralization has just started, the localization of mineral was correlated with

collagen content. This co-localization of the collagen and mineral progressed through day 21 (**Figure 4**). Collagen and mineral are oriented parallel in bone [11, 12, 22, 24, 26, 27] for optimal strength. While we were unable to determine the orientation of the collagen and mineral, the co-localization of the collagen and mineral within the cultures suggests that the interaction between collagen and mineral is similar for mineral formed by MC3T3-E1 cells. Further, this interaction was not altered by RIS-treatment.

While it has been shown that RIS can inhibit HAP crystal growth in solution [113], *in vivo* [269, 270] and *in vitro* [202, 270], this mechanism alone cannot explain the results seen here. If there was a physiochemical interaction between the RIS and HA (i.e. the RIS was binding to newly formed nodules, blocking further mineralization) we would not have seen a lag in the collagen deposition at the same time points. This could however be part of the reason for the decrease in the rate of mineralization at day 14 and 21 that is recovered at day 28.

It also did not appear that at these concentrations the RIS was cytotoxic to the osteoblasts, because as time progressed, the cell layer appeared to get thicker (as evidenced by an increase in the amide II absorbance over time). So it seems unlikely that RIS slowed collagen production and mineralization through necrosis or apoptosis of the osteoblasts. Therefore, we hypothesize that RIS altered the function and activity of the osteoblasts, possibly through decreased protein prenylation, delaying the production of a collagenous extracellular matrix, which is needed for mineralization to occur. In addition, RIS-induced inhibition of crystal growth could have also contributed to the delayed differentiation timeline [203].

RIS causes accumulation of unprenylated proteins within osteoclasts [271-274] as well as in other cell types [105, 126, 255, 272, 275]. It is possible that there was an initial build up of RIS within the treated osteoblasts that caused an increase in unprenylated proteins. This protein build-up could have ultimately caused a decrease in the production and release of collagen and matrix vesicles needed for mineralization.

The current study does have limitations. This study was performed in a cell line derived from mouse osteoblasts not human osteoblast. Additionally the system examined the direct effect of RIS on osteoblasts only. *In vivo* the remodeling interaction of the osteoclasts and osteoblasts is important. *In vivo* it's likely that osteoclasts are exposed to high levels of BPs [276] when the BP is released from resorbed bone, but it's unclear whether bone associated osteoblasts are exposed to high drug levels. Despite this, our studies do show that RIS directly affected osteoblast collagen production and matrix mineralization. Additional studies, using co-cultures of osteoclast and osteoblast cells, as well as the use of human cell lines, are needed.

In summary, we have shown that treatment of MC3T3-E1 cells with 10 μM RIS temporarily delayed the production of bone matrix. Because the delays were seen in both the collagen deposition and mineralization, it appears that the RIS altered the activity and function of the osteoblasts. Collagen deposition, which is needed for mineralization to occur, could have been slowed by a build up of unprenylated proteins within the osteoblast. .Further a lack of a collagenous-matrix would delay the release of osteoblast marker genes and slow mineralization. However, the differences between control and RIS-treated cells were transient, as seen by similar levels of collagen and mineralization by day 28. This is important clinically. While BPs might delay initial collagen deposition and matrix mineralization, the effect is temporary and matrix production and mineralization seems unaffected in the long term.

III.VI Acknowledgements

M.R. was supported by the Alliance for Better Bone Health and a BNL Laboratory-Directed Research and Development (LDRD) grant (05-048). The NSLS is supported by the United States Department of Energy under contract DE-AC02-98CH10886. Procter and Gamble Pharmaceuticals, Inc. kindly provided the risedronate.

III.VII Tables

Day	p-value median	p-value 25%	p-value 75%
4	1.0	0.773	0.248
11	0.773	0.773	1.0
14	0.021	0.021	0.021
21	0.021	0.021	0.021
28	1.0	1.0	0.773

Table 2: Shows the U-values for mineralization of the control and RIS-treated samples compared using the Mann-Whitney U-test at each time point.

Day	p-value median	p-value 25%	p-value 75%
4	1.0	1.0	1.0
11	0.317	0.317	0.282
14	0.010	0.047	0.020
21	0.021	0.020	0.021
28	1.0	1.0	0.773

Table 3: Shows the U-values for collagen content of the control and RIS-treated samples compared using the Mann-Whitney U-test at each time point.

III.VIII Figures

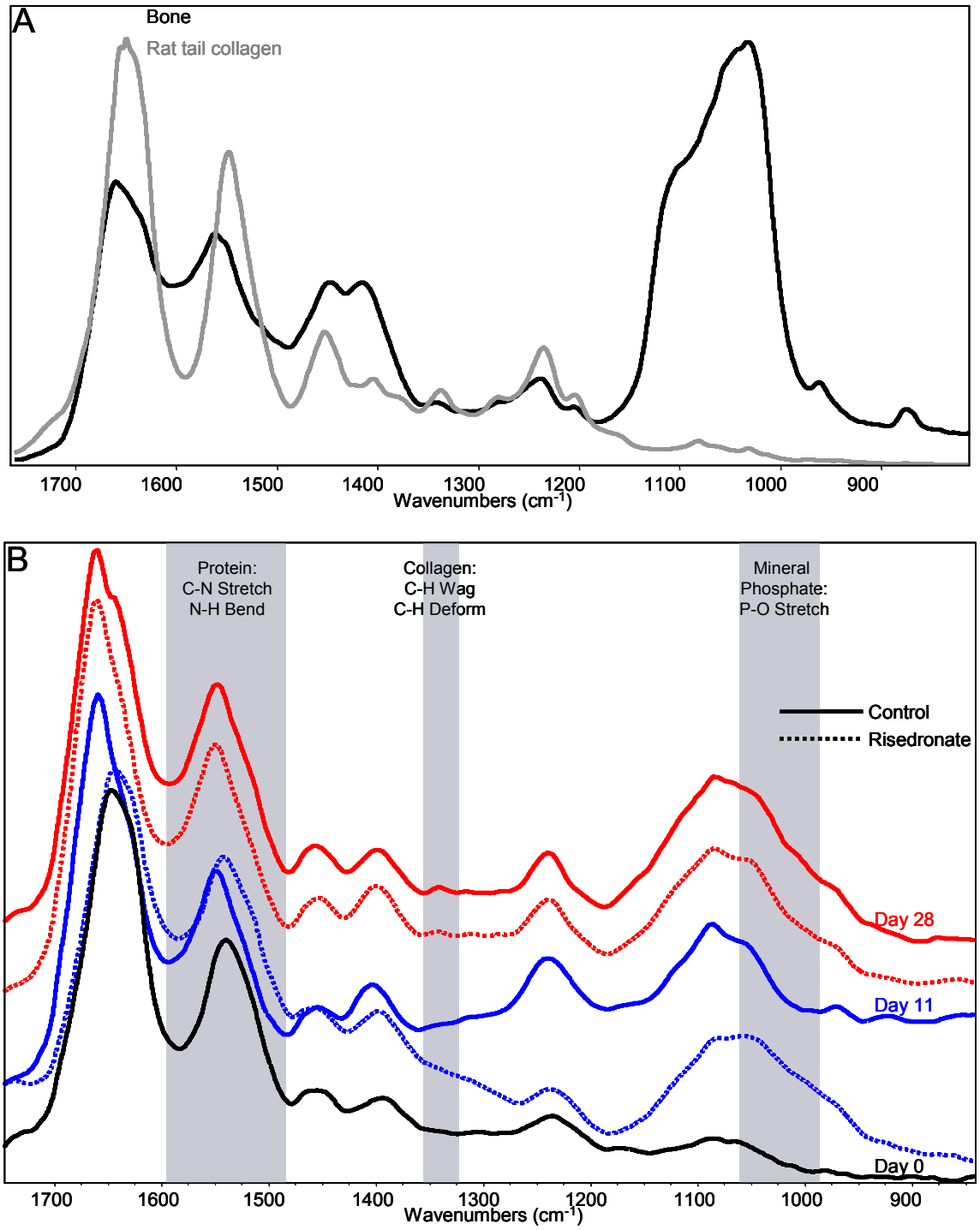

Figure 7: (A) Infrared spectra of rat tail collagen and fully mineralized bone. These spectra were used to help chose which regions of the infrared spectrum of (B) mineralizing osteoblasts should be analyzed. Infrared spectra from day 0, day 11 and day 28 for control and RIS-treated cells. The v1, v3 phosphate peak increases in absorbance and area with time, demonstrating active mineralization.

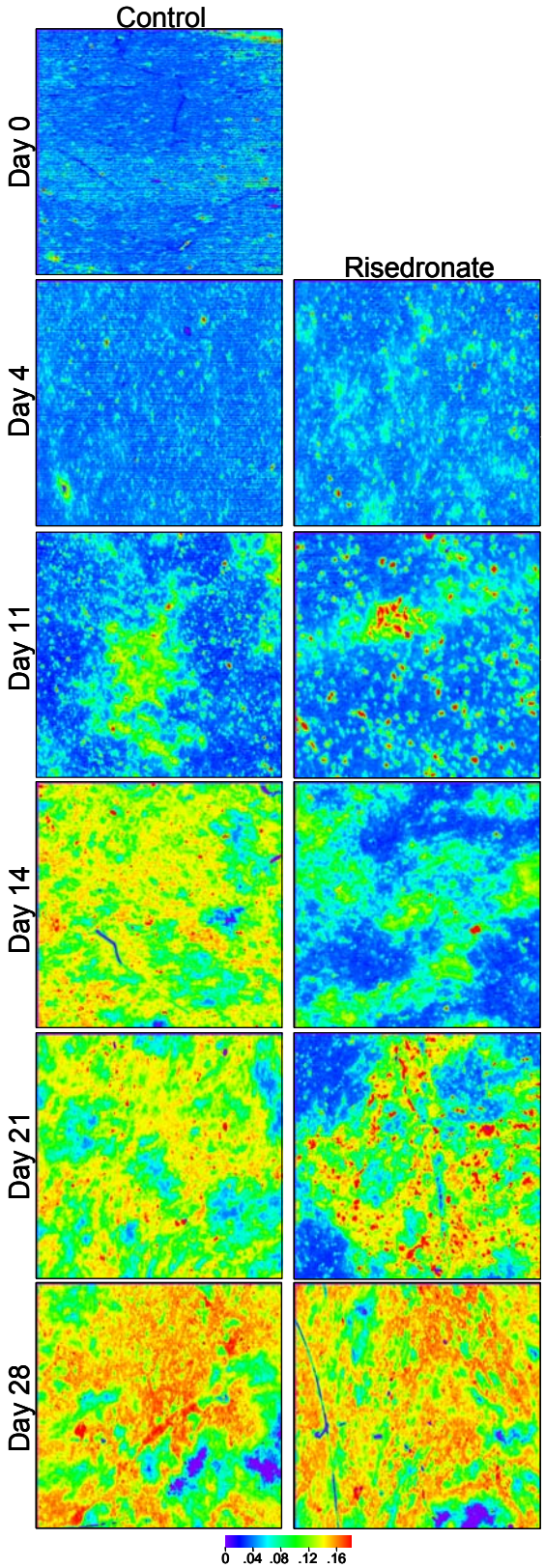

Figure 8: Infrared images of the level of mineralization for each time point for control and RIS-treated cells. The mineralization begins around day 11 and continues to increase through day 28. Mineralization is lagged at day 14 and 21 for the RIS-treated cells.

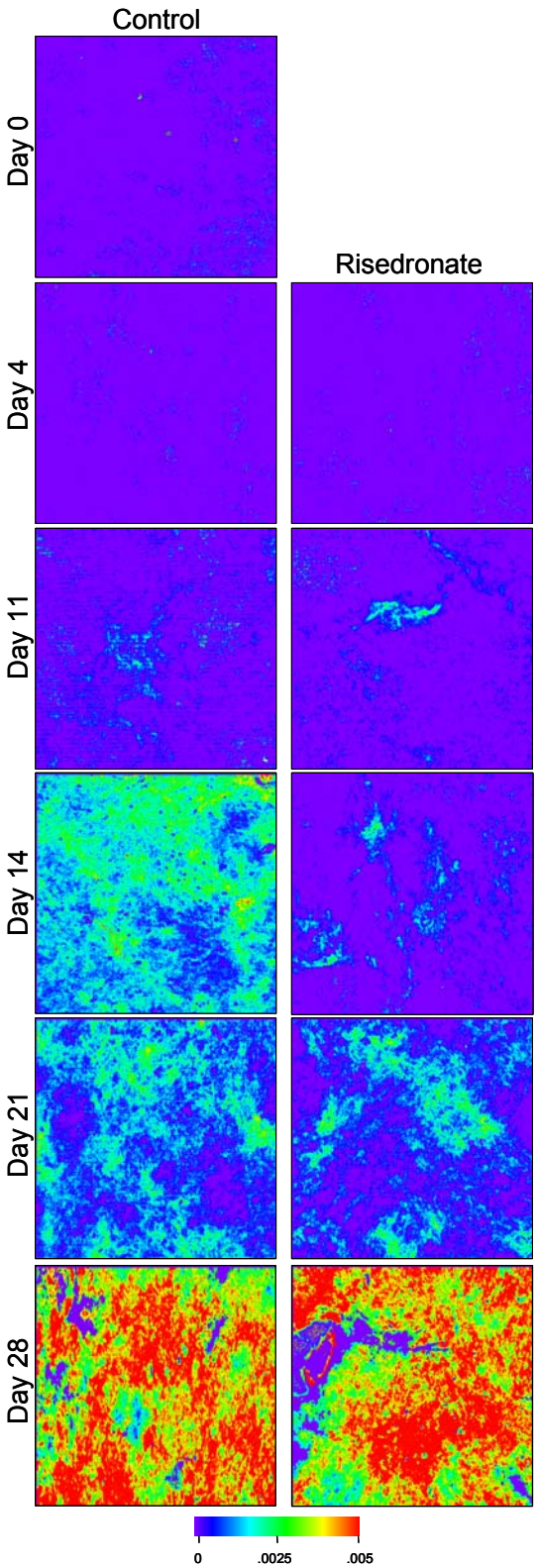

Figure 9: Infrared images of the collagen content for each time point for control and RIS-treated cells. The collagen content begins to increase at around day 14 for the control cells. This is lagged in the RIS-treated cells, but collagen content is the same for both control and RIS-treated cells by day 28.

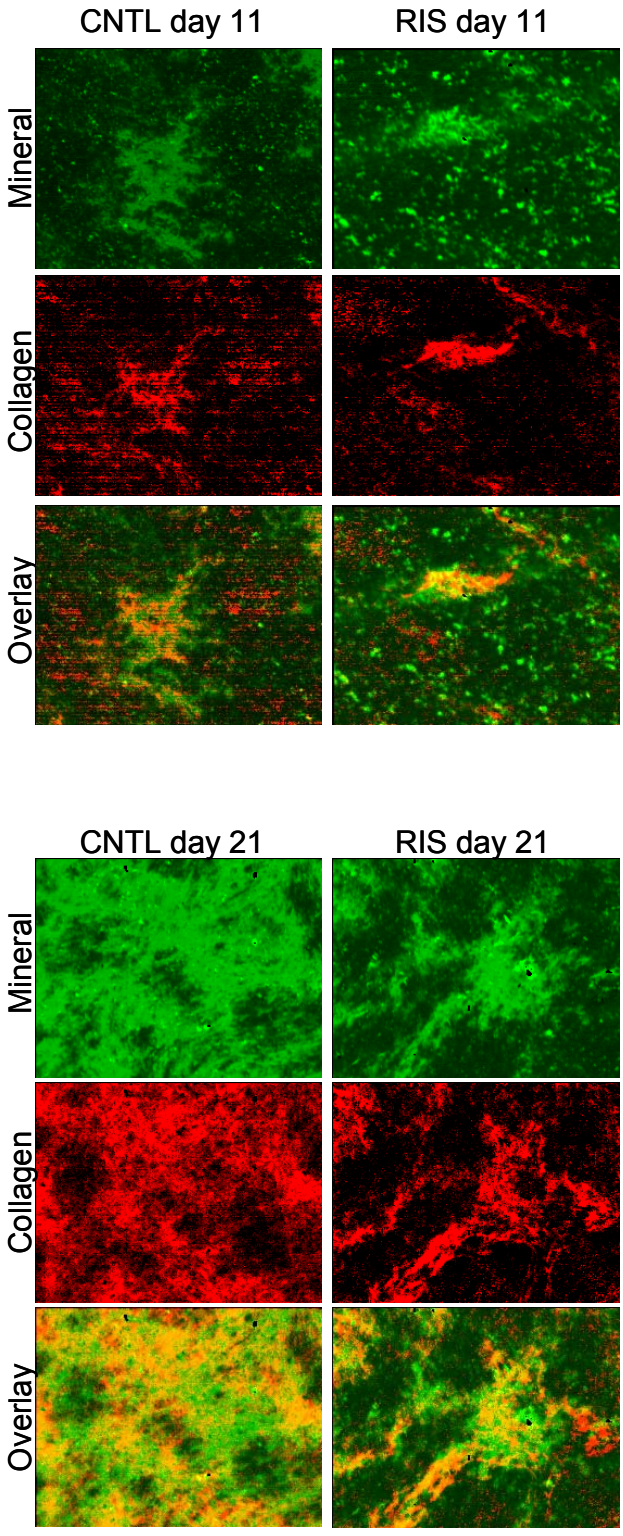

Figure 10: Overlaid images of the mineralization and collagen content for day 11 and day 21 control and RIS-treated cells. The green images represent the mineral, and the red images represent the collagen content. When the images are overlaid, areas appearing yellow show a correlation between the mineral and collagen content.

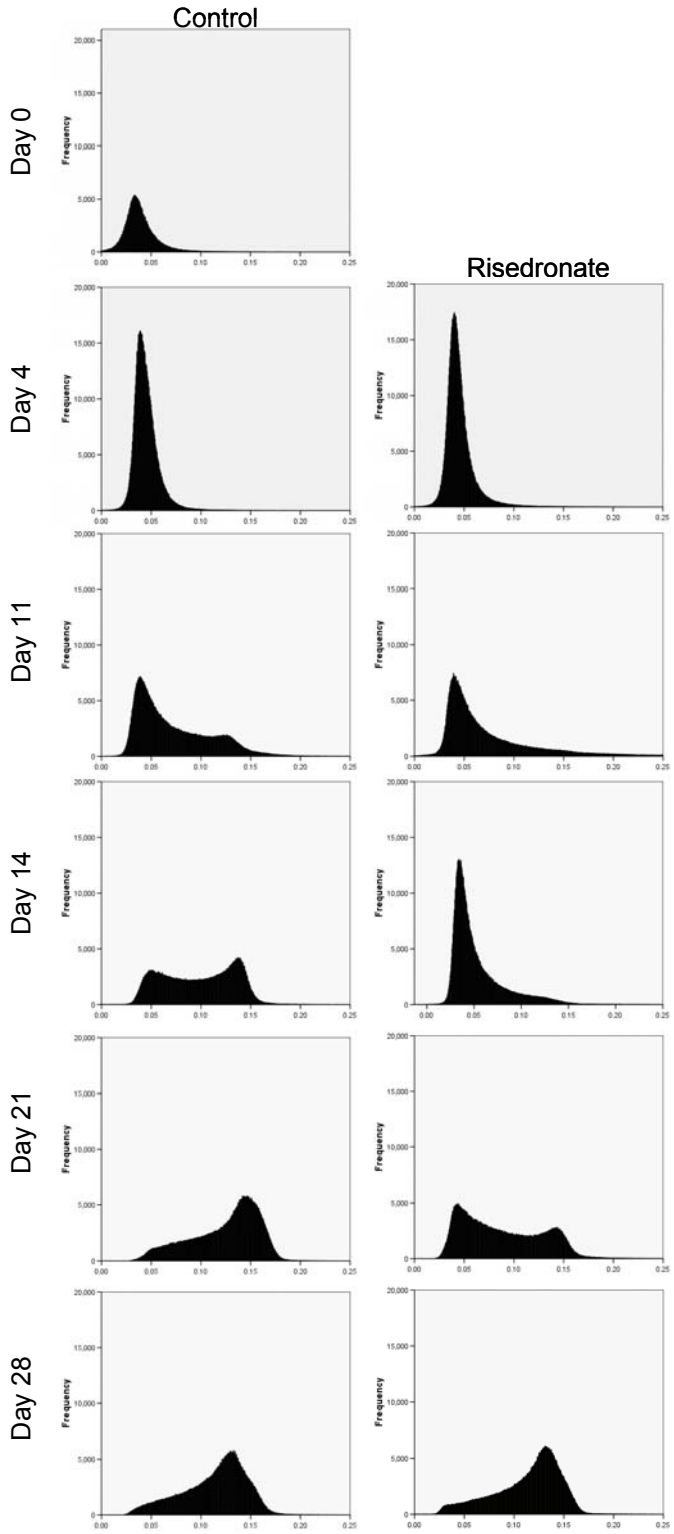

Figure 11: Combined (n=4) distributions of the mineralization as a function of time for control and RIS-treated cells. Bin size of 0.0005. The distribution becomes bimodal for the control cells beginning at day 11, showing the start of mineralization. This bimodal distribution is lagged in the RIS-treated cells, but by day 28 there are no differences between the control and RIS-treated cells.

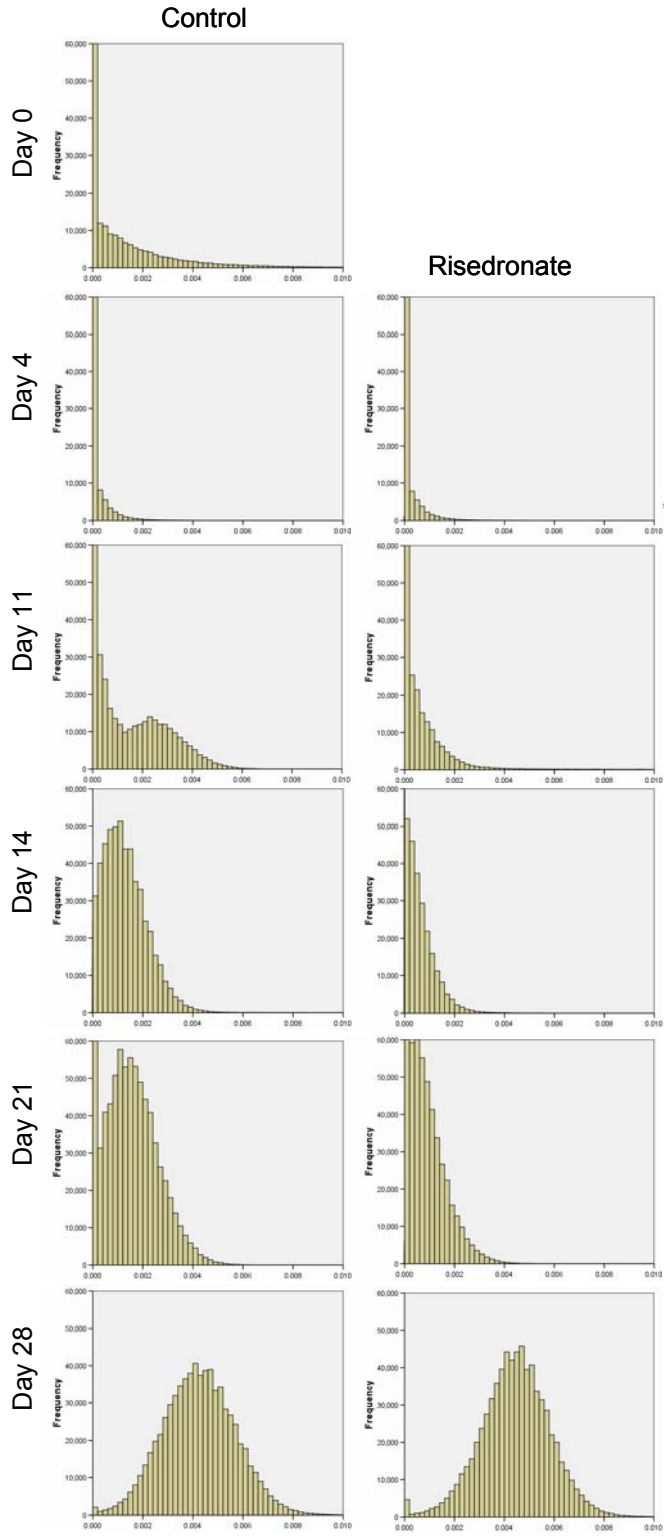

Figure 12: Combined (n=4) distributions of the collagen as a function of time for control and RIS-treated cells. Bin size 0.0002. Collagen content is minimal until day 11. At day 14 and day 21 the collagen content is lagged in the RIS-treated cells but catches up by day 28.

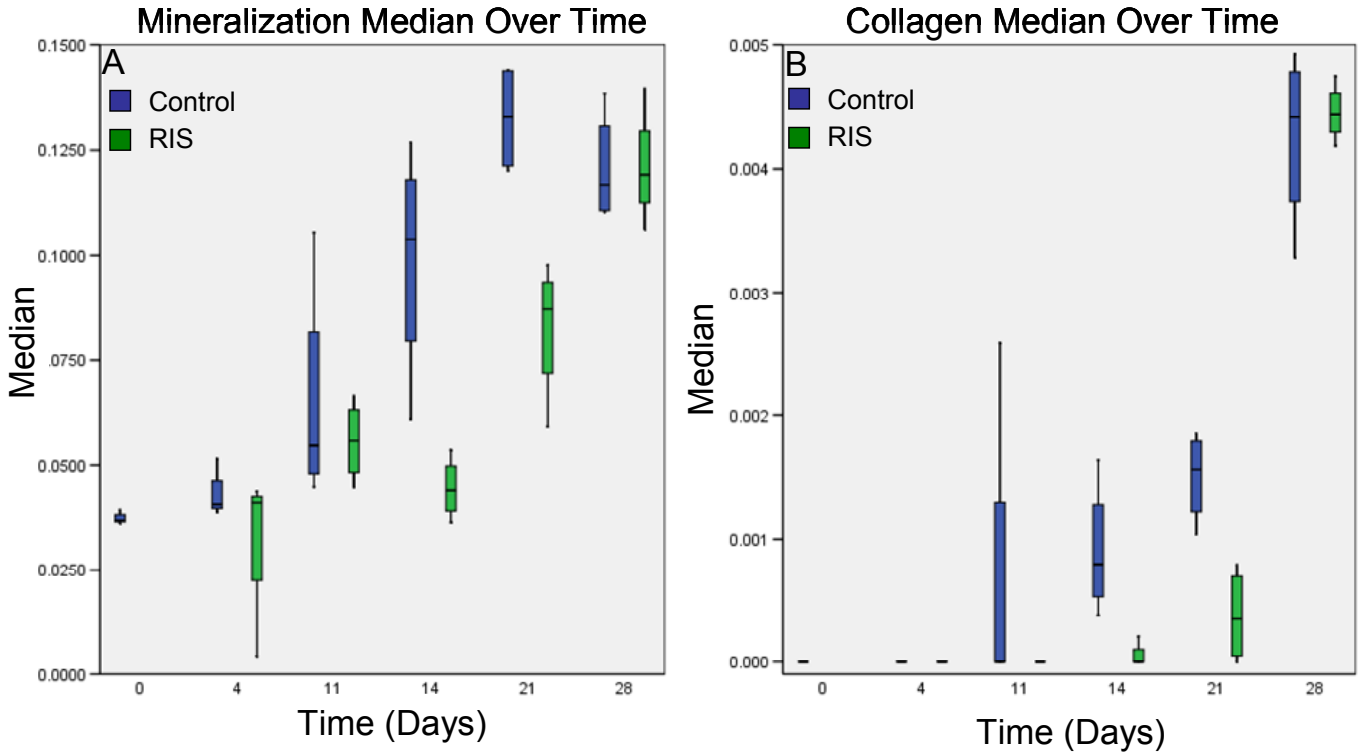

Figure 13: (A) Box plot of the mineralization medians over time for control (blue) and RIS-treated (green) cells. The error bars represent the 25th and 75th percentile. There was a significant difference in the mineralization between control and RIS-treated cells at day 14 (p=0.021) and day 21 (p=0.021). (B) Box plot of the collagen content medians over time for control (blue) and RIS-treated (green) cells. The error bars represent the 25th and 75th percentile. The median at day 0 and 4 is zero for both control and RIS-treated cells and is significantly different between control and RIS-treated cells at day 14 (p=0.010) and 21 (p=0.021).

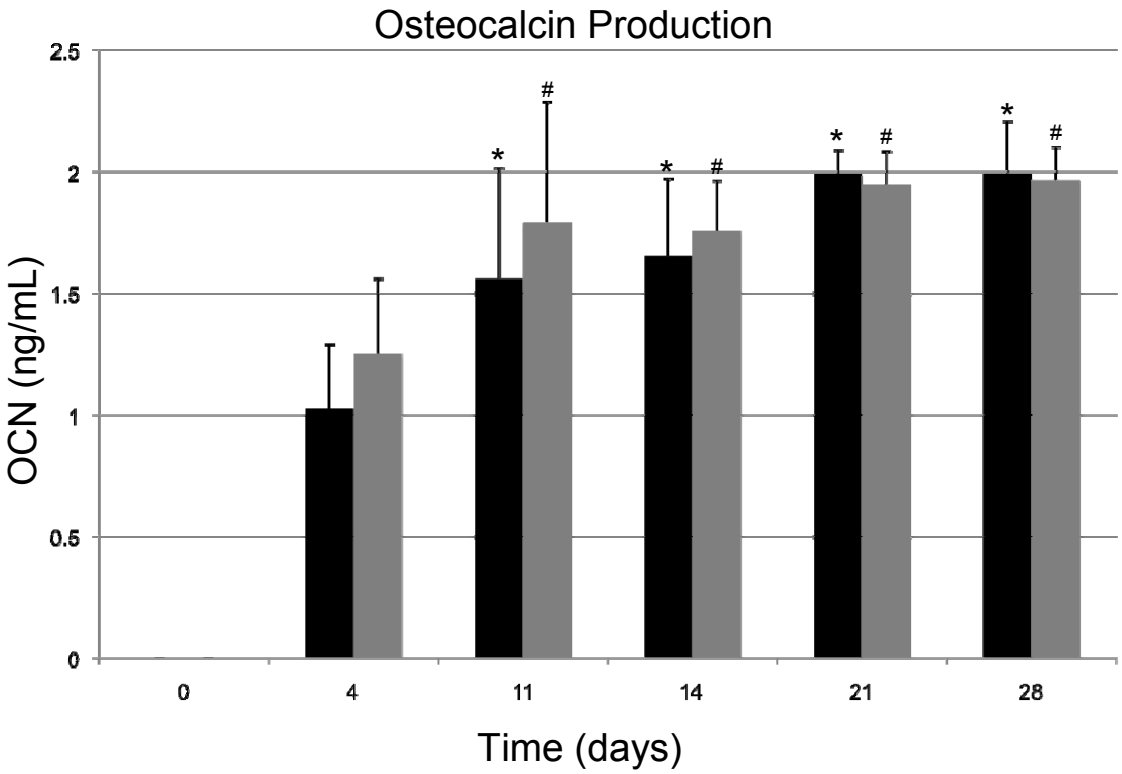

Figure 14: Amount of OCN for the control (black bars) and RIS-treated (grey bars) cells as a function of time. There are no significant differences between the amount of OCN in control and RIS-treated cells as any time point. * denotes a significant difference from day 0 in the control cells. # denotes a significant difference from day 0 in RIS-treated cells.

Chapter IV: Morphology of mineral formed by MC3T3-E1 cells is not altered by risedronate treatment

IV.I Abstract

Osteoporosis is a wide spread bone disease that leads to decreased BMD, altered tissue architecture and increased fracture risk. BPs are currently the most widely used treatment for osteoporosis. While much is known about how BPs act on osteoclasts and how bone remodeling is suppressed, little is known about how BP-treatment might alter the quality of newly forming bone matrix. BPs have been shown to bind to mineral in solution and *in vivo*, so we hypothesized that they may bind to mineral formed *in vitro*, altering its morphology. The structure of bone and orientation of its organic and mineral components plays an important role in the mechanical properties of the tissue, and changes to this structure could affect bone quality. This study examines whether RIS treatment alters the nanostructure of the mineral formed by MC3T3-E1 osteoblasts. Synchrotron nano-TXM was used at 8 keV to study the structure of mineral and collagen formed by untreated and RIS-treated MC3T3-E1 cells at 0, 4, 11, 14, 21, and 28 days. Mineral began to form on day 11 as nanometer-sized aggregates of mineral. By day 21 the aggregates had come together to form larger micrometer-sized nodules. Comparison of the mineral structure to that of amorphous calcium phosphate (ACP) and crystalline hydroxyapatite (HAP) revealed that the mineral formed by MC3T3-E1 cells appeared to be a cross between the ACP and HAP morphology. The mineral nodules were made up of smaller aggregates, like the ACP, however the overall shape of the nodule and aggregates was similar to that of HAP. Since collagen has a similar density to air, imaging of the collagen fibrils provided no contrast at 8 keV. Further, treatment of the cells with RIS did not alter the structure of the mineral. Understanding how RIS-treatment might alter the morphology of newly formed tissue is important for determining the long term affects that BP-treatment could have on the mechanical properties of bone.

IV.II Introduction

Osteoporosis is a disease that affects millions of Americans and costs billions of dollars each year for fracture treatment and care [74]. BPs are currently the most widely used treatment for osteoporosis as they have been shown to slow the damaging effects of the disease. While the use of BPs for disease treatment has been investigated for the past 30 years, long term physiological, quality, and mechanical effects are still being investigated. Because BPs accumulate in bone tissue, it is important to understand how bone metabolism and remodeling are altered during long term treatment.

Bone and mineralizing tissue are anisotropic materials that consist of organic and mineralized components. The main protein in bone (85-90%) is type I collagen. Collagen molecules (~1 nm) come together to form collagen fibrils, which have a diameter of ~100 nm. *In vivo* and *in vitro,* ascorbic acid stimulates osteoblasts to increase procollagen hydroxylation [64], which results in the formation and secretion of collagen fibrils. Type I collagen fibrils with diameters of become rectilinearly organized to form 1 μm collagen fibers [13, 14]. Within 24 hours of induction, osteoblasts begin to form a type I collagen matrix which develops 60-70 nm axial periodicity after about 7 days [53].

The mineral in bone is a poorly crystalline hydroxyapatite, specifically $Ca_{10}[PO_4]_6[OH]_2$, that becomes substituted with carbonate over time [4]. Plate-like mineral crystals, ranging in size from 5-60 nm [9-12], fill in 35 nm holes within the collagen matrix and eventually become closely packed and parallel to one another [19-21, 268]. As the tissue ages, the mineral crystals grow and begin to overlap with the collagen fibers within the matrix [9].

The orientation of both the collagen and mineral separately add mechanical strength to bone. In healthy tissue, collagen provides bone with ductility [5-8] and its periodic and parallel arrangement [14, 17, 18] helps to enhance stiffness and strength [15, 16, 277-279]. Changes in collagen orientation could account for altered mechanical properties in osteoporotic bone [14, 17, 280]. Moreover, bone rigidity is attributed to the mineral phase

of its matrix [207, 281]. While there has been conflicting evidence that alterations to mineral crystal size play a role in osteoporosis [11, 71-73, 282, 283], it is known that larger mineral crystals tend to reduce the stiffness of the tissue [284]. Changes to the morphology of the mineral could also affect bone mechanics [21].

Interaction of the mineral and collagen matrix is also important to bone strength and development. A well-organized matrix of collagen is essential for the deposition of physiologic mineral [50-55]. Within the matrix it is believe that the collagen fibers and mineral crystals are oriented parallel to one another to provide optimal mechanical strength [11, 12, 22, 24, 26, 27]. Additionally, while collagen and mineral each contribute certain mechanical properties to bone, the interaction of the two constituents also adds to the mechanics of the tissue. It has been shown that although collagen supports most of the strain that bone experiences, it also disperses some of that strain to the mineral crystals [285]. Collagen further shields the mineral from excessive stress through even distribution of the forces throughout the matrix [28, 29]. It is apparent that any changes in the structure of the collagen or mineral could alter the mechanical stability of bone tissue.

Recently, a full-field hard x-ray microscope, based on an Xradia™ nanoXCT full-field transmission x-ray microscope (TXM), was designed and implemented at SSRL. The microscope can image bone tissue in phase contrast mode with a 3-D spatial resolution of 25-60 nm which enables the imaging of the nanoscale structure of mineralized bone tissue. Results can be correlated with mechanical information from nanoindentation [191, 192] to provide an understanding of bone fragility at the nanoscale.

The objective of this study was to image the 2-D and 3-D nanostructure of the mineralized matrix formed by MC3T3-E1 osteoblasts using nano-TXM to specifically determine how the collagen and mineralized matrix might be affected by RIS-treatment. BPs have been shown to bind to mineral, and so we hypothesized that mineral morphology could be altered by RIS-treatment. While previous studies have shown that the rate of collagen

deposition can be affected by BP-treatment bone morphometry is not altered [286], and so we further hypothesized that collagen fibril orientation within the matrix would not be altered .

IV.III Materials and Methods

Cell Culture

A mineralizing sub-clone (sub-clone 4) of MC3T3-E1 mouse osteoblasts (ATCC, Manassas, VA) was grown in α-MEM with 10% fetal bovine serum (Sigma-Aldrich, Missouri), 1% sodium pyruvate (Sigma-Aldrich, Missouri), 1% Penicillin-streptomycin (Sigma-Aldrich, Missouri) and 1% Amphotericin β (Sigma-Aldrich, Missouri) at 37^{o}C in a fully humidified atmosphere of 5% CO_2. At confluence, (day 0) the medium was supplemented with 5 μg/mL ascorbic acid (Sigma-Aldrich, Missouri) and 4 mM sodium phosphate monobasic (Sigma-Aldrich, Missouri) to initiate mineralization. RIS-treated cells were also supplemented with 10 μM of RIS. Medium, supplements and RIS were changed every 2-3 days and samples were removed after 0, 4, 11, 14, 21, and 28 days in mineralizing medium.

For x-ray data collection, the cells were grown on 10 x 5 mm piece of mylar film that was 0.01 inches thick. Mylar film was used for a substrate because it is transparent to x-rays. When the films were removed from the medium they were washed twice in distilled water and once in 75% ethyl alcohol and dried. A total of 22 samples (control: day 0, 4, 11, 14, 21, 28; RIS: day 4, 11, 14, 21, 28, n=2 for each time point) were grown for x-ray data collection.

Risedronate

RIS monosodium hemipentahydrate powder was obtained from Procter & Gamble Pharmaceuticals (Cincinnati, OH). The drug was dissolved in sterile water, the pH adjusted to 7.4 with 1 M NaOH, then filter-sterilized through a 0.22 μm filter before use.

Calcium Phosphate Standards

ACP and HAP (Sigma Aldrich, Missouri) were used as standards to assess the type of mineral the MC3T3-E1 cells were forming. A few grains, approximately 5 μm in diameter, of the calcium phosphate powders were placed between two pieces of kapton tape. 6-10 grains of ACP and HAP were located within each sample and imaged in phase contrast mode. One grain of each type of powder was chosen for tomographic 3-D imaging, to compare to the mineral formed by the MC3T3-E1 osteoblasts.

Nano-Transmission X-ray Microscopy

X-ray data were collected using the Xradia™ nanoXCT at beamline BL6-2 at SSRL [189]. The energy was tuned to 8 keV using a double crystal monochromator. The x-rays illuminated the sample, and a gold/SiN zone plate magnified the image onto a 2-D CCD detector, cooled to -70^{o}C. All images were collected using TXMConfigure and TXMController software (Xradia™ Concord, CA), in phase contrast mode utilizing the phase ring, where the reference image were collected through an empty sample holder. Reference and average phase contrast images were collected with a bin of 1, with 2 second exposure times, with a total of 20 scans. At later time points (~ day 11 and later) 6 areas containing mineral nodules were found using a light microscope and the coordinates were recorded. Average images were then collected in these 6 areas in phase contrast mode. One nodule from each sample was chosen to perform tomographic 3-D imaging. For samples between 0-4 days, 6 areas were chosen from each sample for 2-D imaging to demonstrate that no mineral was present.

3-D tomographic imaging was performed with a bin of 2, and 2 second exposure. Images were collected between at most -70^{o} to +70^{o}, in 0.5^{o} increments. Phase contrast images collected in 3-D tomographic mode were reconstructed and formatted into mpg files using TXMRecontructor and TXM3DViewer software (Xradia™ Concord, CA), respectively.

IV.IV Results

We were able to begin finding mineralized regions at day 11 for both the control and RIS-treated cells. Mineralization began as diffuse nanometer-sized aggregates (**Figure 15**). **Figure 16** shows the comparison between ACP, HAP and mineral formed by day 21 control and RIS-treated cells. The visible images showed the area that was imaged by the nano-TXM (in between the white crosshairs). The corresponding phase contrast images showed the mineral morphology of each sample.

In **Figure 16B**, the ACP had a nodular appearance. The 5 μm nodule of mineral appeared to be made up of smaller 200-700 nm aggregates, which all had a fairly spherical shape. The HAP (**Figure 16D**) had a flatter appearance. Its structure appeared more rigid and rectangular when compared to the ACP, and it appeared as if it was made up of smaller granules.

Examination of the morphology of the mineral formed by the day 21 control cells (**Figure 16F**) appeared to be a cross between the morphology of the ACP and the HAP. The mineral nodule appeared to be made up of smaller aggregates, like that of the ACP. However, the overall appearance had a flatter plate-like form, similar to the HAP.

Comparison of the day 21 control (**Figure 16F**) and RIS-treated mineral (**Figure 16H**) revealed that there were no differences between the nanoscale morphology of the mineral formed by the MC3T3-E1 osteoblasts. Results were similar for all other time points, suggesting that the morphology of the mineral formed by MC3T3-E1 osteoblasts was not changed by RIS-treatment.

Additionally, examination of the mineral morphology at day 11 (**Figure 15**) and day 21 (**Figure 16F and 16H**) suggested that at the onset of mineralization, small nanometer-sized grains of mineral aggregate within the same area. As time progresses, these aggregates grow in size and eventually form a larger micrometer-sized mineral nodule.

We were unable to image the collagen fibers that form the matrix needed for physiological mineralization to occur. It appeared that the density of the collagen was too close to the density of air, which resulted in very little image contrast at 8 keV. Moreover, because the mineral within the cultures was so dense, it could have further overpowered the contrast of the collagen.

IV.V: Discussion

In this study, we imaged the nanoscale morphology of mineral formed by MC3T3-E1 cells and compared it to calcium phosphate standards. Additionally, we examined if treatment with RIS caused alterations in the mineral produced by these cells. Because of BPs high binding affinity for mineral [113], we hypothesized that RIS might bind to mineral formed by MC3T3-E1 osteoblasts, altering its appearance.

While we were able to determine the morphology of the mineral formed by the osteoblasts, imaging of the collagen fibrils was not possible. It appeared that in phase contrast mode, the density of the collagen was too close to air to obtain contrast. While imaging of the collagen fibrils within the culture was not possible, due to similarities in the density of air and collagen, it is known that a collagen matrix is needed for mineralization [50-53] and we previously saw that this line of cells produced collagen (**Chapter III**). Therefore, we can assume that a collagenous matrix was present but we were unable to determine if the mineral formed by these cells was associated with that collagenous matrix or whether it was ectopic.

Mineral formed by MC3T3-E1 cells is initially deposited by matrix vesicles that are associated with the organic matrix [53]. Small mineral nodules are formed when the mineral within the matrix vesicle is secreted. These nodules increase in number and size over time, act as nucleation sites for further mineralization, and eventually some of the nodules fuse. MC3T3-E1 cells form two types of mineral [63]. Ectopic mineral, which is not associated with the collagenous extracellular matrix, forms when the amount of phosphate within the media is >4.0 mM [65]. This type of mineral, due to

precipitation of phosphate from the medium, has a granular appearance and is believed to be nonphysiological [287, 288]. On the other hand, extracellular matrix-associated mineral that forms at lower concentrations of available phosphate resembles that found in woven bone [53, 65]. However, a stable, cross-linked collagenous matrix is necessary for this type of mineralization to occur [50-53]. It has been shown that the matrix-associated mineral formed by osteoblasts (of different lineages) appears as spherical nodules [40, 53]. Further, diffraction analysis of mineral nodules showed them to be non-oriented HAP, with crystal sizes ranging from 13-16 nm [40, 51, 55].

It is believed that calcification of the organic matrix of bone occurs in two phases; nucleation of the mineral, followed by growth of the mineral crystal [289]. Mineral within bone has been classified as poorly crystalline HAP [4]. However, the exact structure of bone mineral is hard to pinpoint because cationic calcium and anionic phosphate substitutions can occur altering the mineral stoichiometry [38, 183, 290]. Additionally, as bone matures, mineral crystal size and perfection increase [184, 187]. Changes to the mineral crystallites in bone can contribute to fragility at the microscopic level because physical properties of bone, such as solubility, hardness, brittleness, and thermal stability are altered [291, 292]. Changes in just one of these properties could affect the overall fragility of the bone tissue.

Comparison of the morphology of the mineral formed in the control cultures revealed that mineral begins as nanometer-sized diffuse particulates which eventually come together to form a larger mineral nodules. The nanoscale morphology and appearance of the mineral nodules formed by MC3T3-E1 is a cross between the ACP and HAP. The nodules the cells produced appeared to be made up of smaller aggregates, like the ACP mineral. However, the smaller aggregates that make up the mineral nodules were not round, like those of ACP. They had a flatter, more squared appearance like those in the HAP. This is consistent with the fact that mineral within bone tissue is characterized as poorly crystalline HAP [4] and that it has a plate-like appearance [19, 20, 268].

While the affects of BP-treatment on osteoblasts has been studied *in vitro* [134, 201-203] and *in vivo* [131, 136, 137, 139, 193-200] the quality and structure of the mineral formed during treatment has not been investigated. It is known that BP-treatment decreases mineralization [131, 134, 136-139, 193-203], but the process by which mineralization is decreased is not well defined. BPs have been shown to bind to HAP both *in vitro* [113, 202] and *in vivo* [203, 293], and have also been shown to prevent precipitation of calcium phosphate from solution, slow the transformation of ACP to HAP, inhibit the aggregation of crystals and hinder crystal dissolution [294, 295]. Additionally, BPs may biologically affect HAP crystals by altering crystal size, growth, aggregation, and dissolution. They may also have an affect on how mineral crystals interact with collagen, charged ions, proteins and glycosaminoglycans within the bone matrix [296]. *In vivo* BPs have been shown to localize to areas where new bone is being formed, because newly forming HAP crystals provide large surface areas of exposed mineral that the BP can attach to [112]. All of these properties suggest that *in vitro*, BPs would attach to newly formed mineral and cause some alteration to its nanoscale morphology.

Therefore it is possible that alterations in the mineralization timeline, as seen in **Chapter III**, could occur if the structure of the mineral was altered. However, in this study we saw no morphological differences in the mineral formed by control and RIS-treated samples, suggesting that changes in mineral morphology do not contribute to decreased mineralization in the MC3T3-E1 osteoblast model of bone formation.

This study did have some limitations in that we were unable to view the collagen fibril network that supported the mineral growth. Further studies, where the collagen fibrils are labeled with metallic particles for easier viewing, are currently being considered. The ability to see if the interaction of the collagen matrix and mineral crystals is changed by BP-treatment is of much interest and could further help understand how treatment might alter the mechanical properties of the tissue. Moreover, phase contrast nano-TXM is

currently qualitative and does not provide quantitative or compositional information about the material being examined.

In conclusion, we have shown that the mineral formed by MC3T3-E1 osteoblasts starts as diffuse nanometer-sized aggregates, that act as nucleation sites for mineral growth. These aggregates grow in size and eventually form larger micrometer-sized mineral nodules. The mineral nodules had similar morphology to both ACP and HAP, in that their overall shape was plate-like, like HAP, but they appeared more like ACP on the nanometer scale. Bone mineral is known to be poorly crystalline HAP with plate-like features, which is comparable to what we saw in this study. Additionally we have shown that RIS-treatment does not alter the structure of the mineral formed by osteoblasts. This study helps to understand how BP-treatment might affect bone quality in patients undergoing long term treatment.

IV.VI: Figures

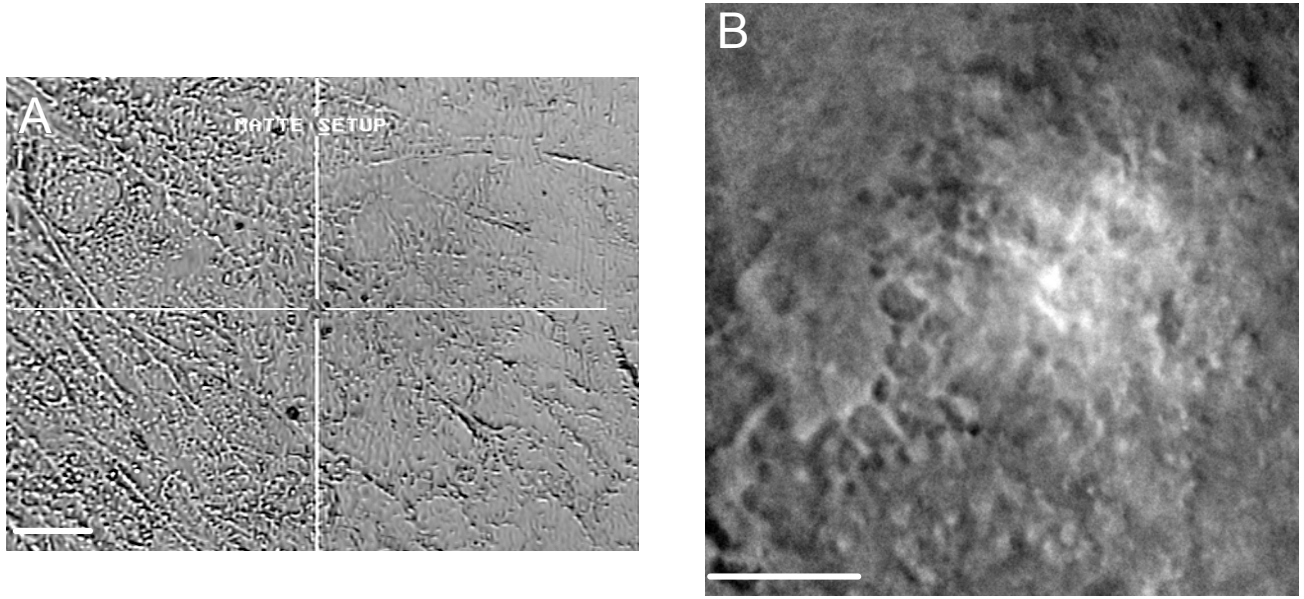

Figure 15: (A) 50X visible image of day 11 MC3T3-E1 mineralizing osteoblasts. Scale bar is 100 μm. (B) Phase contrast image of diffuse mineral formed by the MC3T3-E1 cells at day 11. The individual aggregates are less than 1 μm in diameter. Scale bar is 3.75 μm.

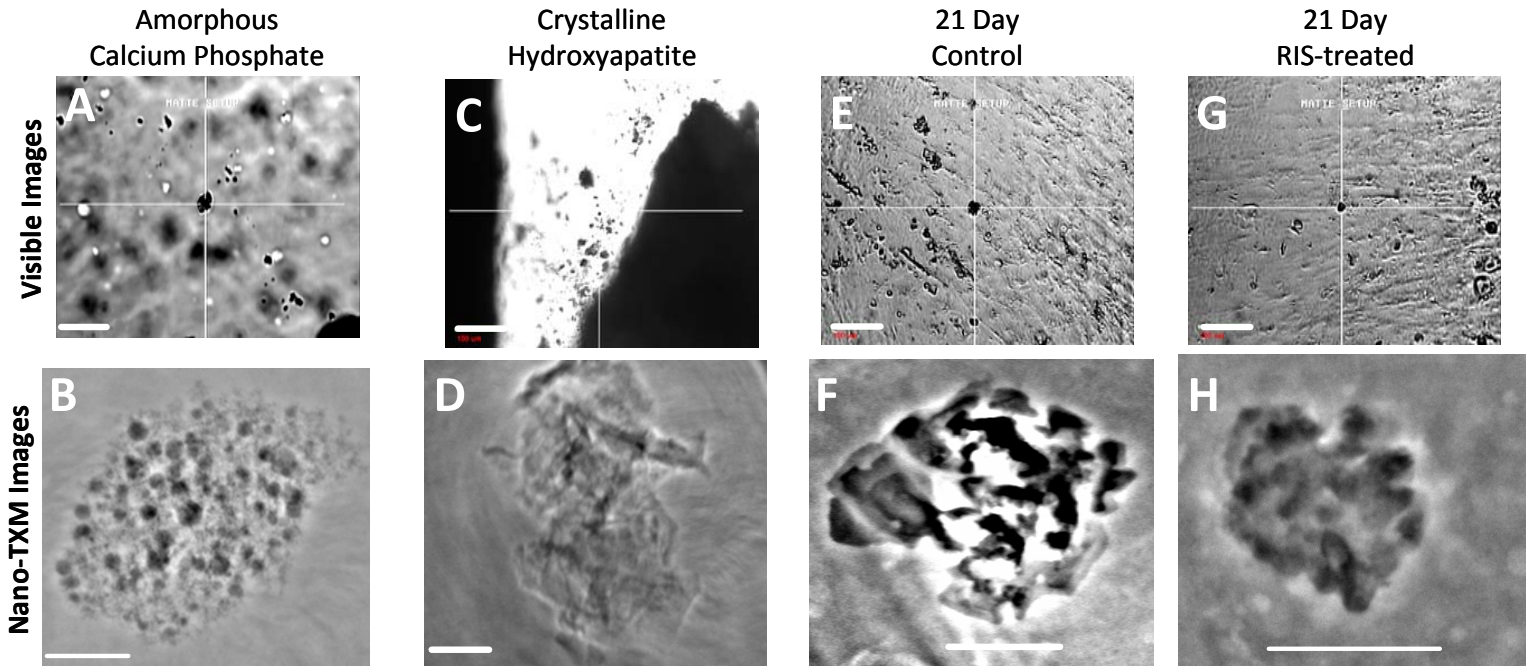

Figure 16: 50X visible image of (A) a grain of amorphous calcium phosphate (B) imaged in phase contrast mode and (C) a 50X visible image of a grain of crystalline calcium phosphate (D) imaged in phase contrast mode, for comparison to the mineral examined from the control and RIS-treated MC3T3-E1 cells. (E) 50X visible image of 21 day control cells imaged in (F) phase contrast mode. The mineral nodule is approximately 7 μm in diameter. (G) Visible image of a mineral nodule from 21 day RIS-treated cells imaged in (H) phase contrast mode. It appears that the mineral structure of osteoblasts is similar to that of amorphous hydroxyapatite and additionally that it is not changed by RIS-treatment. Scale bar in the visible images is 100 μm and the scale bar for the phase contrast images is 2.5 μm.

Chapter V: Discussion

Bisphosphonates are currently the most frequently used treatment for osteoporosis. It is known that they counteract the damaging effects of the disease by increasing BMD [81, 120, 297, 298], decreasing fracture risk [81, 84, 299-302], and restoring microarchitecture [303-307]. However, BPs themselves have been shown to have adverse affects on the tissue. They have been shown to increase mineralization [100, 121] and microdamage [122] in existing bone, making it more brittle [100, 101, 121, 286]. Additionally, they have been shown to decrease mineral and collagen production and proliferation of osteoblasts *in vitro* [134, 135, 201-204] and *in vivo* [131, 136, 137, 139, 193-200].

Chemical composition of bone is intimately tied to its mechanical properties, suggesting that chemical and structural changes caused by long term BP-treatment could have an effect on bone fragility. For example, bone strength has been shown to be dependant on mass, microstructure, geometry and material properties [308]. Understanding how composition plays a role in mechanics is important to determine how each constituent of bone contributes to its overall strength and how changes in composition and morphology could translate to decreased bone mechanics and increased fragility.

It is unclear how bone composition and structure are affected by BP-treatment and whether changes to bone quality with treatment could have long term mechanical consequences. For example, it is unclear if increased mineralization of existing bone, caused by BP-treatment, makes the tissue more susceptible to microdamage. **Specific Aim 1** addressed this uncertainty by probing the chemical composition of untreated and BP-treated bone in and around areas of microdamage. This was undertaken to determine if BP-induced over mineralization was correlated with microdamage formation.

Further, it is not known if the composition and structure of bone formed during BP-treatment is altered. **Specific Aim 2** was designed to examine the chemical composition and organization of mineralized matrix formed by untreated and RIS-treated osteoblasts, to determine if BP-treated altered the function and

activity of bone forming cells. Since BP's have been shown to have effects on the cell types involved in bone formation and remodeling it is possible that they also have an effect on the chemistry and structure of existing and newly formed bone. Therefore, it is important to understand how BP-treatment might alter the chemical composition, morphology, and quality of existing and newly formed bone and mineral, because this has a direct effect on the mechanical properties and fragility of the tissue.

V.I BP-induced accumulation of microdamage is not caused by over mineralization

We hypothesized that microdamage would be concentrated to older areas of tissue where mineralization and carbonate accumulation are increased leading to brittle tissue. However, we did not see increased levels of mineralization in areas of microdamage or the surrounding undamaged tissue in control and BP-treated animals [205]. We saw that within the microcrack, collagen cross-linking was decreased due to stretching and breakage of the collagenous matrix. This could have lead to the decreased carbonate accumulation seen within the microcracks, as mineral is displaced from the damaged matrix and carbonated mineral preferentially dissolves. Several groups have hypothesized that over mineralization [61, 309], caused by BP-mediated bone resorption is the cause of increased accumulation of microdamage [121, 143]. Specifically that microdamage would be accumulated within areas of over mineralization because this area of the tissue was more brittle. However this hypothesis has not been previous tested.

For the first time we have probed the chemical composition of microdamaged tissue as well as the surrounding undamaged bone, specifically examining the level of mineralization, to confirm the hypothesis that others had proposed. Surprisingly, we saw that bone was not over mineralized in areas of microdamage. Actually, we saw a decrease in the absorption intensity of the phosphate peaks in the IR spectra from within the microcracks. This decrease in intensity was accompanied by a decrease in the intensity of the amide I protein

peak and therefore attributed to dissolution of bone mineral due to stretching and breakage of the collagenous matrix [205, 219]. So while the level of mineralization (protein:phosphate ratio) was unchanged between microdamaged and undamaged bone, the quantity of mineral and collagen cross-links within the microcrack decreased.

Changes in existing bone composition due to BP-treatment have been previously demonstrated *in vivo*. As previously mentioned BPs have been shown to increase mineralization of existing tissue [100, 101, 121, 286, 309-311], increase the homogeneity of tissue mineralization [100, 312], and slightly decrease levels of low mineralized bone [313, 314]. Additionally accumulation of advanced glycation end-products has been shown with BP-treatment [136]. Increases in bone strength with BP-treatment have been attributed to increased mineralization [100, 309]. However, over mineralization and accumulation of advanced glycation end-products leads to increased brittleness of the tissue [61, 315, 316] which could further increase the occurrence of microcracks [121].

Women who present with osteoporotic fracture tend to be distributed either in the highest or the lowest quartile of the mineralization spectrum [317], and mineralization of their bones tends to be less heterogeneous [312]. Increased mineral content in osteoporosis has been correlated with increased tensile strength and elastic modulus [318] and reduced tissue toughness [312]. Additionally, decreased elastic modulus, yield stress [281], and increased fragility [178] are associated with low mineral content. These findings demonstrate that a reduced mineral to matrix ratio affects the mechanical properties of the tissue, and could play a role in microdamage accumulation. These finding are what lead us to believe that microdamage would be associated with areas of over mineralized tissue.

Since we did not see increased mineralization in areas of microdamage and it's surrounding undamaged tissue it is likely that the process of slowed remodeling leads to increases in microdamage accumulation. This is consistent with the fact that examination of the undamaged tissue yielded homogenous composition. If microdamage was a result of localized areas of increased

mineralization we would have seen this in the undamaged tissue closest to the microcracks. Instead, we saw a clear compositional distinction between undamaged tissue and the microcrack, which we attributed to crack formation. Others have also shown that microdamage accumulation is likely due to slowed remodeling [141].

Regardless of the fact that microdamage was not confined to areas with increased mineralization, microdamage accumulation can still have an effect on the mechanics of the tissue. Increased microdamage can lead to a decrease in elastic modulus [319] and decreased bone toughness [122, 123]. However, microdamage-induced changes in mechanical properties of the tissue may be offset by increased mineralization [170, 298, 303], because it has been shown that slight increases in mineralization can lead to increased strength [100, 309]. However the relationship between mineralization and strength needs to be carefully monitored; while low mineralization is known to be associated with low stiffness, strength, and elastic modulus [92-94, 188, 320, 321], over mineralization leads to increased brittleness of the tissue [61, 315]. As mineralization increases and bone becomes more brittle, the amount of plastic deformation the bone can withstand decreases and bone breaks with less strain. Hence a higher level of mineralization renders bone more likely to fracture when exposed to stress. Thus, bone with greater strength and stiffness may also be more brittle and more, rather than less, likely to fracture.

Even though microdamage accumulation was not associated with over mineralization, we did show that the formation of microcracks lead to localized changes in bone composition, which could have further implications on bone fragility.

V.II Chemical composition changes are associated with microcrack formation

While microdamage was not associated with areas of over mineralization, we did see that the local composition within the microcrack was altered [205]. We attributed this composition change with microcrack formation rather than being

the cause of it. More specifically, we saw a decrease in the carbonate accumulation within the microcrack. Further, we saw an increase in acid phosphate content and altered collagen cross-linking within the crack, when compared with the surrounding undamaged tissue. Mineralization and crystallinity were not changed within areas of microdamage.

When a microcrack is formed the collagenous matrix of the tissue is stretched and sometimes broken [219]. When this occurs, mineral crystals associated with the stretched and broken matrix are displaced [206]. Changes in mineral composition, as a result of stress and pressure, have been previously demonstrated in synthetic apatites [224, 233] and bone [225]. Mineral that contains higher levels of carbonate would be more likely to dissolve in this microenvironment because it is more soluble [35, 36]. Therefore, the compositional changes that we observed are likely due to stretching and breakage of the collagen matrix during crack formation, dissociation of mineral from the matrix, and dissolution of carbonated apatite.

Our group previously showed that globally BP-treatment does not alter the chemical composition of damaged bone tissue [121]. However, to date, compositional analysis of microcracks and the surrounding undamaged bone has not been undertaken. Further, determining if BP-mediated compositional changes contribute to microdamage accumulation has not been investigated. For the first time we have shown that microdamage accumulation causes localized compositional changes in areas of microcrack formation. These chemical changes, paired with increased microdamage accumulation with BP-treatment could have further implications on bone fragility.

Even though microdamage does not appear to be caused by changes in bone composition, it does lead to localized alterations in bone composition [205]. Therefore, it is still important to understand accumulation of microdamage can contribute to overall bone fragility. The relationship between microdamage and reduction in mechanical properties are not directly proportionate [322]. Bone with low levels of microdamage has been shown to be mechanically similar to non-damaged tissue, while medium and high levels of damage induced

disproportionate reductions in post-yield deformation. Additionally, increases in microdamage accumulation have been shown to decrease bone toughness [122, 235], stiffness [155, 323], and elastic modulus [319]. However, some have suggested that increased fracture rates and decreased mechanical properties of BP-treated tissue are associated with increased mineralization, not microdamage accumulation [324], while still others saw no deterioration in mechanics with microdamage accumulation [170]. This is relevant from a clinical standpoint, as it has been suggested that people with low BMD who are being treated with bisphosphonates also accumulate microdamage [172, 232]. Further, if microdamage is causing localized compositional changes in the tissue, this could lead to additional changes in bone mechanics. Because we saw increased microdamage accumulation with BP-treatment in our animal model, investigation into the clinical long-term effects of BP-treatment should be undertaken.

The conventional wisdom is that collagen and collagen cross-links are primarily correlated to the post-yield properties of bone [15, 16]. However, it has been shown that collagen can also have an effect on the pre-yield properties of the tissue, such as tensile stiffness and strength, [94, 325, 326], toughness, ductility, and viscoelasticity [180, 259, 327]. As the collagenous matrix of bone is deposited, collagen fibrils begin to cross-link. Collagen cross-links may play a role in mechanical stability of bone tissue [234, 326, 328], as they are thought to contribute to bones tensile strength and viscoelasticity [296]. Bone toughness has also been associated with alterations to the collagen network [234]. The amount of non-reducible:reducible collagen cross-links has been shown to increase with age [220, 296, 329]. A decreased collagen cross-linking ratio, as seen here, is associated with reduced and broken cross-links [218] and collagen denaturation [230].

Further, decreased carbonate accumulation and increased acid phosphate could lead to increased fragility. Carbonate (CO_3^{2-}) and acid phosphate (HPO_4^{2-}) are frequently substituted into the phosphate (PO_4^{3-}) anionic sites within the bone matrix [291, 330]. Because carbonated apatites are more likely to dissolve when compared to unsubstituted hydroxyapatite [35-37], carbonate substitutions make

the bone lattice less stable. The mechanical consequences of carbonate substitution are not well understood because it has been shown to increase [34, 221], decrease [183, 222], and remain constant [61] during aging. Acid phosphate is found in immature bone and decreases with age [38-40, 187]. Increased acid phosphate has been shown in osteoporotic tissue, suggesting it plays a role in increase bone fragility [186]. Therefore, microdamage induced compositional changes in collagen and mineral, as seen here, could make bone more fragile.

We have shown that BPs induce changes to the chemical composition of bone through the accumulation of microdamage. These changes could lead to further decreased mechanical stability in osteoporotic patients. Because bone formation is coupled to resorption and compositional changes were observed in existing bone as a result of BP-treatment, it was feasible to hypothesize that BPs would have an effect on bone formation as well.

V.III RIS-treatment delays the collagen deposition and mineralization of osteoblasts in vitro

It has been previously shown that BP-treatment can have an effect on the collagen deposition and mineralization rate of osteoblasts in culture, and so we hypothesized that RIS-treatment would have a similar effect. We have shown that while the time line of collagen and mineral deposition of osteoblasts is interrupted by RIS-treatment at 14 and 21 days of treatment, the lag in matrix development is only temporary [236]. It is likely that uptake of RIS from culture caused increased amounts of unprenylated proteins within the osteoblasts, which slowed the deposition of the collagen matrix. A collagenous matrix is required for mineralization to occur, so when the collagen deposition is disrupted, so is mineralization [243]. These results are in agreement with previous *in vivo* studies where BPs have been shown to slow the occurrence of new bone formation sites [131, 136, 331-333], as well as inhibit further bone formation at pre-existing bone-forming surfaces [137]. *In vivo* changes in mineralization are possibly due to osteoblasts internalizing the BPs which directly alters their function [136]. Or

osteoblast function could be indirectly regulated through exposure of osteoclasts to BPs [131]. Regardless, the long term consequences of remodeling suppression on chemical composition, caused by BP-treatment, and their impact on mechanical properties of the tissue are incompletely understood.

While the intended cellular target of BPs is osteoclasts and their activity, it has recently been demonstrated that BPs also have an effect on osteoblast cells. BPs have been shown to stimulate osteoblasts, promoting osteoblast proliferation [133 , 237, 334] and increasing production of osteoblast-differentiation markers like ALP [133-135, 335] and OCN [133, 203, 335]. Additionally they have been shown to further increase type I collagen synthesis [133, 135, 203, 334, 336, 337] and mineral production [134, 135, 203]. These increases, caused by BPs, would eventually lead to an increase in mineralized matrix.

Similar to our findings, BPs have also been shown to have inhibitory effects on osteoblasts. Specifically, decreasing cell viability [202, 204], proliferation [135, 200, 254], causing apoptosis and inhibition of protein prenylation [202, 275]. Decreased collagen synthesis [204], ALP production [254] and mineral deposition [193, 200, 201, 203, 338] have also been demonstrated. While these actions would lead to decreased mineralization and bone formation it is difficult to make general conclusions about the affect BPs have on osteoblasts, because of such contradictory results.

Conflicting affects of BPs on osteoblast cells is likely due to the varied binding affinity of different BPs [113, 293] as well as their anti-resorption capabilities. Additionally, varied doses of BPs cause differing affects on osteoblasts [134, 202, 237, 334, 335]. For example, higher doses of ALN have been shown to suppress osteoblast mineralization while lower doses promote it [203]. Differences in cell type (i.e. animal versus human derived osteoblasts) could also play a role in the varied affects BPs have on cell proliferation and differentiation. The affect of BPs on new bone formation is only beginning to be investigated because recent studies have suggested in addition to their actions on osteoclasts BPs may also affect osteoblasts.

Although results from previous studies has been contradictory, this work was designed to specifically examine the effects of RIS on osteoblasts and determine how newly formed bone composition was altered by this specific BP-treatment. While many groups have investigated the effects of BPs on osteoblasts, most have indirectly quantified collagen deposition and mineralization through measurements of markers of these processes. For example, mineralization can be correlated with OCN and ALP production. Further, collagen synthesis can be estimated via hydroxyproline measurements. To our knowledge, the chemical composition of mineralizing osteoblasts, treated with BPs, has not been previously probed using FTIRI. Further, deposition of collagen and mineral has not been spatially correlated in untreated and BP-treated cultures.

If RIS had the same effect on osteoblasts *in vivo* as it did in our *in vitro* study, decreased amounts of collagen and mineral could lead to decreased toughness and rigidity, respectively. Bone with low collagen content tends to be less ductile and have a lower tensile strength because of a reduction in cross-links [296]. Low collagen content has also been associated with more brittle bone [339]. Bone with low levels of mineral tends to have lower stiffness and strength [320].

Additionally, if protein prenylation is being slowed within the osteoblasts, this could lead to inactivation of the proteins required for the cell to function. This could cause osteoblast apoptosis, which would also lead to decreased collagen synthesis and mineralization. Because the mineralization and collagen deposition of control and RIS-treated cells is eventually similar, it is unlikely that the temporary lags seen here would influence the long term mechanics of newly formed bone, if the same trend was followed *in vivo*.

We have shown that RIS temporarily delays the collagen deposition and matrix mineralization of MC3T3-E1 cells. BPs are known to bind to HAP inhibiting its formation and dissolution [113, 116, 202, 203, 270], and may biologically affect HAP crystals. Additionally, they may have an effect on the interaction of the collagenous matrix and the mineral produced by osteoblasts [296]. Therefore,

it is possible that the temporary deposition delays we saw are caused by changes in the mineral and collagen morphology caused by BP-treatment.

V.IV The morphology of newly deposited mineral is not changed by RIS-treatment

BPs have been shown to bind to mineral and so we hypothesize that mineral structure could be altered in RIS-treated osteoblasts. Further we believed that the collagen fibril orientation of the matrix formed by MC3T3-E1 osteoblasts will not be altered by RIS-treatment. However, this study we showed that the morphology of the mineral formed by MC3T3-E1 osteoblasts was not altered by BP-treatment. Further, the mineral that the cells formed had a similar appearance to poorly crystalline HAP found in bone (**Chapter IV**). Alterations to mineral structure have been previously shown with BP-treatment [296, 314, 340, 341]. Specifically, BP-treatment has been shown to be correlated with both a decrease [314] and an increase [340, 341] in mineral crystal size. Additionally, they have been shown to arrest increases in crystallinity that normally occur with age [296] and increase the homogeneity of mineral crystals [340]. In our study we did not measure changes in mineral crystal size, and so we were unable to correlate our results with those previously reported. BPs have also been shown to bind to HAP [113] which could also lead to alterations in the morphology of the mineral crystals as they form.

While x-ray diffraction has been utilized to characterize the type and size of mineral MC3T3-E1 mouse osteoblasts form [40, 51, 55], the nanoscale morphology of the mineral has not been investigated. Further, it appears that nanoscale imaging of the interaction of the collagen fibers and mineral nodules has not previously been attempted. While we weren't able to image the collagen fibers, we were still able to visualize the poorly crystalline morphology of the mineral the MC3T3-E1 cells formed. Additionally we were able to demonstrate that the nanoscale crystal morphology of the mineral was not altered by BP-treatment.

A clear relationship between decreased bone microarchitecture and increased fracture has recently been demonstrated, showing the importance of

bone structure on fragility [79]. In normal bone, mineral crystals range in size from 5-60 nm [11, 19, 342, 343], have plate-like geometry [19, 20, 268], and are closely packed and parallel to one another [19-21]. As tissue ages, mineral crystal size and perfection increase [12, 188]. However, in any individual, there will be a broad distribution of mineral crystal sizes, because of ongoing remodeling [314]. Bone tissue will contain newly deposited and older mineral that will lead to variations in crystal size. This is in line with our finding; we saw that mineralization began (day 11) as areas of nanometer-sized (~1000 nm) granules, which aggregated together to form micrometer-sized nodules

Due to changes in ion substitutions, mineral crystal size and perfection are known to increase as bone matures [38, 183, 187, 290]. Changes in mineral morphology can be linked to decreased mechanical stability and increased fragility [226]. Alterations to mineral crystal size and shape could have lead to decreased elastic modulus and strength [226]. Larger and more crystalline minerals have been shown in osteoporosis [71-73, 178], demonstrating larger crystals are associated with more brittle tissue. Larger crystals would also tend to reduce the stiffness of the bone [284]. Further, in diseased states (such as osteogenesis imperfecta), mineral shape has been shown to change [21]. Further, elastic modulus has been significantly correlated to tissue crystallinity in maturing mouse tissue [188]. Therefore, had our studies shown that the mineral morphology was altered by BP-treatment, changes to the mechanical integrity and fragility of the tissue could have also been expected.

Further, solubility, hardness, brittleness, and thermal stability of the tissue can be changed when ion substitutions occur [291, 292], ultimately affecting the overall fragility of the bone tissue. For example, when carbonate (CO_3^{2-}) replaces phosphate (PO_4^{3-}) [291, 330] the bone lattice becomes less stable, because carbonated apatites are more likely to dissolve when compared to unsubstituted HAP [35-37]. Additionally when fluoride was used to treat osteoporosis, crystal structure was altered [344, 345], decreasing elasticity and bone strength and thereby increasing fracture risk, [43-45].

Changes to collagen fibril organization can also contribute to mechanical instability. Disorganized and altered collagen structure has been shown in osteoporotic tissue [14, 17, 280]. Variations in collagen fibril orientation are linked to variations in bone elastic modulus [278]. For example less longitudinally oriented collagen fibrils leads to decreased strength [346]. Therefore, it is clear that the organization of the bone matrix plays a significant mechanical role in bone fragility [15, 16]. Alterations to the collagen fibril organization could also have implications on the mechanics of newly formed mineral. Additional studies, where visualization of the collagen fibril organization are necessary in order to rule out this mechanism as a possible long term effect of BP-treatment.

While BPs have been shown to have many effects on the mechanics of bone tissue, which could be related to alterations in mineral morphology, we saw no such evidence in our studies (**Chapter IV**). While a temporary lag in new mineral formation was seen with RIS-treatment, this was not permanent and did not appear to be a result of morphological changes in mineral. While BP-treatment did not appear to alter the structure of newly forming tissue, it does cause increased damage and compositional changes to existing tissue that could compromise mechanical stability and lead to increased fragility.

V.V Summary

The concept that bone composition and structure can alter mechanical properties of the tissue becomes important in assessing the overall positive effects of this current treatment for osteoporosis. We have shown that BP-treatment does not affect the chemical composition of existing or newly formed bone tissue, which could have lead to compromised mechanical properties. Further, the structure of newly forming mineral is not altered by RIS-treatment. However, the structure of existing tissue is afflicted in that microdamage accumulation is increased which, if not paired with increases in mineralization, could lead to compromised mechanical properties and increased fragility with long term BP treatment.

Chapter VI: Conclusion

VI.I Limitations

Existing Bone

While microdamage accumulation has been demonstrated in patients undergoing BP-treatment [232], the dose that was administered in the microdamage studies was 5-6 times the clinical daily dose. This was done so that assessment of long term microdamage accumulation could be performed. However, similar levels of microdamage accumulation may not be seen in humans because of lower administered doses. Additionally, while we hypothesized that compositional changes were attributed to microcrack formation and not the cause of it, we were unable to confirm that this was precisely the case.

Newly Formed Mineral

Outcomes of BP-treatment *in vitro* and even *in vivo* in animals are hard to extrapolate to effects that would occur within the human body. In the body, bone formation is coupled to bone resorption through interactions of osteoblasts, osteoclasts, and the surface of bone undergoing remodeling. *In vivo*, osteoclasts are exposed to higher amounts of BP than osteoblasts [276], and even then osteoblasts are only exposed to BPs that have been released from the bone surface by the action of osteoclasts. Therefore it is hard to determine what effect BPs would have on osteoblasts within the body, when only studied as a one component system.

Additionally, it is difficult to determine what concentration of BPs osteoblasts and other cells are exposed to *in vivo* because each BP has a different binding affinity for bone. The skeletal retention of BPs is very long and at any given time various concentrations of BPs could be in the blood stream depending on whether bone resorption is occurring in areas of the tissue that have bound BPs.

While we anticipated being able to view the collagen fibers, using phase contrast nano-TXM, within our system, density similarities between air and the

matrix made this difficult. And so we were also unable to determine if the mineral we were studying was supported by a collagenous matrix. This is a significant limitation of the x-ray study, as it was possible we were examining ectopic mineral and not matrix-associated mineral. Only mineral supported by a collagenous matrix is representative of woven bone.

VI.II Future Work

Future work in understanding how BPs affect the whole remodeling process are important to determine how long term osteoporosis treatment could alter bone mechanics and fragility.

Bone remodeling is a process that involves the coupled action of osteoclasts and osteoblasts. Therefore a system where active remodeling is occurring would be more relevant to understand how BPs affect the overall physiology, composition, and quality of the resulting tissue. Future work should be performed in an *in vitro* system of osteoblasts, osteoclasts and a remodeling surface, to more accurately depict what is occurring in the human body. This would lead to a clearer and more precise understanding of how BPs would affect each step of the remodeling process. Additionally we did not study the effects of BPs on human osteoblast cells. Repeating the current study, using a human osteoblasts cell line, may yield different results that are more applicable to clinical outcomes.

We were only able to postulate why RIS-treatment slowed the mineral and collagen deposition timeline in the cells. The ability to see the location of the BPs *in vitro* and even *in vivo* could help determine how treatment affects existing bone and bone formation. Fluorescently and near infrared labeled BPs have recently been created and experiments with these tagged BPs would be helpful to understand how BPs bind to bone and interact with bone remodeling cells. This could ultimately lead to an understanding of the mechanism by which BPs affect bone composition and structure.

Additionally, as we were not able to view the collagen within the mineralizing osteoblasts, it would be helpful to examine ways in which the phase contrast of the collagen within the culture could be viewed using nano-TXM. One

option would be to find a way to tag the collagen fibers with gold nanoparticles. The particles would have a high phase contrast and would therefore highlight where the collagen fibers were located.

Lastly, *in vivo* animal studies need to be carried out, using clinical doses of BPs to determine how new bone formation is affected by treatment. The use of tagged BPs, as mentioned above, help to determine how the drugs interact with osteoblasts and what role they play in new bone formation. Fluorochrome labels, such as oxytetracyline, calcein alizarin and xylenol, could also be used so that bone composition and structure can be examined as a function of age and drug-treatment.

VI.III Summary

The major goal of this thesis was to determine if BP-treatment had any effect on the chemical composition or morphology of existing and newly formed bone tissue. This was achieved through two specific aims; one examining the chemical composition and structure of existing bone treated with ALN or RIS and comparing it to control tissue, and the other determining how the collagen and mineral deposition of osteoblasts was affected by treatment. Results of this research can help to understand how BPs, which are designed to help combat bone fragility, might alter bone mechanics through chemical and structural changes during long term treatment.

We have shown that ALN and RIS treatment do not alter the chemical composition of existing bone, changing its mechanical properties and making it more fragile. However, chemical composition is altered due to the accumulation of microdamage within treated tissue. Microdamage leads to collagen breakage and dissolution of mineral within the crack and could ultimately lead to bone with decreased toughness, stiffness and elastic modulus.

Additionally, RIS-treatment causes a temporary lag in the deposition of collagen and mineral, by osteoblast cells. Because the delays were seen in both the collagen deposition and mineralization, it appears that the RIS altered the activity and function of the osteoblasts. Collagen deposition, which is needed for mineralization to occur, could have been slowed by a build up of unprenylated

proteins within the osteoblast. Further a lack of a collagenous-matrix would delay the release of osteoblast marker genes and slow mineralization. This lag could lead to decreased mechanical stability of the tissue and increased fragility if similar trends are followed *in vivo*. While the structure of newly formed mineral is not affected by BP-treatment, accumulation of microdamage in existing tissue, along with compositional changes that occur as a result of microdamage, could eventually lead to mechanical instability and fragility in the tissue.

While it is hard to directly extrapolate these results to the clinical setting, it does suggest that further studies need to be carried out to determine if BP-treatment, designed to specifically decrease fracture risk, could eventually lead to tissue with increased fragility.

Bibliography

1. Lakes, R., Materials with Structural Hierarchy. *Nature*, 1993. **361**(6412): p. 511-515.

2. Rho, J.Y., L. Kuhn-Spearing, and P. Zioupos, Mechanical properties and the hierarchical structure of bone. *Med Eng Phys*, 1998. **20**(2): p. 92-102.

3. Weiner, S. and W. Traub, Bone-Structure - from Angstroms to Microns. *Faseb Journal*, 1992. **6**(3): p. 879-885.

4. Wopenka, B. and J.D. Pasteris, A mineralogical perspective on the apatite in bone. *Mat Sci Eng C-Biomim*, 2005. **25**(2): p. 131-143.

5. Boskey, A.L., T.M. Wright, and R.D. Blank, Collagen and Bone Strength. *J. Bone Min. Res.*, 1999. **14**(3): p. 330-333.

6. McCalden, R.W., et al., Age-related changes in the tensile properties of cortical bone. The relative importance of changes in porosity, mineralization, and microstructure. *J Bone Joint Surg Am*, 1993. **75**(8): p. 1193-205.

7. Danielsen, C.C., T.T. Andreassen, and L. Mosekilde, Mechanical properties of collagen from decalcified rat femur in relation to age and in vitro maturation. *Calcif Tissue Int*, 1986. **39**(2): p. 69-73.

8. Oxlund, H., et al., Reduced concentrations of collagen cross-links are associated with reduced strength of bone. *Bone*, 1995. **17**(4 Suppl): p. 365S-371S.

9. Arsenault, A.L., Crystal-collagen relationships in calcified turkey leg tendons visualized by selected-area dark field electron microscopy. *Calcif Tissue Int*, 1988. **43**(4): p. 202-12.

10. Robinson, R.A., An electron-microscopic study of the crystalline inorganic component of bone and its relationship to the organic matrix. *J Bone Joint Surg Am*, 1952. **34-A**(2): p. 389-435; passim.

11. Rubin, M.A., et al., TEM analysis of the nanostructure of normal and osteoporotic human trabecular bone. *Bone*, 2003. **33**(3): p. 270-82.

12. Weiner, S. and W. Traub, Crystal size and organization in bone. *Connect Tissue Res*, 1989. **21**(1-4): p. 259-65.

13. Adachi, E., I. Hopkinson, and T. Hayashi, Basement-membrane stromal relationships: interactions between collagen fibrils and the lamina densa. *Int Rev Cytol*, 1997. **173**: p. 73-156.

14. Tzaphlidou, M. and H. Kafantari, Influence of nutritional factors on bone collagen fibrils in ovariectomized rats. *Bone*, 2000. **27**(5): p. 635-8.

15. Evans, F.G. and R. Vincentelli, Relation of collagen fiber orientation to some mechanical properties of human cortical bone. *J Biomech*, 1969. **2**(1): p. 63-71.

16. Reilly, D.T., A.H. Burstein, and V.H. Frankel, The elastic modulus for bone. *J Biomech*, 1974. **7**(3): p. 271-5.

17. Kafantari, H., et al., Structural alterations in rat skin and bone collagen fibrils induced by ovariectomy. *Bone*, 2000. **26**(4): p. 349-53.

18. Kounadi, E., G. Fountos, and M. Tzaphlidou, The influence of inflammation-mediated osteopenia (IMO) on the structure of rabbit bone and skin collagen fibrils. *Connect Tissue Res*, 1998. **37**(1-2): p. 69-76.

19. Eppell, S.J., et al., Shape and size of isolated bone mineralites measured using atomic force microscopy. *J Orthop Res*, 2001. **19**(6): p. 1027-34.

20. Jackson, S.A., A.G. Cartwright, and D. Lewis, The morphology of bone mineral crystals. *Calcif Tissue Res*, 1978. **25**(3): p. 217-22.

21. Landis, W.J., The strength of a calcified tissue depends in part on the molecular structure and organization of its constituent mineral crystals in their organic matrix. *Bone*, 1995. **16**(5): p. 533-44.

22. Fratzl, P., et al., Nucleation and growth of mineral crystals in bone studied by small-angle X-ray scattering. *Calcif Tissue Int*, 1991. **48**(6): p. 407-13.

23. Hassenkam, T., et al., High-resolution AFM imaging of intact and fractured trabecular bone. *Bone*, 2004. **35**(1): p. 4-10.

24. Landis, W.J., et al., Structural relations between collagen and mineral in bone as determined by high voltage electron microscopic tomography. *Microsc Res Tech*, 1996. **33**(2): p. 192-202.

25. Tong, W., et al., Size and shape of mineralites in young bovine bone measured by atomic force microscopy. *Calcif Tissue Int*, 2003. **72**(5): p. 592-8.

26. Rinnerthaler, S., et al., Scanning small angle X-ray scattering analysis of human bone sections. *Calcif Tissue Int*, 1999. **64**(5): p. 422-9.

27. Wolff, J., Uber die innere Architectur der knochen und ihre Bedeutung fur die Fragen vom Knochenwachsthum. *Archiv fur pathologische Anatomie und Physiologie*, 1870. **50**: p. 389-450.

28. Fratzl, P., et al., Abnormal bone mineralization after fluoride treatment in osteoporosis: a small-angle x-ray-scattering study. *J Bone Miner Res*, 1994. **9**(10): p. 1541-9.

29. Gao, H., et al., Materials become insensitive to flaws at nanoscale: lessons from nature. *Proc Natl Acad Sci U S A*, 2003. **100**(10): p. 5597-600.

30. Gupta, H.S., et al., Nanoscale deformation mechanisms in bone. *Nano Letters*, 2005. **5**(10): p. 2108-2111.

31. Legros, R.Z., N. Balmain, and G. Bonel, Structure and Composition of the Mineral Phase of Periosteal Bone. *J Chem Res-S*, 1986. **1**: p. 8-9.

32. Pellegrino, E. and R. Blitz, Mineralization in the chick embroyo. I. Monohydrogen phosphate and carbonate relationships during maturation of the bone crystal complex. *Calcified Tissue Res*, 1971: p. 128-135.

33. Rey, C., et al., The carbonate environment in bone mineral: a resolution-enhanced Fourier Transform Infrared Spectroscopy Study. *Calcif Tissue Int*, 1989. **45**(3): p. 157-64.

34. Rey, C., et al., Fourier transform infrared spectroscopic study of the carbonate ions in bone mineral during aging. *Calcif Tissue Int*, 1991. **49**(4): p. 251-8.

35. Baig, A.A., et al., Relationships among carbonated apatite solubility, crystallite size, and microstrain parameters. *Calcif Tissue Int*, 1999. **64**(5): p. 437-49.

36. LeGeros, R.Z. and M.S. Tung, Chemical stability of carbonate- and fluoride-containing apatites. *Caries Res*, 1983. **17**(5): p. 419-29.

37. Nelson, D.G., et al., Effect of carbonate and fluoride on the dissolution behaviour of synthetic apatites. *Caries Res*, 1983. **17**(3): p. 200-11.

38. Gadaleta, S.J., et al., Fourier transform infrared spectroscopy of the solution-mediated conversion of amorphous calcium phosphate to hydroxyapatite: new correlations between X-ray diffraction and infrared data. *Calcif Tissue Int*, 1996. **58**(1): p. 9-16.

39. Huang, R.Y., et al., Characterization of bone mineral composition in the proximal tibia of cynomolgus monkeys: effect of ovariectomy and nandrolone decanoate treatment. *Bone*, 2002. **30**(3): p. 492-7.

40. Rey, C., et al., Structural and chemical characteristics and maturation of the calcium- phosphate crystals formed during the calcification of the organic matrix synthesized by chicken osteoblasts in cell culture. *J Bone Miner Res*, 1995. **10**(10): p. 1577-88.

41. Kleerekoper, M., The role of fluoride in the prevention of osteoporosis. *Endocrinol Metab Clin North Am*, 1998. **27**(2): p. 441-52.

42. Lau, K.H., et al., A proposed mechanism of the mitogenic action of fluoride on bone cells: inhibition of the activity of an osteoblastic acid phosphatase. *Metabolism*, 1989. **38**(9): p. 858-68.

43. Gambacciani, M., et al., Treatment of postmenopausal vertebral osteopenia with monofluorophospate: a long-term calcium-controlled study. *Osteoporos Int*, 1995. **5**(6): p. 467-71.

44. Haguenauer, D., et al., Fluoride for the treatment of postmenopausal osteoporotic fractures: a meta-analysis. *Osteoporos Int*, 2000. **11**(9): p. 727-38.

45. Meunier, P.J., et al., Fluoride salts are no better at preventing new vertebral fractures than calcium-vitamin D in postmenopausal osteoporosis: the FAVOStudy. *Osteoporos Int*, 1998. **8**(1): p. 4-12.

46. Riggs, B.L., et al., Effect of fluoride treatment on the fracture rate in postmenopausal women with osteoporosis. *N Engl J Med*, 1990. **322**(12): p. 802-9.

47. Campbell, J.R., et al., The association between environmental lead exposure and bone density in children. *Environ Health Perspect*, 2004. **112**(11): p. 1200-3.

48. Escribano, A., et al., Effect of lead on bone development and bone mass: a morphometric, densitometric, and histomorphometric study in growing rats. *Calcif Tissue Int*, 1997. **60**(2): p. 200-3.

49. Gruber, H.E., et al., Osteopenia induced by long-term, low- and high-level exposure of the adult rat to lead. *Miner Electrolyte Metab*, 1997. **23**(2): p. 65-73.

50. Aronow, M.A. and L.C. Gerstenfeld, Culture conditions requisite for maximal expression of the osteoblast phenotype. *J Bone Miner Res*, 1988. **3**(Suppl 1): p. S136.

51. Franceschi, R.T. and B.S. Iyer, Relationship between collagen synthesis and expression of the osteoblast phenotype in MC3T3-E1 cells. *J Bone Miner Res*, 1992. **7**(2): p. 235-46.

52. Glimcher, M.J., A.J. Hodge, and F.O. Schmitt, Macromolecular Aggregation States in Relation to Mineralization: The Collagen-Hydroxyapatite System as Studied in Vitro. *Proc Natl Acad Sci U S A*, 1957. **43**(10): p. 860-7.

53. Sudo, H., et al., In vitro differentiation and calcification in a new clonal osteogenic cell line derived from newborn mouse calvaria. *J Cell Biol*, 1983. **96**(1): p. 191-8.

54. Gokhale, J., P.G. Robey, and A.L. Boskey, The biochemistry of bone, in *Osteoporosis*, R. Marcus, D. Feldman, and J. Kelsey, Editors. 2001, Academic Press: San Diego.

55. Meng, Y., et al., Biomineralization of a Self-Assembled Extracellular Matrix for Bone Tissue Engineering. *Tissue Eng Part A*, 2008.

56. Marieb, E., Human Anatomy and Physiology. 4 ed, ed. L. Fogel. 1998, Menlo Park: Benjamin/Cummings Science Publishing.

57. Parfitt, A.M., Bone remodeling and bone loss: understanding the pathophysiology of osteoporosis. *Clin Obstet Gynecol*, 1987. **30**(4): p. 789-811.

58. Marotti, G., A. Favia, and A.Z. Zallone, Quantitative analysis on the rate of secondary bone mineralization. *Calcif Tissue Res*, 1972. **10**(1): p. 67-81.

59. Wergedal, J.E. and D.J. Baylink, Electron microprobe measurements of bone mineralization rate in vivo. *Am J Physiol*, 1974. **226**(2): p. 345-52.

60. Amprino, R. and A. Engstrom, Studies on x ray absorption and diffraction of bone tissue. *Acta Anat (Basel)*, 1952. **15**(1-2): p. 1-22.

61. Akkus, O., et al., Aging of microstructural compartments in human compact bone. *J Bone Miner Res*, 2003. **18**(6): p. 1012-9.

62. Huang, R.Y., et al., In situ chemistry of osteoporosis revealed by synchrotron infrared microspectroscopy. *Bone*, 2003. **33**(4): p. 514-21.

63. Wang, D., et al., Isolation and characterization of MC3T3-E1 preosteoblast subclones with distinct in vitro and in vivo differentiation/mineralization potential. *J Bone Miner Res*, 1999. **14**(6): p. 893-903.

64. Schwarz, R.I., P. Kleinman, and N. Owens, Ascorbate can act as an inducer of the collagen pathway because most steps are tightly coupled. *Ann N Y Acad Sci*, 1987. **498**: p. 172-85.

65. Marsh, M.E., et al., Mineralization of bone-like extracellular matrix in the absence of functional osteoblasts. *J Bone Miner Res*, 1995. **10**(11): p. 1635-43.

66. Anderson, H.C., R. Garimella, and S.E. Tague, The role of matrix vesicles in growth plate development and biomineralization. *Front Biosci*, 2005. **10**: p. 822-37.

67. Anderson, H.C., Molecular biology of matrix vesicles. *Clin Orthop Relat Res*, 1995(314): p. 266-80.

68. Anderson, H.C., Matrix vesicles and calcification. *Curr Rheumatol Rep*, 2003. **5**(3): p. 222-6.

69. Jepsen, K.J., et al., Type I collagen mutation alters the strength and fatigue behavior of Mov13 cortical tissue. *J Biomech*, 1997. **30**(11-12): p. 1141-7.

70. Kozloff, K.M., et al., Brittle IV mouse model for osteogenesis imperfecta IV demonstrates postpubertal adaptations to improve whole bone strength. *J Bone Miner Res*, 2004. **19**(4): p. 614-22.

71. Gadeleta, S.J., et al., A physical, chemical, and mechanical study of lumbar vertebrae from normal, ovariectomized, and nandrolone decanoate-treated cynomolgus monkeys (Macaca fascicularis). *Bone*, 2000. **27**(4): p. 541-50.

72. Burnell, J.M., et al., Bone matrix and mineral abnormalities in postmenopausal osteoporosis. *Metabolism*, 1982. **31**(11): p. 1113-20.

73. Thompson, D.D., et al., Comparison of bone apatite in osteoporotic and normal Eskimos. *Calcif Tissue Int*, 1983. **35**(3): p. 392-3.

74. WHO, Prevention and Management of Osteoporosis. Report of a WHO Scientific Group. 2003, Geneva, Switzerland: WHO Technical Report Series, No 921.

75. Peck, W.A., P. Burkhardt, and C. Christiansen, Consensus development conference: diagnosis, prophylaxis, and treatment of osteoporosis. *Am J Med*, 1993. **94**(6): p. 646-50.

76. Cooper, C., Epidemiology of Osteoporosis, in *Primer on the Metabolic Bone Diseases and Disorders of Mineral Metabolism*, M.J. Favus, Editor. 2003, American Society of Bone and Mineral Research.

77. Barou, O., et al., High-resolution three-dimensional micro-computed tomography detects bone loss and changes in trabecular architecture early: comparison with DEXA and bone histomorphometry in a rat model of disuse osteoporosis. *Invest Radiol*, 2002. **37**(1): p. 40-6.

78. Chappard, D., et al., Bone microarchitecture in males with corticosteroid-induced osteoporosis. *Osteoporos Int*, 2006.

79. Genant, H.K., et al., Severity of vertebral fracture reflects deterioration of bone microarchitecture. *Osteoporos Int*, 2007. **18**(1): p. 69-76.

80. Laib, A., et al., 3D micro-computed tomography of trabecular and cortical bone architecture with application to a rat model of immobilisation osteoporosis. *Med Biol Eng Comput*, 2000. **38**(3): p. 326-32.

81. Chesnut, I.C., et al., Effects of oral ibandronate administered daily or intermittently on fracture risk in postmenopausal osteoporosis. *J Bone Miner Res*, 2004. **19**(8): p. 1241-9.

82. Ensrud, K.E., et al., Treatment with Alendronate Prevents Fractures in women at highest risk: results from the Fracture Intervention Trial. *Arch Intern Med*, 1997. **157**: p. 2617-2624.

83. Ettinger, B., et al., Reduction of vertebral fracture risk in postmenopausal women with osteoporosis treated with raloxifene: results from a 3-year randomized clinical trial. Multiple Outcomes of Raloxifene Evaluation (MORE) Investigators. *Jama*, 1999. **282**(7): p. 637-45.

84. Harrington, J.T., et al., Risedronate rapidly reduces the risk for nonvertebral fractures in women with postmenopausal osteoporosis. *Calcif Tissue Int*, 2004. **74**(2): p. 129-35.

85. Harris, S.T., et al., Effects of risedronate treatment on vertebral and nonvertebral fractures in women with postmenopausal osteoporosis: a randomized controlled trial. Vertebral Efficacy With Risedronate Therapy (VERT) Study Group. *Jama*, 1999. **282**(14): p. 1344-52.

86. Stewart, A., et al., Bone density and bone turnover in patients with osteoarthritis and osteoporosis. *J Rheumatol*, 1999. **26**(3): p. 622-6.

87. Kanis, J.A., et al., Ten year probabilities of osteoporotic fractures according to BMD and diagnostic thresholds. *Osteoporos Int*, 2001. **12**(12): p. 989-95.

88. Garnero, P., et al., Increased bone turnover in late postmenopausal women is a major determinant of osteoporosis. *J Bone Miner Res*, 1996. **11**(3): p. 337-49.

89. De Laet, C.E., et al., Bone density and risk of hip fracture in men and women: cross sectional analysis. *Bmj*, 1997. **315**(7102): p. 221-5.

90. Schuit, S.C., et al., Fracture incidence and association with bone mineral density in elderly men and women: the Rotterdam Study. *Bone*, 2004. **34**(1): p. 195-202.

91. Currey, J.D., The mechanical consequences of variation in the mineral content of bone. *J Biomech*, 1969. **2**: p. 1-11.

92. Currey, J.D., The relationship between stiffness and the mineral content of bone. *J Biomech*, 1969. **2**: p. 477-480.

93. Currey, J.D., The Effect of Porosity and Mineral-Content on the Youngs Modulus of Elasticity of Compact-Bone. *J Biomech*, 1988. **21**(2): p. 131-139.

94. Currey, J.D., Role of collagen and other organics in the mechanical properties of bone. *Osteoporos Int*, 2003. **14**: p. S29-S36.

95. Vose, G. and A. Kubala, Bone Strength-Ots relationship to x-ray determined ash content. *Human Biology*, 1959. **31**: p. 261-2790.

96. Sherman, S. and E.C. Hadley, Aging and bone quality: an underexplored frontier. *Calcif Tissue Int*, 1993. **53 Suppl 1**: p. S1.

97. Marshall, D., O. Johnell, and H. Wedel, Meta-analysis of how well measures of bone mineral density predict occurrence of osteoporotic fractures. *Bmj*, 1996. **312**(7041): p. 1254-9.

98. Judex, S., et al., Combining high-resolution micro-computed tomography with material composition to define the quality of bone tissue. *Curr Osteoporos Rep*, 2003. **1**(1): p. 11-9.

99. Hong, H., et al., Effect of Risedronate on Bone Strength and Work to Failure Determined by Simulation of Clinically-Measured Bone Loss and Mineralization Changes and FEA. *J Bone Miner Res*, 2008. **23**(S1).

100. Boivin, G.Y., et al., Alendronate increases bone strength by increasing the mean degree of mineralization of bone tissue in osteoporotic women. *Bone*, 2000. **27**(5): p. 687-94.

101. Meunier, P.J. and G. Boivin, Bone mineral density reflects bone mass but also the degree of mineralization of bone: therapeutic implications. *Bone*, 1997. **21**(5): p. 373-7.

102. Fisher, J.E., et al., Alendronate mechanism of action: geranylgeraniol, an intermediate in the mevalonate pathway, prevents inhibition of osteoclast formation, bone resorption, and kinase activation in vitro. *Proc Natl Acad Sci U S A*, 1999. **96**(1): p. 133-8.

103. Fisher, L.W., et al., Osteonectin content in human osteogenesis imperfecta bone shows a range similar to that of two bovine models of OI. *Calcif Tissue Int*, 1987. **40**(5): p. 260-4.

104. Hughes, D.E., et al., Bisphosphonates promote apoptosis in murine osteoclasts in vitro and in vivo. *J Bone Miner Res*, 1995. **10**(10): p. 1478-87.

105. Luckman, S.P., et al., Nitrogen-containing bisphosphonates inhibit the mevalonate pathway and prevent post-translational prenylation of GTP-binding proteins, including Ras. *J Bone Miner Res*, 1998. **13**(4): p. 581-9.

106. Rogers, M.J., et al., Molecular mechanisms of action of bisphosphonates. *Bone*, 1999. **24**: p. 73S-79S.

107. Frith, J.C., et al., Clodronate and liposome-encapsulated clodronate are metabolized to a toxic ATP analog, adenosine 5'-(beta, gamma-dichloromethylene) triphosphate, by mammalian cells in vitro. *J Bone Miner Res*, 1997. **12**(9): p. 1358-67.

108. Reszka, A.A. and G.A. Rodan, Bisphosphonate mechanism of action. *Curr Rheumatol Rep*, 2003. **5**(1): p. 65-74.

109. Watts, N., Bisphosphonates, statins, osteoporosis, and atherosclerosis. *South Med J*, 2002. **95**(6): p. 578-82.

110. Sato, M., et al., Bisphosphonate action. Alendronate localization in rat bone and effects on osteoclast ultrastructure. *J Clin Invest*, 1991. **88**(6): p. 2095-105.

111. Azuma, Y., et al., Alendronate distributed on bone surfaces inhibits osteoclastic bone resorption in vitro and in experimental hypercalcemia models. *Bone*, 1995. **16**(2): p. 235-45.

112. Masarachia, P., et al., Comparison of the distribution of 3H-alendronate and 3H-etidronate in rat and mouse bones. *Bone*, 1996. **19**(3): p. 281-90.

113. Nancollas, G.H., et al., Novel insights into actions of bisphosphonates on bone: differences in interactions with hydroxyapatite. *Bone*, 2006. **38**(5): p. 617-27.

114. Monkkonen, J. and P. Ylitalo, The tissue distribution of clodronate (dichloromethylene bisphosphonate) in mice. The effects of vehicle and the route of administration. *Eur J Drug Metab Pharmacokinet*, 1990. **15**(3): p. 239-43.

115. Fleisch, H., R.G. Russell, and M.D. Francis, Diphosphonates inhibit hydroxyapatite dissolution in vitro and bone resorption in tissue culture and in vivo. *Science*, 1969. **165**(899): p. 1262-4.

116. Francis, M.D., R.G. Russell, and H. Fleisch, Diphosphonates inhibit formation of calcium phosphate crystals in vitro and pathological calcification in vivo. *Science*, 1969. **165**(899): p. 1264-6.

117. Fleisch, H., Bisphosphonates--history and experimental basis. *Bone*, 1987. **8 Suppl 1**: p. S23-8.

118. Chavassieux, P.M., et al., Histomorphometric assessment of the long-term effects of alendronate on bone quality and remodeling in patients with osteoporosis. *J Clin Invest*, 1997. **100**(6): p. 1475-80.

119. Delmas, P.D., How does antiresorptive therapy decrease the risk of fracture in women with osteoporosis? *Bone*, 2000. **27**(1): p. 1-3.

120. Rosen, C.J., et al., Treatment with once-weekly alendronate 70 mg compared with once-weekly risedronate 35 mg in women with postmenopausal osteoporosis: a randomized double-blind study. *J Bone Miner Res*, 2005. **20**(1): p. 141-51.

121. Burr, D.B., et al., Tissue mineralization is increased following 1-year treatment with high doses of bisphosphonates in dogs. *Bone*, 2003. **33**(6): p. 960-9.

122. Mashiba, T., et al., Suppressed bone turnover by bisphosphonates increases microdamage accumulation and reduces some biomechanical properties in dog rib. *J Bone Miner Res*, 2000. **15**(4): p. 613-20.

123. Mashiba, T., et al., Effects of suppressed bone turnover by bisphosphonates on microdamage accumulation and biomechanical properties in clinically relevant skeletal sites in beagles. *Bone*, 2001. **28**(5): p. 524-31.

124. Halasy-Nagy, J.M., G.A. Rodan, and A.A. Reszka, Inhibition of bone resorption by alendronate and risedronate does not require osteoclast apoptosis. *Bone*, 2001. **29**(6): p. 553-9.

125. Dunford, J.E., et al., Structure-activity relationships for inhibition of farnesyl diphosphate synthase in vitro and inhibition of bone resorption in

vivo by nitrogen-containing bisphosphonates. *J Pharmacol Exp Ther*, 2001. **296**(2): p. 235-42.

126. Coxon, F.P., et al., Visualizing mineral binding and uptake of bisphosphonate by osteoclasts and non-resorbing cells. *Bone*, 2008. **42**(5): p. 848-60.

127. Fisher, J.E., G.A. Rodan, and A.A. Reszka, In vivo effects of bisphosphonates on the osteoclast mevalonate pathway. *Endocrinology*, 2000. **141**(12): p. 4793-6.

128. Fleisch, H., Bisphosphonates in osteoporosis: an introduction. *Osteoporos Int*, 1993. **3 Suppl 3**: p. S3-5.

129. Ono, K. and S. Wada, [Regulation of calcification by bisphosphonates]. *Clin Calcium*, 2004. **14**(6): p. 60-3.

130. Williams, G. and J.D. Sallis, Structural factors influencing the ability of compounds to inhibit hydroxyapatite formation. *Calcif Tissue Int*, 1982. **34**(2): p. 169-77.

131. Iwata, K., et al., Bisphosphonates suppress periosteal osteoblast activity independently of resorption in rat femur and tibia. *Bone*, 2006. **39**(5): p. 1053-8.

132. Vitte, C., H. Fleisch, and H.L. Guenther, Bisphosphonates induce osteoblasts to secrete an inhibitor of osteoclast-mediated resorption. *Endocrinology*, 1996. **137**(6): p. 2324-33.

133. Fromigue, O. and J.J. Body, Bisphosphonates influence the proliferation and the maturation of normal human osteoblasts. *J Endocrinol Invest*, 2002. **25**(6): p. 539-46.

134. Igarashi, K., et al., Effects of bisphosphonates on alkaline phosphatase activity, mineralization, and prostaglandin E2 synthesis in the clonal osteoblast-like cell line MC3T3-E1. *Prostaglandins Leukot Essent Fatty Acids*, 1997. **56**(2): p. 121-5.

135. Reinholz, G.G., et al., Bisphosphonates directly regulate cell proliferation, differentiation, and gene expression in human osteoblasts. *Cancer Res*, 2000. **60**(21): p. 6001-7.

136. Allen, M.R., et al., Antiremodeling agents influence osteoblast activity differently in modeling and remodeling sites of canine rib. *Calcif Tissue Int*, 2006. **79**(4): p. 255-61.

137. Tobias, J.H., J.W. Chow, and T.J. Chambers, 3-Amino-1-hydroxypropylidine-1-bisphosphonate (AHPrBP) suppresses not only the induction of new, but also the persistence of existing bone-forming surfaces in rat cancellous bone. *Bone*, 1993. **14**(4): p. 619-23.

138. Gasser, A.B., et al., The influence of two diphosphonates on calcium metabolism in the rat. *Clin Sci*, 1972. **43**(1): p. 31-45.

139. Reitsma, P.H., et al., Kinetic studies of bone and mineral metabolism during treatment with (3-amino-1-hydroxypropylidene)-1,1-bisphosphonate (APD) in rats. *Calcif Tissue Int*, 1980. **32**(2): p. 145-57.

140. Burr, D.B., et al., Bone remodeling in response to in vivo fatigue microdamage. *J Biomech*, 1985. **18**(3): p. 189-200.

141. Li, J., T. Mashiba, and D.B. Burr, Bisphosphonate treatment suppresses not only stochastic remodeling but also the targeted repair of microdamage. *Calcif Tissue Int*, 2001. **69**(5): p. 281-6.

142. Mori, S. and D.B. Burr, Increased intracortical remodeling following fatigue damage. *Bone*, 1993. **14**(2): p. 103-9.

143. Zioupos, P. and J.D. Currey, The Extent of Microcracking and the Morphology of Microcracks in Damaged Bone. *J Mat Sci*, 1994. **29**(4): p. 978-986.

144. Schaffler, M.B., K. Choi, and C. Milgrom, Aging and matrix microdamage accumulation in human compact bone. *Bone*, 1995. **17**(6): p. 521-525.

145. Taylor, D. and T.C. Lee, Microdamage and mechanical behaviour: predicting failure and remodelling in compact bone. *J Anat*, 2003. **203**(2): p. 203-11.

146. Sahar, N.D., S.I. Hong, and D.H. Kohn, Micro- and nano-structural analyses of damage in bone. *Micron*, 2005.

147. Norman, T.L. and Z. Wang, Microdamage of human cortical bone: incidence and morphology in long bones. *Bone*, 1997. **20**(4): p. 375-9.

148. Frost, H.M., Presence of microscopic crack in vivo in bone. *H Ford Hosp Med Bull*, 1960. **8**: p. 27-35.

149. Burr, D.B. and R.B. Martin, Calculating the probability that microcracks initiate resorption spaces. *J Biomech*, 1993. **26**(4-5): p. 613-6.

150. Burr, D.B. Damage detection and behavior in bone. in *12th Conference of the European Society of Biomechanics*. 2000. Dublin: Royal Academy of Medicine in Ireland.

151. Bentolila, V., et al., Intracortical remodeling in adult rat long bones after fatigue loading. *Bone*, 1998. **23**(3): p. 275-81.

152. Burr, D.B., et al., Bone microdamage and skeletal fragility in osteoporotic and stress fractures. *J Bone Miner Res*, 1997. **12**(1): p. 6-15.

153. Mori, S., R. Harruff, and D.B. Burr, Microcracks in articular calcified cartilage of human femoral heads. *Arch Pathol Lab Med*, 1993. **117**(2): p. 196-8.

154. Burr, D.B. and T. Stafford, Validity of the bulk-staining technique to separate artifactual from in vivo bone microdamage. *Clin Orthop Relat Res*, 1990(260): p. 305-8.

155. Schaffler, M.B., E.L. Radin, and D.B. Burr, Mechanical and morphological effects of strain rate on fatigue of compact bone. *Bone*, 1989. **10**(3): p. 207-14.

156. Boyce, T.M., et al., Damage type and strain mode associations in human compact bone bending fatigue. *J Orthop Res*, 1998. **16**(3): p. 322-9.

157. Reilly, G.C. and J.D. Currey, The development of microcracking and failure in bone depends on the loading mode to which it is adapted. *J Exp Biol*, 1999. **202**(Pt 5): p. 543-52.

158. Fazzalari, N.L., J.S. Kuliwaba, and M.R. Forwood, Cancellous bone microdamage in the proximal femur: influence of age and osteoarthritis on damage morphology and regional distribution. *Bone*, 2002. **31**(6): p. 697-702.

159. Mori, S., et al., Trabecular bone volume and microdamage accumulation in the femoral heads of women with and without femoral neck fractures. *Bone*, 1997. **21**(6): p. 521-6.

160. Zarrinkalam, K.H., et al., New insights into the propagation of fatigue damage in cortical bone using confocal microscopy and chelating fluorochromes. *Eur J Morphol*, 2005. **42**(1-2): p. 81-90.

161. Birdwood, G., Understanding Osteoporosis and its treatment, A guide for physicians and their patients. 1996, Pearl River: New York.

162. Chapurlat, R.D. and P.D. Delmas, Bone microdamage: a clinical perspective. *Osteoporos Int*, 2009.

163. Taylor, D., Fatigue of bone and bones: an analysis based on stressed volume. *J Orthop Res*, 1998. **16**(2): p. 163-9.

164. Flora, L., et al., Comparative skeletal effects of two disphosphonates in dogs. *Metab Bone Dis Relat Res*, 1980. **2S**: p. 389-407.

165. Carter, D.R. and W.C. Hayes, Compact bone fatigue damage--I. Residual strength and stiffness. *J Biomech*, 1977. **10**(5-6): p. 325-37.

166. Danova, N.A., et al., Degradation of bone structural properties by accumulation and coalescence of microcracks. *Bone*, 2003. **33**(2): p. 197-205.

167. Norman, T.L., et al., Influence of microdamage on fracture toughness of the human femur and tibia. *Bone*, 1998. **23**(3): p. 303-6.

168. Muir, P., et al., Effect of fatigue loading and associated matrix microdamage on bone blood flow and interstitial fluid flow. *Bone*, 2007. **40**(4): p. 948-56.

169. Martinez-Reina, J., et al., On the role of bone damage in calcium homeostasis. *J Theor Biol*, 2008. **254**(3): p. 704-12.

170. Allen, M.R., et al., Alterations in canine vertebral bone turnover, microdamage accumulation, and biomechanical properties following 1-year treatment with clinical treatment doses of risedronate or alendronate. *Bone*, 2006. **39**(4): p. 872-9.

171. Chapurlat, R.D., et al., Microcrack frequency and bone remodeling in postmenopausal osteoporotic women on long-term bisphosphonates: a bone biopsy study. *J Bone Miner Res*, 2007. **22**(10): p. 1502-9.

172. Stepan, J.J., et al., Low bone mineral density is associated with bone microdamage accumulation in postmenopausal women with osteoporosis. *Bone*, 2007. **41**(3): p. 378-85.

173. Pavia, D.L., G.M. Lampman, and G.S. Kriz, Introduction to Spectroscopy: a guide for students of organic chemistry. 1979, Philadelphia: Saunders College Publishing.

174. Humecki, H., Practical Applications of Infrared Microspectroscopy. 1995, New York: Marcel Dekker, Inc.

175. Rey, C., et al., Resolution-enhanced Fourier transform infrared spectroscopy study of the environment of phosphate ions in the early deposits of a solid phase of calcium-phosphate in bone and enamel, and their evolution with age. I: Investigations in the upsilon 4 PO4 domain. *Calcif Tissue Int*, 1990. **46**(6): p. 384-94.

176. Rey, C., et al., Resolution-enhanced Fourier transform infrared spectroscopy study of the environment of phosphate ions in the early deposits of solid phase calcium phosphate in bone and enamel and their evolution with age: 2. Investigations in the ν_3 PO_4 domain. *Calc. Tissue Int.*, 1991. **49**: p. 383-388.

177. Boskey, A.L., Bone mineral and matrix. Are they altered in osteoporosis? *Orthop Clin North Am*, 1990. **21**(1): p. 19-29.

178. Boskey, A.L., et al., Comparison of mineral quality and quantity in iliac crest biopsies from high- and low-turnover osteoporosis: an FT-IR microspectroscopic investigation. *Osteoporos Int*, 2005. **16**(12): p. 2031-8.

179. Miller, L.M., et al., A Method for Examining the Chemical Basis for Bone Disease: Synchrotron Infrared Microspectroscopy. *Cellular and Molec Biol*, 1998. **44**(1): p. 117-127.

180. Paschalis, E., et al., Spectroscopic determination of collagen cross-links at the ultrastructural level, and its application to osteoporosis. *Bone*, 1998. **23**: p. S342.

181. Paschalis, E.P., et al., FTIR microspectroscopic analysis of human iliac crest biopsies from untreated osteoporotic bone. *Calcif Tissue Int*, 1997. **61**(6): p. 487-92.

182. Gadaleta, S.J., et al., Fourier transform infrared microscopy of calcified turkey leg tendon. *Calcif. Tissue Int.*, 1996. **58**: p. 17-23.

183. Paschalis, E.P., et al., FTIR microspectroscopic analysis of human osteonal bone. *Calcif Tissue Int*, 1996. **59**(6): p. 480-7.

184. Paschalis, E.P., et al., Fourier transform infrared microspectroscopic analysis identifies alterations in mineral properties in bones from mice transgenic for type X collagen. *Bone*, 1996. **19**(2): p. 151-6.

185. Miller, L.M., et al., Combining IR spectroscopy and fluorescence imaging in a single microscope: Biomedical applications using a synchrotron infrared source. *Rev. Sci. Instr.*, 2002. **73**: p. 1357-1360.

186. Miller, L.M., J. Tibrewala, and C.S. Carlson, Examination of Bone Chemical Composition in Osteoporosis Using Fluorescence-Assisted Synchrotron Infrared Microspectroscopy. *Cellular and Molec. Biol.*, 2000. **46**: p. 1035-44.

187. Miller, L.M., et al., In situ analysis of mineral content and crystallinity in bone using infrared micro-spectroscopy of the nu(4) PO(4)(3-) vibration. *Biochim Biophys Acta*, 2001. **1527**(1-2): p. 11-9.

188. Miller, L.M., et al., Accretion of bone quantity and quality in the developing mouse skeleton. *J Bone Miner Res*, 2007. **22**(7): p. 1037-45.

189. Andrews, J.C., et al., A High Resolution, Hard X-ray Bio-imaging Facility at SSRL. *Synchrotron Radiation News*, 2008. **21**(3): p. 17-26.

190. Tkachuk, A., et al., X-ray computed tomography in Zernike phase contrast mode at 8 keV with 50-nm resolution using anode X-ray source. *Z Kristallogr*, 2007. **222**: p. 650-655.

191. Rho, J.Y., T.Y. Tsui, and G.M. Pharr, Elastic properties of human cortical and trabecular lamellar bone measured by nanoindentation. *Biomaterials*, 1997. **18**(20): p. 1325-30.

192. Rho, J.Y., et al., Variations in the individual thick lamellar properties within osteons by nanoindentation. *Bone*, 1999. **25**(3): p. 295-300.

193. D'Aoust, P., et al., Etidronate (HEBP) promotes osteoblast differentiation and wound closure in rat calvaria. *Cell Tissue Res*, 2000. **302**(3): p. 353-63.

194. Russell, R.G., et al., Effect of diphosphonates and calcitonin on the chemistry and quantitative histology of rat bone. *Calcif Tissue Res*, 1973. **11**(3): p. 179-95.

195. Miller, S.C. and W.S. Jee, Ethane-1-hydroxy-1, 1-diphosphonate (EHDP). Effects on growth and modeling of the rat tibia. *Calcif Tissue Res*, 1975. **18**(3): p. 215-31.

196. King, W.R., M.D. Francis, and W.R. Michael, Effect of disodium ethane-1-hydroxy-1, 1-diphosphonate on bone formation. *Clin Orthop Relat Res*, 1971. **78**: p. 251-70.

197. Schenk, R., et al., Effect of ethane-1-hydroxy-1,1-diphosphonate (EHDP) and dichloromethylene diphosphonate (Cl 2 MDP) on the calcification and resorption of cartilage and bone in the tibial epiphysis and metaphysis of rats. *Calcif Tissue Res*, 1973. **11**(3): p. 196-214.

198. Rosenblum, I.Y., The effectsof disodium ethane-1-hydroxy-1, 1-diphosphonate (EHDP) on mineral and organic components of rat bone. *Calcif Tissue Res*, 1974. **16**(3): p. 239-50.

199. Larsson, A. and S.E. Larsson, Light microscopic and ultrastructural observations on the short-term effects of ethylene-1-hydroxy-1, 1-diphosphonate (EHDP) on rat tibia epiphysis. *Acta Pathol Microbiol Scand [A]*, 1976. **84**(1): p. 17-27.

200. Katoh, Y., et al., Effects of ethane-1-hydroxy-1, 1-diphosphonate on cell differentiation, and proteoglycan and calcium metabolism, in the proximal tibia of young rats. *Bone*, 1991. **12**(2): p. 59-65.

201. Kellinsalmi, M., et al., In vitro comparison of clodronate, pamidronate and zoledronic acid effects on rat osteoclasts and human stem cell-derived osteoblasts. *Basic Clin Pharmacol Toxicol*, 2005. **97**(6): p. 382-91.

202. Idris, A.I., et al., Aminobisphosphonates cause osteoblast apoptosis and inhibit bone nodule formation in vitro. *Calcif Tissue Int*, 2008. **82**(3): p. 191-201.

203. Tsuchimoto, M., et al., Alendronate modulates osteogenesis of human osteoblastic cells in vitro. *Jpn J Pharmacol*, 1994. **66**(1): p. 25-33.

204. Garcia-Moreno, C., et al., Effect of alendronate on cultured normal human osteoblasts. *Bone*, 1998. **22**(3): p. 233-9.

205. Ruppel, M.E., D.B. Burr, and L.M. Miller, Chemical makeup of microdamaged bone differs from undamaged bone. *Bone*, 2006. **39**(2): p. 318-24.

206. Neuman, W.F. and M.W. Neuman, The Chemical Dynamics of Bone Mineral. 1958, Chicago: The University of Chicago Press.

207. Glimcher, M.J., The nature of the mineral component of bone and the mechanisms of calcification, in *Disorders of Bone and Mineral Metabolism*, F.L. Coe and M.J. Favus, Editors. 1992, Raven Press: New York. p. 265-286.

208. Bohic, S., et al., Characterization of the trabecular rat bone mineral: effect of ovariectomy and bisphosphonate treatment. *Bone*, 2000. **26**(4): p. 341-8.

209. Miller, L.M., et al., Applications of fluorescence-assisted infrared microspectroscopy to the study of osteoporosis. *Synchrotron Radiation News*, 1999. **12**(1): p. 21-27.

210. Miller, L.M., et al., Alterations in mineral composition observed in osteoarthritic joints of cynomolgus monkeys. *Bone*, 2004. **35**(2): p. 498-506.

211. Camacho, N.P., W.J. Landis, and A.L. Boskey, Mineral changes in a mouse model of osteogenesis imperfecta detected by Fourier transform infrared microscopy. *Connect Tissue Res*, 1996. **35**(1-4): p. 259-65.

212. Camacho, N.P., et al., The material basis for reduced mechanical properties in OIM mice bones. *J. Bone Min. Res.*, 1999. **14**: p. 264-272.

213. Rey, C., et al., A Resolution-Enhanced Fourier Transform Infrared Spectroscopic Study of the Environment of the CO_3^{2-} Ion in the Mineral Phase of Enamel During its Formation and Maturation. *Calcified Tissue International*, 1991. **49**: p. 259-268.

214. Burr, D.B. and M. Hooser, Alterations to the en bloc basic fuchsin staining protocol for the demonstration of microdamage produced in vivo. *Bone*, 1995. **17**(4): p. 431-3.

215. Lee, T.C., et al., Detecting microdamage in bone. *Journal of Anatomy*, 2003. **203**(2): p. 161-172.

216. Verborgt, O., G.J. Gibson, and M.B. Schaffler, Loss of osteocyte integrity in association with microdamage and bone remodeling after fatigue in vivo. *J Bone Miner Res*, 2000. **15**(1): p. 60-7.

217. Galley, S.A., D.J. Michalek, and S.W. Donahue, A fatigue microcrack alters fluid velocities in a computational model of interstitial fluid flow in cortical bone. *J Biomech*, 2006. **39**(11): p. 2026-33.

218. Paschalis, E.P., et al., Spectroscopic characterization of collagen cross-links in bone. *J. Bone Min. Res.*, 2001. **16**(10): p. 1821-1828.

219. Nalla, R.K., J.H. Kinney, and R.O. Ritchie, Mechanistic fracture criteria for the failure of human cortical bone. *Nat Mater*, 2003. **2**(3): p. 164-8.

220. Paschalis, E.P., et al., Bone fragility and collagen cross-links. *J Bone Miner Res*, 2004. **19**(12): p. 2000-4.

221. Legros, R., N. Balmain, and G. Bonel, Age-related changes in mineral of rat and bovine cortical bone. *Calcif Tissue Int*, 1987. **41**(3): p. 137-44.

222. Ouyang, H., et al., Fourier transform infrared microscopic imaging: effects of estrogen and estrogen deficiency on fracture healing in rat femurs. *Appl Spectrosc*, 2004. **58**(1): p. 1-9.

223. LeGeros, R.Z., Chemical and crystallographic events in the caries process. *J Dent Res*, 1990. **69 Spec No**: p. 567-74; discussion 634-6.

224. Timlin, J.A., et al., Raman spectroscopic imaging markers for fatigue-related microdamage in bovine bone. *Analytical Chem.*, 2000. **72**: p. 2229-36.

225. Carden, A., et al., Ultrastructural changes accompanying the mechanical deformation of bone tissue: a Raman imaging study. *Calcif Tissue Int*, 2003. **72**(2): p. 166-75.

226. Blank, R.D., et al., Spectroscopically determined collagen Pyr/deH-DHLNL cross-link ratio and crystallinity indices differ markedly in recombinant congenic mice with divergent calculated bone tissue strength. *Connect Tissue Res*, 2003. **44**(3-4): p. 134-42.

227. Vashishth, D., et al., Influence of nonenzymatic glycation on biomechanical properties of cortical bone. *Bone*, 2001. **28**(2): p. 195-201.

228. Nalla, R.K., et al., Effect of aging on the toughness of human cortical bone: evaluation by R-curves. *Bone*, 2004. **35**(6): p. 1240-6.

229. Faibish, D., et al., Infrared imaging of calcified tissue in bone biopsies from adults with osteomalacia. *Bone*, 2005. **36**(1): p. 6-12.

230. Lazarev, Y.A., B.A. Grishkovsky, and T.B. Khromova, Amide I band of IR spectrum and structure of collagen and related peptides. *Biopolymers*, 1985. **24**: p. 1449-1478.

231. Silver, F.H., et al., Analysis of mammalian connective tissue: relationship between hierarchical structures and mechanical properties. *J Long Term Eff Med Implants*, 1992. **2**(2-3): p. 165-98.

232. Stepan, J.J., et al. Prevalent Fracture, Low Bone Mineral Density and Ageing are associated with greater histomorphometric indicators of microdamage accumulation in postmenopausal women. in *ASBMR Annual Meeting*. 2005. Nashville, TN.

233. Vaidya, S.N., et al., Pressure-induced crystalline to amorphous transition in hydroxylapatite. *Journal of Materials Science*, 1997. **32**(12): p. 3213-3217.

234. Wang, X., et al., Age-related changes in the collagen network and toughness of bone. *Bone*, 2002. **31**(1): p. 1-7.

235. Zioupos, P., Accumulation of in-vivo fatigue microdamage and its relation to biomechanical properties in ageing human cortical bone. *J Microsc*, 2001. **201**(Pt 2): p. 270-8.

236. Ruppel, M.E., R.J. Phipps, and L.M. Miller, Risedronate-treatment temporarily delays collagen deposition and matrix mineralization of MC3T3-E1 osteoblasts. *Bone*, 2009. **Submitted**.

237. Giuliani, N., et al., Bisphosphonates stimulate formation of osteoblast precursors and mineralized nodules in murine and human bone marrow cultures in vitro and promote early osteoblastogenesis in young and aged mice in vivo. *Bone*, 1998. **22**(5): p. 455-61.

238. Stein, G.S., J.B. Lian, and T.A. Owen, Relationship of cell growth to the regulation of tissue-specific gene expression during osteoblast differentiation. *Faseb J*, 1990. **4**(13): p. 3111-23.

239. Ibaraki, K., et al., Bone matrix mRNA expression in differentiating fetal bovine osteoblasts. *J Bone Miner Res*, 1992. **7**(7): p. 743-54.

240. Beck, G.R., Jr., B. Zerler, and E. Moran, Gene array analysis of osteoblast differentiation. *Cell Growth Differ*, 2001. **12**(2): p. 61-83.

241. Miller, L.M., et al., Synchrotron Infrared Spectroscopy as a Means of Studying the Chemical Composition of Bone: Applications to Osteoarthritis. *SPIE*, 1997. **3153**: p. 141-148.

242. Mochida, Y., et al., Decorin modulates collagen matrix assembly and mineralization. *Matrix Biol*, 2009. **28**(1): p. 44-52.

243. Turecek, C., et al., Collagen cross-linking influences osteoblastic differentiation. *Calcif Tissue Int*, 2008. **82**(5): p. 392-400.

244. Lim, J.Y., et al., Surface energy effects on osteoblast spatial growth and mineralization. *Biomaterials*, 2008. **29**(12): p. 1776-84.

245. Luppen, C.A., et al., Brief bone morphogenetic protein 2 treatment of glucocorticoid-inhibited MC3T3-E1 osteoblasts rescues commitment-associated cell cycle and mineralization without alteration of Runx2. *J Biol Chem*, 2003. **278**(45): p. 44995-5003.

246. Boskey, A.L., et al., Applications of Fourier transform infrared (FT-IR) microscopy to the study of mineralization in bone and cartilage. *Cells and Materials*, 1992. **2**(3): p. 209-220.

247. Bonewald, L.F., et al., von Kossa staining alone is not sufficient to confirm that mineralization in vitro represents bone formation. *Calcif Tissue Int*, 2003. **72**(5): p. 537-47.

248. Subburaman, K., et al., Templated biomineralization on self-assembled protein fibers. *Proc Natl Acad Sci*, 2006. **103**(40): p. 14672-14677.

249. Pernodet, N., et al., Fibronectin Fibrillogenesis on sulfonated polystyrene surface. *J Biomed Mater Res Pt A*, 2003. **64A**(4): p. 684-692.

250. Liu, K.Z., et al., Modification of the extracellular matrix following myocardial infarction monitored by FTIR spectroscopy. *Biochimica Et Biophysica Acta-Molecular Basis of Disease*, 1996. **1315**(2): p. 73-77.

251. Gough, K.M., et al., Fourier transform infrared evaluation of microscopic scarring in the cardiomyopathic heart: effect of chronic AT1 suppression. *Anal Biochem*, 2003. **316**(2): p. 232-42.

252. Camacho, N.P., et al., FTIR microscopic imaging of collagen and proteoglycan in bovine cartilage. *Biopolymers*, 2001. **62**(1): p. 1-8.

253. Jackson, M., M.G. Sowa, and H.H. Mantsch, Infrared spectroscopy: a new frontier in medicine. *Biophys Chem*, 1997. **68**(1-3): p. 109-25.

254. Khokher, M.A. and P. Dandona, Diphosphonates inhibit human osteoblast secretion and proliferation. *Metabolism*, 1989. **38**(2): p. 184-7.

255. Coxon, F.P., et al., Resorbing osteoclasts increase the availability of mineral-bound bisphosphonates to non-resorbing cells. *J Bone Miner Res*, 2005. **20**: p. s260.

256. Gasser, J., et al., Resorbing osteoclasts increase the availability of mineral-bound bisphosphonates to non-resorbing cells. *Bone*, 2006. **38**(3): p. 50-51.

257. Wenstrup, R.J., et al., Discordant expression of osteoblast markers in MC3T3-E1 cells that synthesize a high turnover matrix. *J Biol Chem*, 1996. **271**(17): p. 10271-6.

258. Xiao, G., et al., Ascorbic acid-dependent activation of the osteocalcin promoter in MC3T3-E1 preosteoblasts: requirement for collagen matrix synthesis and the presence of an intact OSE2 sequence. *Mol Endocrinol*, 1997. **11**(8): p. 1103-13.

259. Yamauchi, M.M., D.R. Young, and G.S. Chandler, Crosslinking and new bone collagen syntheses in immobilized and recovering primate osteoporosis. *Bone*, 1988. **9**: p. 415.

260. Yamauchi, M. and E.P. Katz, The post-translational chemistry and molecular packing of mineralizing tendon collagens. *Connect Tissue Res*, 1993. **29**(2): p. 81-98.

261. Gerstenfeld, L.C., et al., Post-translational control of collagen fibrillogenesis in mineralizing cultures of chick osteoblasts. *J Bone Miner Res*, 1993. **8**(9): p. 1031-43.

262. Pornprasertsuk, S., et al., Overexpression of lysyl hydroxylase-2b leads to defective collagen fibrillogenesis and matrix mineralization. *J Bone Miner Res*, 2005. **20**(1): p. 81-7.

263. Pornprasertsuk, S., et al., Lysyl hydroxylase-2b directs collagen cross-linking pathways in MC3T3-E1 cells. *J Bone Miner Res*, 2004. **19**(8): p. 1349-55.

264. Arsenault, A.L., B.W. Frankland, and F.P. Ottensmeyer, Vectorial sequence of mineralization in the turkey leg tendon determined by electron microscopic imaging. *Calcif Tissue Int*, 1991. **48**(1): p. 46-55.

265. Kirsch, T. and R.E. Wuthier, Stimulation of calcification of growth plate cartilage matrix vesicles by binding to type II and X collagens. *J Biol Chem*, 1994. **269**(15): p. 11462-9.

266. Landis, W.J. and A.L. Arsenault, Vesicle- and collagen-mediated calcification in the turkey leg tendon. *Connect Tissue Res*, 1989. **22**(1-4): p. 35-42; discussion 53-61.

267. Wu, L.N., et al., Induction of mineral deposition by primary cultures of chicken growth plate chondrocytes in ascorbate-containing media. Evidence of an association between matrix vesicles and collagen. *J Biol Chem*, 1989. **264**(35): p. 21346-55.

268. Fratzl, P., et al., Structure and mechanical quality of the collagen-mineral nano-composite in bone. *J Mater Chem*, 2004. **14**(14): p. 2115-2123.

269. Fleisch, H., Bisphosphonates. Pharmacology and use in the treatment of tumour-induced hypercalcaemic and metastatic bone disease. *Drugs*, 1991. **42**(6): p. 919-44.

270. Russell, R.G., et al., The influence of pyrophosphate, condensed phosphates, phosphonates and other phosphate compounds on the dissolution of hydroxyapatite in vitro and on bone resorption induced by parathyroid hormone in tissue culture and in thyroparathyroidectomised rats. *Calcif Tissue Res*, 1970. **6**(3): p. 183-96.

271. Coxon, F.P., et al., Phosphonocarboxylate inhibitors of Rab geranylgeranyl transferase disrupt the prenylation and membrane localization of Rab proteins in osteoclasts in vitro and in vivo. *Bone*, 2005. **37**(3): p. 349-58.

272. Dunford, J.E., et al., Inhibition of protein prenylation by bisphosphonates causes sustained activation of Rac, Cdc42, and Rho GTPases. *J Bone Miner Res*, 2006. **21**(5): p. 684-94.

273. Coxon, F.P., et al., Identification of a novel phosphonocarboxylate inhibitor of Rab geranylgeranyl transferase that specifically prevents Rab prenylation in osteoclasts and macrophages. *J Biol Chem*, 2001. **276**(51): p. 48213-22.

274. Coxon, F.P., et al., Protein geranylgeranylation is required for osteoclast formation, function, and survival: inhibition by bisphosphonates and GGTI-298. *J Bone Miner Res*, 2000. **15**(8): p. 1467-76.

275. Luckman, S.P., et al., Heterocycle-containing bisphosphonates cause apoptosis and inhibit bone resorption by preventing protein prenylation: evidence from structure-activity relationships in J774 macrophages. *J Bone Miner Res*, 1998. **13**(11): p. 1668-78.

276. Russell, R.G., Bisphosphonates: mode of action and pharmacology. *Pediatrics*, 2007. **119 Suppl 2**: p. S150-62.

277. Kazanci, M., et al., Bone osteonal tissues by Raman spectral mapping: orientation-composition. *J Struct Biol*, 2006. **156**(3): p. 489-96.

278. Martin, R.B. and D.L. Boardman, The effects of collagen fiber orientation, porosity, density, and mineralization on bovine cortical bone bending properties. *J Biomech*, 1993. **26**(9): p. 1047-54.

279. Puustjarvi, K., et al., Do more highly organized collagen fibrils increase bone mechanical strength in loss of mineral density after one-year running training? *J Bone Miner Res*, 1999. **14**(3): p. 321-9.

280. Fountos, G., et al., The effects of inflammation-mediated osteoporosis (IMO) on the skeletal Ca/P ratio and on the structure of rabbit bone and skin collagen. *Appl Radiat Isot*, 1998. **49**(5-6): p. 657-9.

281. Burstein, A.H., et al., Contribution of collagen and mineral to the elastic-plastic properties of bone. *J Bone Joint Surg Am*, 1975. **57**(7): p. 956-61.

282. Lundon, K., M. Dumitriu, and M. Grynpas, The long-term effect of ovariectomy on the quality and quantity of cancellous bone in young macaques. *Bone Miner*, 1994. **24**(2): p. 135-49.

283. Simmons, E.D., Jr., K.P. Pritzker, and M.D. Grynpas, Age-related changes in the human femoral cortex. *J Orthop Res*, 1991. **9**(2): p. 155-67.

284. Jager, I. and P. Fratzl, Mineralized collagen fibrils: a mechanical model with a staggered arrangement of mineral particles. *Biophys J*, 2000. **79**(4): p. 1737-46.

285. Gupta, H.S., et al., Cooperative deformation of mineral and collagen in bone at the nanoscale. *Proc Natl Acad Sci U S A*, 2006. **103**(47): p. 17741-6.

286. Roschger, P., et al., Alendronate increases degree and uniformity of mineralization in cancellous bone and decreases the porosity in cortical bone of osteoporotic women. *Bone*, 2001. **29**(2): p. 185-91.

287. Khouja, H.I., et al., Calcium and orthophosphate deposits in vitro do not imply osteoblast-mediated mineralization: mineralization by betaglycerophosphate in the absence of osteoblasts. *Bone*, 1990. **11**(6): p. 385-91.

288. Chung, C.H., et al., Mechanism of action of beta-glycerophosphate on bone cell mineralization. *Calcif Tissue Int*, 1992. **51**(4): p. 305-11.

289. Glimcher, M.J., Molecular biology of mineralized tissues with particular reference to bone. *Rev Mod Phys*, 1959. **31**(2): p. 359-393.

290. Paschalis, E.P., et al., FTIR microspectroscopic analysis of normal human cortical and trabecular bone. *Calcif Tissue Int*, 1997. **61**(6): p. 480-6.

291. Elliott, J.C., Calcium phosphate biominerals. *Rev Mineral Geochem*, 2002. **48**: p. 427-453.

292. Gross, K.A. and C.C. Berndt, Biomedical application of apatites. *Rev Mineral Geochem*, 2002. **48**: p. 631-672.

293. Henneman, Z.J., et al., Bisphosphonate binding affinity as assessed by inhibition of carbonated apatite dissolution in vitro. *J Biomed Mater Res A*, 2008. **85**(4): p. 993-1000.

294. Jung, A., S. Bisaz, and H. Fleisch, The binding of pyrophosphate and two diphosphonates by hydroxyapatite crystals. *Calcif Tissue Res*, 1973. **11**(4): p. 269-80.

295. Ebrahimpour, A. and M.D. Francis, Bisphosphonate therapy in acute and chronic bone loss: physical chemical considerations in bisphosphonate-related therapies, in *Bisphosphonate on Bone*, O.L. Bijvoet, et al., Editors. 1995, Elsevier Publishing: Amsterdam. p. 125-136.

296. Durchschlag, E., et al., Bone material properties in trabecular bone from human iliac crest biopsies after 3- and 5-year treatment with risedronate*. J Bone Miner Res*, 2006. **21**(10): p. 1581-90.

297. Balena, R., et al., The effects of 2-year treatment with the aminobisphosphonate alendronate on bone metabolism, bone histomorphometry, and bone strength in ovariectomized nonhuman primates*. J Clin Invest*, 1993. **92**(6): p. 2577-86.

298. Komatsubara, S., et al., Suppressed bone turnover by long-term bisphosphonate treatment accumulates microdamage but maintains intrinsic material properties in cortical bone of dog rib*. J Bone Miner Res*, 2004. **19**(6): p. 999-1005.

299. Liberman, U.A., et al., Effect of oral alendronate on bone mineral density and the incidence of fractures in postmenopausal osteoporosis. The Alendronate Phase III Osteoporosis Treatment Study Group*. N Engl J Med*, 1995. **333**(22): p. 1437-43.

300. Liberman, U.A., et al., Hip and non-spine fracture risk reductions differ among antiresorptive agents: Evidence from randomised controlled trials*. Int J Clin Pract*, 2006. **60**(11): p. 1394-400.

301. Roux, C., et al., Efficacy of risedronate on clinical vertebral fractures within six months*. Curr Med Res Opin*, 2004. **20**(4): p. 433-9.

302. Silverman, S.L., et al., Effectiveness of bisphosphonates on nonvertebral and hip fractures in the first year of therapy: the risedronate and alendronate (REAL) cohort study*. Osteoporos Int*, 2007. **18**(1): p. 25-34.

303. Day, J.S., et al., Bisphosphonate treatment affects trabecular bone apparent modulus through micro-architecture rather than matrix properties*. J Orthop Res*, 2004. **22**(3): p. 465-71.

304. Borah, B., et al., Risedronate preserves trabecular architecture and increases bone strength in vertebra of ovariectomized minipigs as measured by three-dimensional microcomputed tomography*. J Bone Miner Res*, 2002. **17**(7): p. 1139-47.

305. Borah, B., et al., Risedronate preserves bone architecture in postmenopausal women with osteoporosis as measured by three-dimensional microcomputed tomography. *Bone*, 2004. **34**(4): p. 736-46.

306. Dufresne, T.E., et al., Risedronate preserves bone architecture in early postmenopausal women in 1 year as measured by three-dimensional microcomputed tomography. *Calcif Tissue Int*, 2003. **73**(5): p. 423-32.

307. Recker, R., et al., Trabecular bone microarchitecture after alendronate treatment of osteoporotic women. *Curr Med Res Opin*, 2005. **21**(2): p. 185-94.

308. Loveridge, N., et al., Bone mineralization density and femoral neck fragility. *Bone*, 2004. **35**(4): p. 929-41.

309. Borah, B., et al., The effect of risedronate on bone mineralization as measured by micro-computed tomography with synchrotron radiation: correlation to histomorphometric indices of turnover. *Bone*, 2005. **37**(1): p. 1-9.

310. Boivin, G., et al., Contribution of raloxifene and calcium and vitamin D3 supplementation to the increase of the degree of mineralization of bone in postmenopausal women. *J Clin Endocrinol Metab*, 2003. **88**(9): p. 4199-205.

311. Boivin, G., et al., Influence of estrogen therapy at conventional and high doses on the degree of mineralization of iliac bone tissue: a quantitative microradiographic analysis in postmenopausal women. *Bone*, 2005. **36**(3): p. 562-7.

312. Kendall, K., Control of cracks by interfaces in composites. *Proceedings of the Royal Society of London. Series A, Mathematical and Physical Sciences*, 1975. **341**(1627): p. 409-428.

313. Zoehrer, R., et al., Effects of 3- and 5-year treatment with risedronate on bone mineralization density distribution in triple biopsies of the iliac crest in postmenopausal women. *J Bone Miner Res*, 2006. **21**(7): p. 1106-12.

314. Grynpas, M.D., et al., Changes in bone mineralization, architecture and mechanical properties due to long-term (1 year) administration of pamidronate (APD) to adult dogs. *Osteoporos Int*, 1992. **2**(2): p. 74-81.

315. Currey, J.D., K. Brear, and P. Zioupos, The effects of ageing and changes in mineral content in degrading the toughness of human femora. *J Biomech*, 1996. **29**(2): p. 257-60.

316. Vashishth, D., The role of the collagen matrix in skeletal fragility. *Curr Osteoporos Rep*, 2007. **5**(2): p. 62-6.

317. Ciarelli, T.E., D.P. Fyhrie, and A.M. Parfitt, Effects of vertebral bone fragility and bone formation rate on the mineralization levels of cancellous bone from white females. *Bone*, 2003. **32**(3): p. 311-5.

318. McNamara, L.M., et al., Strength of cancellous bone trabecular tissue from normal, ovariectomized and drug-treated rats over the course of ageing. *Bone*, 2006. **39**(2): p. 392-400.

319. Burr, D.B., et al., Does microdamage accumulation affect the mechanical properties of bone? *J Biomech*, 1998. **31**(4): p. 337-45.

320. Hernandez, C.J., et al., The influence of bone volume fraction and ash fraction on bone strength and modulus. *Bone*, 2001. **29**(1): p. 74-8.

321. Currey, J.D., Tensile yield in compact bone is determined by strain, post-yield behaviour by mineral content. *J Biomech*, 2004. **37**(4): p. 549-56.

322. Schaffler, M.B., Role of bone turnover in microdamage. *Osteoporos Int*, 2003. **14 Suppl 5**: p. 73-80.

323. Forwood, M.R. and A.W. Parker, Microdamage in response to repetitive torsional loading in the rat tibia. *Calcif Tissue Int*, 1989. **45**(1): p. 47-53.

324. Hirano, T., et al., Does suppression of bone turnover impair mechanical properties by allowing microdamage accumulation? *Bone*, 2000. **27**(1): p. 13-20.

325. Garnero, P., et al., Extracellular post-translational modifications of collagen are major determinants of biomechanical properties of fetal bovine cortical bone. *Bone*, 2006. **38**(3): p. 300-9.

326. Zioupos, P., J.D. Currey, and A.J. Hamer, The role of collagen in the declining mechanical properties of aging human cortical bone. *J Biomed Mater Res*, 1999. **45**(2): p. 108-16.

327. Yamauchi, M., D.T. Woodley, and G.L. Mechanic, Aging and cross-linking of skin collagen. *Biochem Biophys Res Commun*, 1988. **152**(2): p. 898-903.

328. Viguet-Carrin, S., P. Garnero, and P.D. Delmas, The role of collagen in bone strength. *Osteoporos Int*, 2006. **17**(3): p. 319-36.

329. Paschalis, E.P., et al., Distribution of collagen cross-links in normal human trabecular bone. *J Bone Miner Res*, 2003. **18**(11): p. 1942-6.

330. LeGeros, R.Z., Calcium phosphates in demineralization/remineralization processes. *J Clin Dent*, 1999. **10**(2): p. 65-73.

331. Baumann, B.D. and T.J. Wronski, Response of cortical bone to antiresorptive agents and parathyroid hormone in aged ovariectomized rats. *Bone*, 1995. **16**(2): p. 247-53.

332. Bikle, D.D., et al., Alendronate increases skeletal mass of growing rats during unloading by inhibiting resorption of calcified cartilage. *J Bone Miner Res*, 1994. **9**(11): p. 1777-87.

333. Pataki, A., et al., Effects of short-term treatment with the bisphosphonates zoledronate and pamidronate on rat bone: a comparative histomorphometric study on the cancellous bone formed before, during, and after treatment. *Anat Rec*, 1997. **249**(4): p. 458-68.

334. Im, G.I., et al., Osteoblast proliferation and maturation by bisphosphonates. *Biomaterials*, 2004. **25**(18): p. 4105-15.

335. Itoh, F., et al., Clodronate stimulates osteoblast differentiation in ST2 and MC3T3-E1 cells and rat organ cultures. *Eur J Pharmacol*, 2003. **477**(1): p. 9-16.

336. Varghese, S. and E. Canalis, Alendronate stimulates collagenase 3 expression in osteoblasts by posttranscriptional mechanisms. *J Bone Miner Res*, 2000. **15**(12): p. 2345-51.

337. von Knoch, F., et al., Effects of bisphosphonates on proliferation and osteoblast differentiation of human bone marrow stromal cells. *Biomaterials*, 2005. **26**(34): p. 6941-9.

338. Tenenbaum, H.C., M. Torontali, and B. Sukhu, Effects of bisphosphonates and inorganic pyrophosphate on osteogenesis in vitro. *Bone*, 1992. **13**(3): p. 249-55.

339. Keaveny, T.M., et al., Collagen status and brittleness of human cortical bone in the elderly. *J Bone Miner Res*, 2003. **18** ((suppl 12)): p. S307.

340. Monier-Faugere, M.C., et al., Intermittent and continuous administration of the bisphosphonate ibandronate in ovariohysterectomized beagle dogs: effects on bone morphometry and mineral properties. *J Bone Miner Res*, 1999. **14**(10): p. 1768-78.

341. Rohanizadeh, R., et al., Ultrastructural properties of bone mineral of control and tiludronate-treated osteoporotic rat. *Calcif Tissue Int*, 2000. **67**(4): p. 330-6.

342. Ziv, V. and S. Weiner, Bone crystal sizes: a comparison of transmission electron microscopic and X-ray diffraction line width broadening techniques. *Connect Tissue Res*, 1994. **30**(3): p. 165-75.

343. Camacho, N.P., et al., Complementary information on bone ultrastructure from scanning small angle X-ray scattering and Fourier-transform infrared microspectroscopy. *Bone*, 1999. **25**(3): p. 287-93.

344. Aaron, J.E., M.C. de Vernejoul, and J.A. Kanis, The effect of sodium fluoride on trabecular architecture. *Bone*, 1991. **12**(5): p. 307-10.

345. Eriksen, E.F., L. Mosekilde, and F. Melsen, Effect of sodium fluoride, calcium, phosphate, and vitamin D2 on trabecular bone balance and remodeling in osteoporotics. *Bone*, 1985. **6**(5): p. 381-9.

346. Martin, R.B. and J. Ishida, The relative effects of collagen fiber orientation, porosity, density, and mineralization on bone strength. *J Biomech*, 1989. **22**(5): p. 419-26.